The Geotechnical Bearing Capacity of Old Timber Piles

F.J. van Daatselaar

The Geotechnical Bearing Capacity of Old Timber Piles

by

F.J. van Daatselaar

To obtain the degree of Master of Science
at the Delft University of Technology,
to be defended publicly on
28 - 11 - 2019

Student number:	4389832	
Duration:	March, 2019 – November, 2019	
Committee:	Dr. ir. M. Korff,	TU Delft, Department of Geo-Engineering (Chair)
	ir. J.C. Landwehr,	Deltares
	Prof. dr. ir. K.G. Gavin,	TU Delft, Deparment of Geo-Engineering
	Prof. dr. ir. J.W.G. van de Kuilen,	TU Delft, Department of Engineering Structures
	Drs W.F. Gard	TU Delft, Department of Engineering Structures

An electronic version of this thesis is available at `http://repository.tudelft.nl/`.

Cover photo: Pile Extraction on the Oudezijdse Achterburgwal, taken on 15 - 05 - 2019.

TU Delft Delft University of Technology

Deltares Enabling Delta Life

Preface

The document before you is the result of nine months of graduation work performed at Deltares.

The work would not have been possible without all the members of my committee who provided me with guidance and feedback; Hans Landwehr, Ken Gavin and Jan Willem van de Kuilen. A special thanks to Mandy Korff and Wolfgang Gard who were always available for my questions.

Furthermore, I am grateful to all the lab technicians who helped me out during my time performing tests in the CiTG basement during the summer; Wim Verwaal, Jens van den Berg and Joost van Meel. Thanks to Marc Friebel especially, who did not only help me with the samples and the set up, but also made my time there so much more fun.

I would also like to thank the municipality of Amsterdam, Erik Hutcheson especially, who made it possible for me to witness the extraction of the piles on the OZAW and who was even as kind as to bring one of the piles to Delft for my research.

I will also take this opportunity to express my gratefulness to my family, my friends and all the wonderful people I have met during my studies in the past two years, many of whom have also become my friends. Your support, advice and occasional distractions are what kept me going throughout.

Lastly to David, my love and best friend. Thank you for your endless patience in handling your often nervous and stressed out girlfriend. Not just in the last nine months, but throughout my whole academic career at TU Delft. Even though I am often to stubborn to use it, I always take your advice to heart. You always have faith in me, especially when I don't. I can't wait to see what the future has in store for us.

E.J. van Daatselaar
Delft, November 2019

Summary

In this thesis the geotechnical bearing capacity of old timber piles in Amsterdam is studied. This is necessary because many structures such as quay walls, bridges and houses in the (historic) city centre of Amsterdam are founded on timber piles with ages ranging between 80 and 300 years old. The assessment of the foundation is currently done using many assumptions, these are needed because the piles are not easily accessible and old construction drawings are not always available or accurate. Furthermore, the effect that bacterial degradation of the wood has on the interface friction between soil and wood has never been studied in detail. In the assessment it is currently assumed that degradation has no effect on the geotechnical bearing capacity (Kalt and Dusseldorp (2018)), while in the old Dapperbuurt tests it was found that old piles had a reduced shaft capacity of 40% (Korff (2013)). The study is split into two parts; firstly a laboratory study into the effect of bacterial degradation on the interface friction between sand and wood has been performed, and secondly a sensitivity analysis into the geotechnical bearing capacity of timber piles in Amsterdam soil has been carried out.

The laboratory tests have been performed using an alternative to a regular direct shear box set up to determine what the difference in interface friction is between sand and fresh timber piles and degraded timber piles. The degraded timber pile was extracted on the Oudezijdese Achterburgwal in Amsterdam and has served as foundation pile under a quay wall for approximately 100 years. The sand was chosen to resemble that of the first sand layer in Amsterdam. The effect of a slime layer, a by-product of bacterial degradation, was further studied using Xanthan gum as an imitation for the slime.

The alternative set up gave consistent results which resembled those of a regular direct shear box and agreed well with the values that were expected from literature studies ($\delta = \frac{3}{4} \times \phi$). The application of a slime layer had an effect on the interface friction between fresh wood and sand, causing a decrease of the interface friction angle of up to 5° on one of the new wood samples. Contrary to the fresh piles, this effect was not seen when the old pile was tested with slime. Also no difference was observed between tests on old wood and test on fresh wood without slime. All in all the 40% reduction that was found from the Dapperbuurt was not confirmed in these tests. Two possible causes are that due to the soft wood structure, sand grains indented into the wood, leading to a higher measured friction angle. Or that the degraded wood sample was not severely degraded.

It is recommended to perform additional tests on wood samples that show more severe degradation, and to perform additional tests with a higher applied normal load. Also, tests on clay should be performed, since the reduction of shaft friction in the Dapperbuurt was found in soft layers, and indentation can not occur in clay.

Secondly, a Monte Carlo analysis has been performed, calculating the total and ultimate bearing capacity of a pile on two locations in Amsterdam, while varying the embedment in the first sand layer and the pile dimensions (length, tapering and diameters). The used parameters were derived from two data sets of extracted piles from Amsterdam. Using this data, the assumptions that are currently being made regarding pile parameters and bearing capacities have been assessed. Furthermore, the effect that a potential reduction in shaft capacity of up to 40% has on total and ultimate bearing capacities has been be studied.

It is found that the assumptions that are made regarding the pile parameters are too optimistic. The assumed parameters do not correspond to the mean value that is found from the data set, often leading to values of the bearing capacity that are too high.

It was concluded that a reduction in shaft capacity did not have a large effect on the total capacity, as this is mainly made up of base capacity, which is not affected by degradation. The ultimate capacity was influenced more severely, as the shaft friction from the Holocene layers can provide quite a big contribution to the ultimate bearing capacity. The most important effect of α_{red} is how it influences the axial load and neutral point of a pile. Assuming that the reduction of the shaft friction works on both positive and negative skin friction, the axial load decreases with decreasing α_{red}, which has a positive effect on the calculation of the wood strength of the pile. The location of the neutral point relative to the case where there is no reduction depends on the soil profile. If sandy layers with more resistance are located at shallow depths, α_{red} usually

causes a reduction in the negative skin friction , leading to a relatively lower neutral point. If the layers with more resistance are located near the pile tip, α_{red} mainly influences the positive skin friction, leading to a relatively higher neutral point.

It is recommended that more detailed studies are performed into the pile parameters and their relation to each other. With better correlations and more information, pile capacities can be determined with a higher level of certainty. Additional pile extractions are also recommended to find more information on the embedment of the pile in the sand layer, as no information is currently available, even though this parameter has a large effect on the bearing capacity of a pile. Moreover, the municipality of Amsterdam is adviced to reevaluate their current set of assumptions regarding pile parameters using the two large data sets that were used here and any additional data from pile extractions that will be performed in the future.

Contents

1 Introduction

1.1. Problem Description

Many structures, such as houses, bridges and quay walls, in the centre of Amsterdam are founded on timber piles. With pile ages varying between 80 and 300 years, the end of the technical life time of these structures is coming close or has already passed. Recently, the need to assess and replace these structures has become acknowledged. In order to determine which structures need to be prioritized, the remaining bearing capacity needs to be assessed accurately.

Since foundation are often not easily accessible, and construction drawings are often absent or not correct, the municipality uses many assumptions when calculating the bearing capacity of timber piles. The method which is currently used to assess the quality of these piles, the F3o, in combination with the assumptions are thought to be too conservative. Often, the calculated bearing capacity is not sufficient even though there is no visible damage to the structure. Therefore it is necessary to conduct additional research into the geotechnical bearing capacity of old timber piles. This research includes an assessment of the assumptions that are currently being made regarding pile parameters and bearing capacities.

Furthermore, it needs to be studied what effect bacterial degradation has on the bearing capacity of timber piles. There is currently no consensus on the subject, as the municipality of Amsterdam assumes that it has no effect on the geotechnical bearing capacity (Kalt and Dusseldorp (2018)), while literature described a potential reduction in the shaft capacity of up to 40% (Korff (2013)).

1.2. Research Plan

The main research question of this thesis is: "What is the effect of wood degradation on the geotechnical bearing capacity of old timber piles?" An answer to this question will be provided by following two tracks. The first track focuses on what the effect of bacterial degradation is on the interface friction between sand and wood. The second track will focus on what the effect of a potential reduction of the shaft friction is on the calculated bearing capacity of a pile in Amsterdam.

For the first track, direct shear tests are performed on samples of old timber piles which are extracted from a quay wall on the Oudezijdse Achterburgwal in the historic city centre of Amsterdam. Direct shear tests on samples of old timber piles have already been performed by Lantinga (2015), but the effect of a bacterial slime layer was not studied. This track is divided into three sub questions:

1. What is the effect of a degraded wood structure on the interface friction?
2. What is the effect of a slime layer on the interface friction?
3. What is the difference in interface friction between 'old' and 'new' piles?

Secondly, it is studied how a decrease in shaft friction affects the total and ultimate bearing capacity of a timber pile in Amsterdam. For this purpose a Monte Carlo analysis is performed. This sensitivity analysis will be made for two locations in the city of Amsterdam with different subsurface conditions. Realistic pile parameters will be obtained from two large data sets of previously extracted piles in Amsterdam. The input and output of this analysis will also be compared to assumptions that the municipality currently makes when assessing the geotechnical bearing capacity of timber piles. Again, three sub questions are defined:

1. What parameter distributions should be used as input for the analysis and how do these relate to the parameters that the municipality uses?
2. What is the geotechnical bearing capacity of timber piles in Amsterdam and how is the uncertainty affected by the input parameters?
3. How is the (distribution of) the geotechnical bearing capacity affected by a reduction in shaft friction due to bacterial degradation?

1.3. Scope

This thesis focuses on the bearing capacity of old timber piles in the city of Amsterdam, more specifically, of timber piles situated under bridges. Although it is expected that much of the same principles will hold for timber piles under quay walls and houses. Most of the bridges with timber pile foundations in Amsterdam are located in the historic city centre and in the eastern, western and southern districts. North of the IJ there is a relatively small amount. That is why the scope of this thesis is limited to the area which is shown in figure 1.1.

Figure 1.1: Area of Amsterdam within the scope of this thesis

Regarding wood degradation, only bacterial degradation will be studied. This choice has been made because timber piles under bridges will have generally been completely submerged during their lifetime. In these, almost anaerobic conditions, fungal degradation cannot occur and will therefore not be studied.

Considering the geotechnical bearing capacity, only the axial capacity of single piles is studied. Pile group effects, redistribution of loads, lateral loading and ageing effects are not included in this study.

1.4. Outline

In chapter two, the necessary literature is described. This includes an overview of the geology of Amsterdam, a description of typical foundations and pile dimensions in Amsterdam as well as a list of assumptions that are being used currently when assessing timber pile foundations. Also, the method which is used to calculate the geotechnical bearing capacity is described, and the theory behind shear box tests is explained. Furthermore some global information will be given on wood structure, wood degradation and bacterial slime.

In the third chapter, the performed lab tests are described. First, the set up and the used sand and wood samples are described in detail. The degree of degradation of the old wood sample is described based on drill resistance measurements, microscopy images and water content data. Next the results of the different tests will be shown and interpreted, which will be followed by conclusions and interpretations. Lastly, recommendations for further research will be given.

Chapter four will focus on the Monte Carlo analysis. The first part will describe the input of the analysis; the two locations and the parameter distributions. Next a short recap will be given on how the various calculations are performed, after which the results will be given. Firstly the results of the first location will be given in detail, then the differences between locations 1 and 2 will be described. After this, the effect of bacterial degradation will be described. Lastly, the conclusions will be drawn and recommendations will be made. The last chapter summarizes the conclusions and recommendations from this thesis.

2

Literature

In this chapter the literature that is relevant for the rest of the thesis will be presented. First, some general background information is given on the geology of Amsterdam; the soil profile and its variations will be described. Next, subsections 2.2 to 2.4 will provide the background for the lab tests of chapter three. These subsections include the theory behind direct shear testing, wood structure and bacterial degradation. The last subsections are relevant for chapter four; the Monte Carlo analysis. First, the calculation method for geotechnical bearing capacity of a foundation pile is explained, the next section reports on the history of pile foundations and presents two data sets which are used as input for the Monte Carlo analysis. Lastly, the current method for assessing timber pile foundations is mentioned, as well as the assumptions that have been adopted regarding pile dimensions and bearing capacities.

2.1. Geology

Old timber piles in Amsterdam are mainly founded in the first sand layer. This layer was used as the main foundation layer from the 16^{th} century until the start of the 20^{th} century. Later, heavier buildings and better piling installations led to foundations being placed in the second or even third sand layer. Since old timber piles are considered, the geology and geohydrology from the first sand layer and upwards will be discussed.

2.1.1. General Soil Profile

The first sand layer in Amsterdam was deposited during the last ice age, the Weichselien, at the end of the Pleistocene. Although the ice did not reach the Netherlands it had an important effect on the depositional climate. The sea level during that time was 110 meters lower than it currently is. This dry climate led to sands being deposited mainly by wind, leading to the first sand layer consisting of fine aeolian sands (Boxtel formation) (Keijer (2015)).

The Holocene is the current geological period which started around 10.000 years ago. The ending of the Pleistocene and thus the melting of the glaciers meant a quick rise in the sea water level occurred. Due to several fluctuations in the sea water level, the Holocene layers consist of continental as well as marine deposits. In Amsterdam, the Holocene deposits mainly consist of clay, although in some areas a thin sand layer, known as 'wadsand', is located at a depth of between 7 and 9 meters under NAP. Timber houses from the middle ages were founded in this layer. Later, this layer was also used as a foundation layer by poor people who could not afford long piles which could reach into the first sand layer (Gans (2011)).

Usually a thin layer of peat covers the first sand layer, this layer belongs to the Nieuwkoop formation and is also known as 'basisveen'. This layer was formed during a regressive period, when the sea level was lower and vegetation got a chance to grow, the layer varies in thickness throughout Amsterdam between 1 meter and 10 cm. A transgressive period followed and the peat deposits were covered by marine clays. Due to the start of formation of coastal barriers, the next layer consists of tidal deposits. The Naaldwijk formation typically consists of layers of clay, silt and sand. On top of this formation is another peat layer, known as Hollandveen, which also belongs to the Nieuwkoop formation and ranges between 1 and 3 meters in thickness. The top layer is a manmade fill, made up of sand and rubble (Gans (2011)). Table 2.1 and figure 2.1 give an overview of the general Amsterdam soil profile.

Soil type	Formation	Top [m NAP]	Bottom [m NAP]
Sand fill	Man made	Greenfield	-1.5
Peat (Hollandveen)	Nieuwkoop Formation	-1.5	-5
Clay	Naaldwijk Formation	-5	-7
Sand (Wadsand)	Naaldwijk Formation	-7	-9
Clay	Naaldwijk Formation	-9	-12
Peat (Basisveen)	Nieuwkoop Formation	-12	-12.5
Sand (First Sand layer)	Boxtel Formation	-12.5	-15

Table 2.1: General Soil Profile in Amsterdam

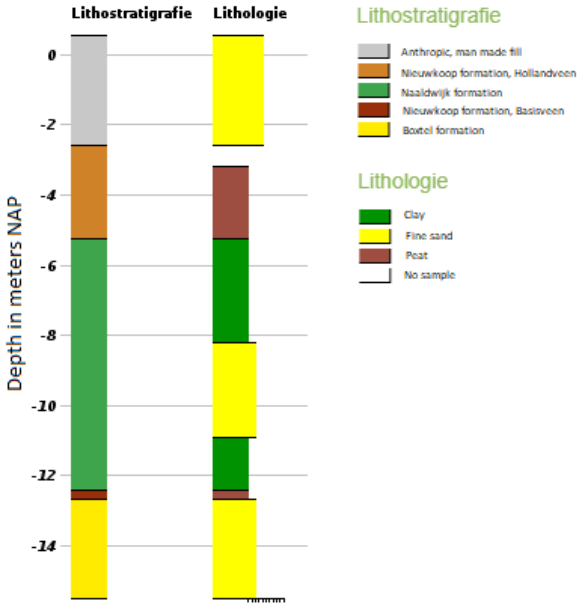

Figure 2.1: Boring of the typical Amsterdam soil profile, after *DINOloket* (2019a)

.

2.1.2. Variation in Soil Profile

Obviously the soil profile is not constant throughout Amsterdam; ancient river activity and the city's many expansions over the years have left their mark in the subsoil. The variation in the most important layers with regard to the geotechnical bearing capacity will be discussed here.

There are two rivers which have had an influence on the subsurface of Amsterdam. Currently, the river Amstel flows through the city, over the years this river has cut several meters into the top layers, about 8 to 9 meters. Along the track of the river (figure 2.2), the top peat layer and part of the clay have been eroded and river clay and sand have been deposited. This variation is only expected to influence the shaft resistance since the first sand layer was not affected.

Figure 2.2: Track of the river Amstel through the city centre with locations of flood planes, after Gans (2011)

.

About 6000 years ago the river IJ was a tidal zone which stretched from the North sea to what is currently the Ijselmeer. With the quick rise of the sea level 5000 years ago, sand was deposited along the North sea coast, closing off the tidal channel. This caused marshlands to be formed behind the coastline, forming the thick layer of peat. The tidal channel has cut deeply into the first, and sometimes even the second, sand layer. A former side-channel of the river IJ is located below the centre of Amsterdam, this has caused the first sand layer to be eroded partly in some areas (Gans (2011)). The variation in depth of the top of the first layer, and the approximate location of the IJ's side channel, is shown in figure 2.3a.

Since Amsterdam was basically a peaty marshland it has always been necessary to apply a fill of sand in order to be able to built and live there properly. The thickness of the sand fill varies significantly, between one and six meters. The downside of applying a thick layer of sand is that the soft peat and clay layers are prone to settlements. Due to high costs and settlements, the thickness of the sand fill was kept as low as possible, especially during the later city expansions (Gans (2011)).

Besides the thickness, the age of the sand fill also varies highly. The sand fills in the historic centre can date back to the 16^{th} century, whereas the outermost districts, such as the Bijlmermeer, were not constructed until 1977. The age of the fill, in combination with its weight have a big influence on the amount of settlement that has already, and is still going to occur. One can assume that in the historic city centre, most of the settlement have already occurred, while in the outer district the greenfield is still settling under the load of the sand fill.

With regard to the geotechnical bearing capacity, this is an important factor to consider when determining the amount of negative skin friction that has already, and is still going to, occur.

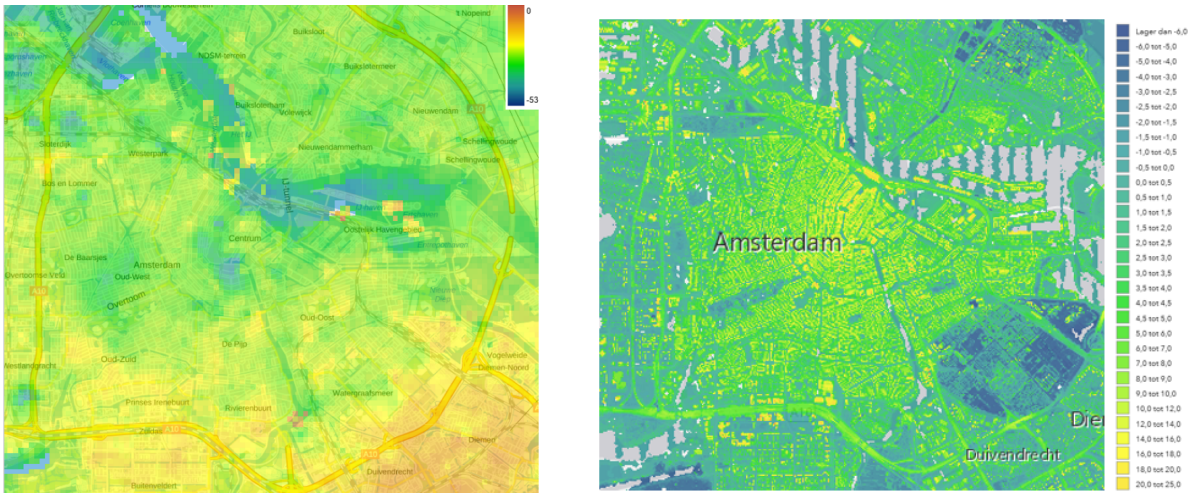

(a) Depth of 1st sand layer (DINO, 2019)

(b) Height of greenfield (AHN, 2019)

Figure 2.3: Variations in soil profile

The height of the greenfield does not vary much throughout the city. Most of the city and its districts have greenfields at between 0.5 and 2 meters above NAP. Some exceptions are the several parks in the city, the Vondelpark, for example, is located at -1 to -2 meters NAP. This is because no sand fill has been placed in the parks. Another area which stands out is part of the Watergraafsmeer, which has its greenfield at between -2 and -5 meters NAP. The reason for this is that the area is a former lake which was drained during the 17^{th} century. In this area the top peat layer is absent and the clay layer lies directly below the sand fill (Gans (2011)). Figure 2.3b shows the heights of greenfield throughout Amsterdam.

2.1.3. Hydrology

Due to these large differences in the height of the greenfield, the ground water table also varies throughout the city, as is shown in figure 2.4. To be able to control the ground water table in all these areas the city has over 40 polders with their own regulation system. The local water authority, Waternet, aims to keep the ground water stable, however, the water level can fluctuate due to for example rainfall, seasonal influences and construction works which require a lowered ground water table. The average ground water table in the centre is usually at -0.4 meters NAP, but is lower in the areas where the greenfield is lower.

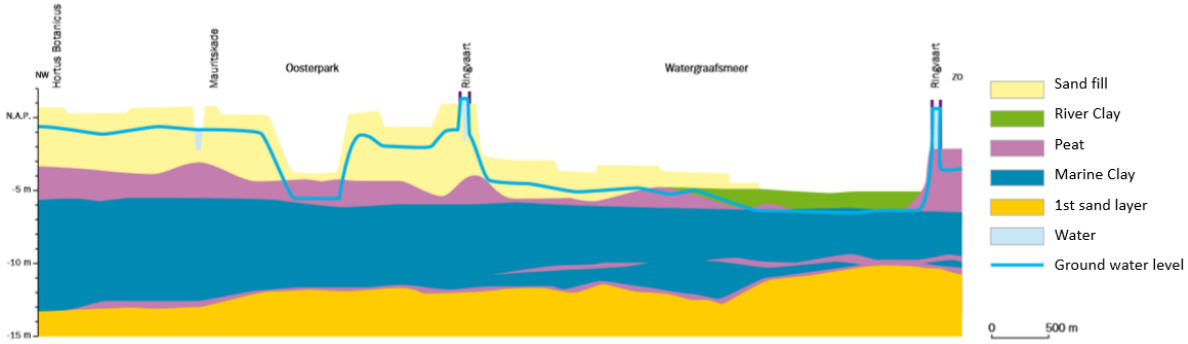

Figure 2.4: Groundwater table in Cross section through Amsterdam, after (Gans, 2011)

Besides the phreatic ground water there is also groundwater present in other soil layers. Both the wad sand layer and the first sand layer are aquifers which have their own hydraulic head. Figure 2.5 shows that the hydraulic head in the wadsand layer follows the phreatic ground water, although the head is slightly lower. This is quite remarkable as the top sand layer and the wadsand layer are separated by 5 meters of clay on this location.

Separating the wadsand from the first sand layer is a 2.5 meters thick clay layer. The hydraulic head in the first sand layer is independent of the conditions on the surface level. The water in this layer is brackish.

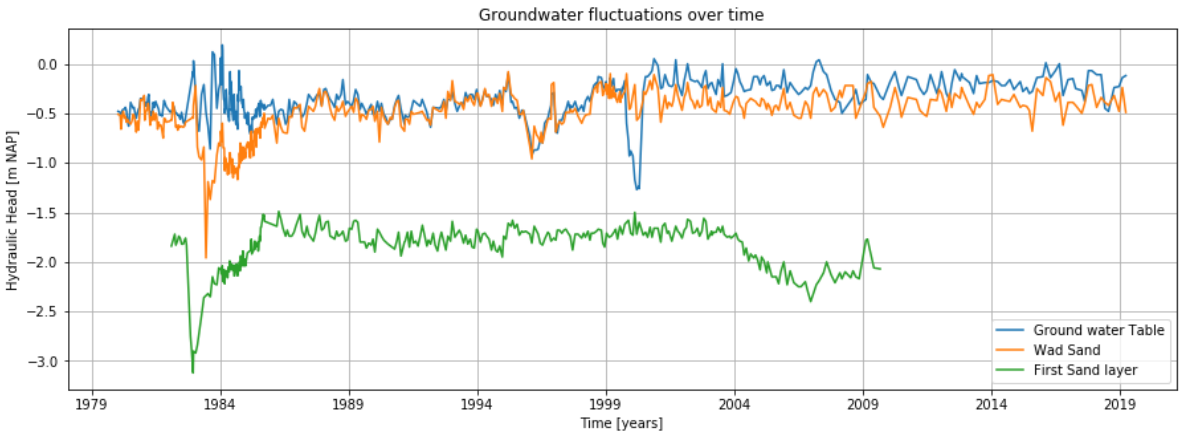

Figure 2.5: Groundwater fluctuations over 40 years of the three water bearing layers, data from Waternet, location is near Waterloo plein

The difference in head between the first sand layer and the other two layers entails that if the intermediate clay layer is interrupted, water will flow into the first sand layer. Consequently, the water tables in the two upper layers will drop. For this reason, one must always be careful when extracting piles from this layer, or performing other works that might cause an interruption of the clay layer.

2.2. Direct Shear tests

Direct shear tests are often used in geotechnics for the determination of the shear strength characteristics, ϕ and c, of soils. During the tests, two parts of a soil specimen are made to slide relative to each other under an applied normal load.

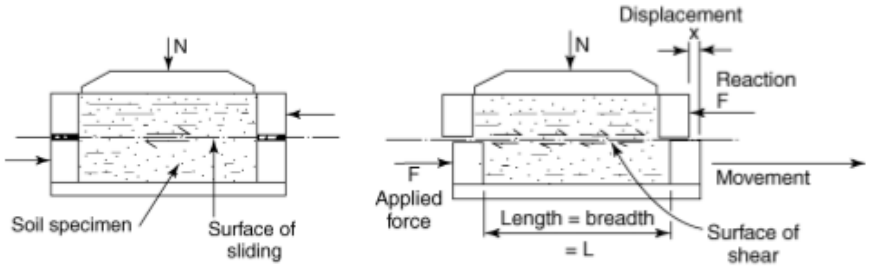

(a) Shear box at start of test (b) Shear box during test

Figure 2.6: Direct Shear Test, from Head (1992)

The test is performed using a direct shear box (figure 2.6), this is a simple apparatus which consists of a square or circular container where the upper half can move relative to the lower half. The test can be either stress-controlled or strain-controlled. Usually this test is strain-controlled: a constant displacement is applied and the reaction force is measured. During the test the shear stress in the sample steadily increases until the maximum shear stress, τ_f, is reached. Following this peak, the shear stress reduces until it reaches the residual shear strength, τ_{res}, at which it remains constant. A typical shear stress-displacement curve for a dense and a loose sample is shown in figure 2.8 a.

2.2.1. Determining friction angle

When this test is performed several times at different normal loads, plotting τ_f against the respective σ_n will result in a straight line. The value of τ_f at the interception of this line and the y-axis equals the soils cohesion and the inclination of the line is equal to the peak friction angle (figure 2.7). If τ_{res} is plotted against σ_n, the residual, or constant volume friction angle, ϕ_{cv} is found. The constant volume friction angle can be several degrees lower than the peak friction angle.

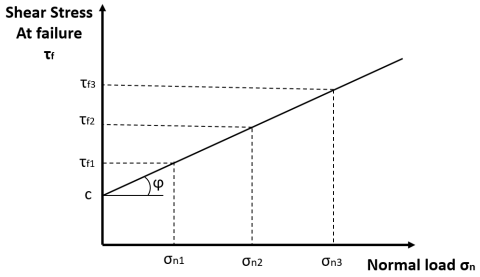

Figure 2.7: Determination of ϕ and c using data of 3 direct shear tests

The determination of the friction angle from this test is based on the Mohr-Coulomb failure criteria, which states that:

$$\tau_f = c + \sigma_n \tan\phi \quad (2.1)$$

where:
$\tau_f = F_{max}$ / Area
σ_n= N / Area
c = Cohesion [kPa]
ϕ = Friction angle of the soil [°]

2.2.2. Influence of Density

The density of the sheared sample has a lot of influence on the observed behaviour during a test. When grains are packed densely, they tend to ride up and over each other when sheared, leading to dilative soil behaviour and an increase in volume. This can be observed during the test as an upward vertical displacement of the top part of the shear box. Similarly, when grains are packed loosely, shearing will cause them to collapse into the open voids, leading to a decrease in volume, as shown in figure 2.8 b and c.

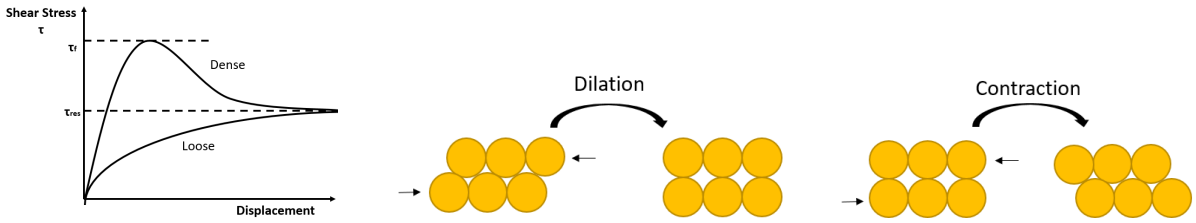

(a) Shear Stress-displacement Curve (b) Dense soil (c) Loose soil

Figure 2.8: Behaviour of sheared soils with different states of packing

As can be imagined it takes a larger force to shear a dense sample to failure compared to a loose sample. This can be seen in the test as a peak in the shear stress - displacement curve. When the test is performed on a loose sample, the peak strength is not reached and the sample immediately goes to the residual strength (figure 2.8 c). The residual strength is independent of the density of the sample and can always be measured to determine the constant volume friction angle ϕ_{cv}. But in order to find the peak friction angle ϕ_p, all tests must be performed at the same density.

2.2.3. Interface Friction

Using shear box tests it is also possible to determine the interface friction properties between a soil and a material. However, since the shear plane in a shear box is very thin, this can only be done on the condition that the tested material has a flat surface. Determining skin friction using direct shear tests is usually done by placing the material in the lower half of the shear box, while the upper half of the box is filled with the soil. In this case the results of the test is not the friction angle of the soil, ϕ, but the interface friction angle, δ. This value is usually presented as a ratio of ϕ.

Potyondy (1961) has done an extensive study on the interface friction between blocks of several construction materials (steel, concrete and wood) and various soils. He found that the four main components which determine skin friction are; the moisture content, the roughness of the surface, the composition on soil and the intensity of normal load. For wood specifically he found that at high normal loads the interface friction increased, probably due to the grains being indented into the soft wood fibres. It is not mentioned what loads are defined as 'high', but highest load that is reported in the paper is equal to 143.6 kPa. Valsangkar and Holm (1997), also reports observations of indentation of particles into the wood specimen. Based on the test results, several coefficients of skin friction are proposed, which are shown in table 2.2. The value for the interface friction angle between wood and soil as used in the NEN 9777-1 is equal to $\delta = \frac{3}{4} \times \phi$.

Soil Type		Factor	
Sand (0.06 < D < 2.0 mm)	Dry , Medium Dense	f_ϕ	0.76
	Saturated, Dense	f_ϕ	0.85
Cohesionless silt (0.002 < D < 0.06 mm)	Dry , Dense	f_ϕ	0.92
	Saturated, Loose	f_ϕ	0.55
	Saturated, Dense	f_ϕ	0.87
Cohesive granular soil (50% Clay + 50% Sand)	Consistency Index 1.0 - 0.5	f_ϕ	0.80
		f_c	0.20
Clay (D<0.06 mm)	Consistency Index 1.0 - 0.73	f_ϕ	0.60
		f_c	0.40
		$f_{c,max}$	0.85

Table 2.2: Skin friction factors for wood (parallel to the to grain) for different soil types, as proposed by Potyondy (1961)
$f_\phi = \delta/\phi$, $f_c = c_a/c$, $f_{c,max} = c_{a,max}/c_{max}$

2.3. Wood Degradation

The main downside of using wood as a construction material is that the material degrades over time, causing it to lose part of its strength. Biological wood degradation can be caused in two ways: degradation due to fungi and degradation due to bacteria. Fungal decay can only occur if the wood is (occasionally) above the groundwater table, as fungi need oxygen for the degrading process. Fungal decay is often the major cause of degradation on the pile head. When the pile was driven the head was below the groundwater table, but (temporarily) lowering it and seasonal changes may have left it dry for some periods. Bacterial decay occurs over the full length of the pile because bacteria can survive in much lower oxygen concentrations, sometimes even in anaerobic conditions (R. Klaassen, den Nijs, and van Beusekom (2000)). In bridges, fungal decay often does not play a role, as the foundation piles are fully submerged. For that reason, the bacterial component is expected to play the largest role in reduction of the geotechnical bearing capacity, as most of the length of the pile is under the groundwater table. For these reasons, bacterial degradation will be the type of degradation that is studied in this thesis.

2.3.1. Wood Structure

In general, there are two types of wood; coniferous and deciduous wood. This thesis will focus only on coniferous wood because most of the timber piles used in Amsterdam are from coniferous wood species. Since wood is a natural material, its characteristics are not isotropic. The strength is higher in some areas compared to others and can differ with the loading direction. Figure 2.9a shows the different parts in the cross section of a timber pile. Firstly, a distinction is made based on the age of the wood. Juvenile wood, the innermost 10 to 15 rings, is the youngest part of the tree and has a much lower strength compared to the mature wood. Another important distinction can be made between heartwood and sapwood. The sapwood is the outer most shell of the cross section, this is where the sap streams occurred in the living tree. Consequently, this part of the wood has a more open structure, which is more susceptible to bacterial degradation. The heartwood part of the cross section did not contain any living cells anymore and due to the presence of certain chemicals it is somewhat protected from degradation. Especially in wood species like pine there is a large difference in susceptibility to degradation between heartwood and sapwood (R. Klaassen et al. (2000)).

(a) Cross Section Timber, from Schreurs (2017)

(b) Properties over Length of Pile, after Lantinga (2015)

Figure 2.9: Macro structure of wood

Besides the differences in the cross section, the differences in wood strength also play a role over the length of the pile. Figure 2.9b shows the development of the different zones over the length of the tree. It shows that the thickness of the sapwood and the juvenile wood remains constant over the length, resulting in a combination of juvenile wood and sapwood at the top of the tree. When the tree is used as foundation pile it is flipped: the top of the tree becomes the tip of the pile. Therefore, this relatively weak part which is quite susceptible to degradation becomes the part of the pile where most of the bearing capacity is mobilized. The degree in which this plays a role depends on the length of the tree compared to the length of the pile, in other words; how much of the tip was removed before installation.

The microstructure of coniferous wood is shown in figure 2.10. The structure is mostly made up of tracheids, these long strands are in contact with each other by pits. Pits are tiny openings in the cell wall which allow water to move from one cell to another. For water transport in the radial direction, pits are also present at the intersection between rays and tracheids, these pits are called cross-field pits.

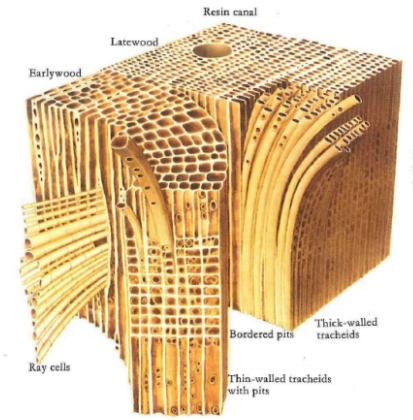

Figure 2.10: Microstructure of soft wood, from Gard (2019).

The shape of these cross-field pits are different for various wood species and thus provides a good way to identify the species of wood. Figure 2.11 shows the shape and names of several types of cross field pits. The types that can be expected when studying foundation piles in Amsterdam are the Windowlike, the Peceoid and the Taxodioid. Taxodoid are typical for firs (*Abies*) and piceoid crossfield pits are found in spruce (*Picae*). Pines (*Pinus*) can have either windowlike or pinoid cross field pits, depending on the specific species. The species of pine that is used as foundation pile is the *Pinus Sylvestris*, which has windowlike crossfield pits (Ilvessalo-Pfäffli (1995)).

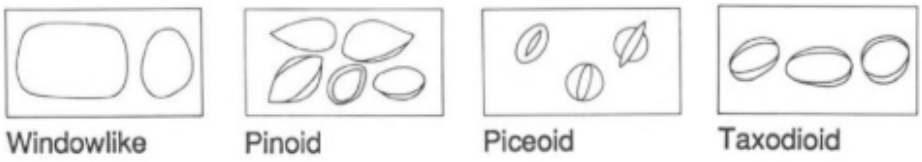

Figure 2.11: Shapes of cross field pits of soft wood species, after Ilvessalo-Pfäffli (1995)

On a much smaller scale, the wood's cell walls are built up of three components; lignine, cellulose and hemicellulose. These work together similar to the components of a concrete beam; the cellulose strings act as the reinforcement, taking up tensile forces. The lignine provides the timber with compressive strength, like the mortar in concrete. Similarly to cement, hemicellulose binds the other two together (R. Klaassen et al. (2000)).

2.3.2. Bacterial Degradation

The main types of bacteria that are responsible for wood decay are the Tunneling Bacteria (TB) and the Erosion Bacteria (EB). The speed at which the EB can break down the wood is lower than that of TB, but EB is better resistant to extreme conditions. It can survive in lower oxygen concentrations and at higher temperatures. Both bacteria mainly break down the cellulose and hemicellulose in the cell wall. The break down of the lignin is not possible without the presence of oxygen (R. Klaassen et al. (2000)).

Bacterial degradation is often limited to the sapwood part of the cross section. This is because the structure in this area is more open and allows bacteria to enter the wood more easily. This often results in a "soft shell" of deteriorated wood around the perimeter of the pile.

The ease with which bacteria can affect the wood, and therefore the speed, is highly dependent on the wood species. Pine sapwood has a more open structure compared to the sapwood of spruce, therefore pinewood is more prone to severe degradation. Also, sapwood of pine is usually thicker than that of Spruce (R. Klaassen et al. (2000)).

Not only wood species has an influence on the speed and amount of degradation, the soil conditions also play a major role. R. Klaassen et al. (2000) describes that degradation in peat and clay layers is less than in sand layers. This has to do with the amount water, and therefore the amount of oxygen, flowing past the pile.

Another factor that is mainly present in peat, is that all the oxygen that enter the layer is immediately used for the oxidation process of the organic material, leaving little for the degradation process.

Another theory is that oxygen is transported through the pile by a flow of water from the top to the tip of the pile. Such a water flow makes sense in the case of Amsterdam as there is a large difference in hydraulic head of the phreatic water and the water in the first sand layer, as discussed in paragraph 2.1.3. Since water travels through the path of least resistance this flow could occur if the permeability of the piles is higher than that of the separating soil layers.

Lantinga (2015) investigated the effect of wood degradation on engineering properties of wood. She found that the more degraded the wood, the lower the E-modulus and strength of the wood became.

2.3.3. Effect of Bacterial Degradation on Geotechnical Bearing Capacity

It is currently assumed that bacterial degradation of the wood has no effect on the geotechnical bearing capacity of the pile. This is, however, contradicted by tests performed in the Dapperbuurt in 1974, where it was found that the shaft friction of old piles was potentially 40 percent lower compared to new timber piles (Korff (2013)).

One theory which explains this is a reduction of the friction coefficient between the pile and the soil. This could be caused by a slime layer surrounding the wood (Lantinga (2015)). It is known that wood degrading bacteria produce a layer of slime (R. K. Klaassen (2008)), but it has never been investigated whether this may have an effect on the friction between the pile and the soil.

2.4. Bacterial Slime

The bacterial substance that might be responsible for the decrease in a pile's shaft capacity is actually called the biofilm. This is the habitat of a colony of multiple species of bacteria. The main components of this habitat, which is responsible for its three dimensional slimy structure, are extracellular ploymeric substances (EPS). These subtances are excreted by the bacteria inside the biofilm and are mainly made up of polysaccharides, proteins, lipids, DNA and other humic substances. The first phase of biofilm formation is the adhesion of a single cell to a surface. The bateria starts dividing and forms a micro colony. The bacteria start excreting EPS and the biofilm starts to form. As the biofilm matures, other species of bacteria can enter the EPS matrix Flemming (2011). This proces is shown in figure 2.12.

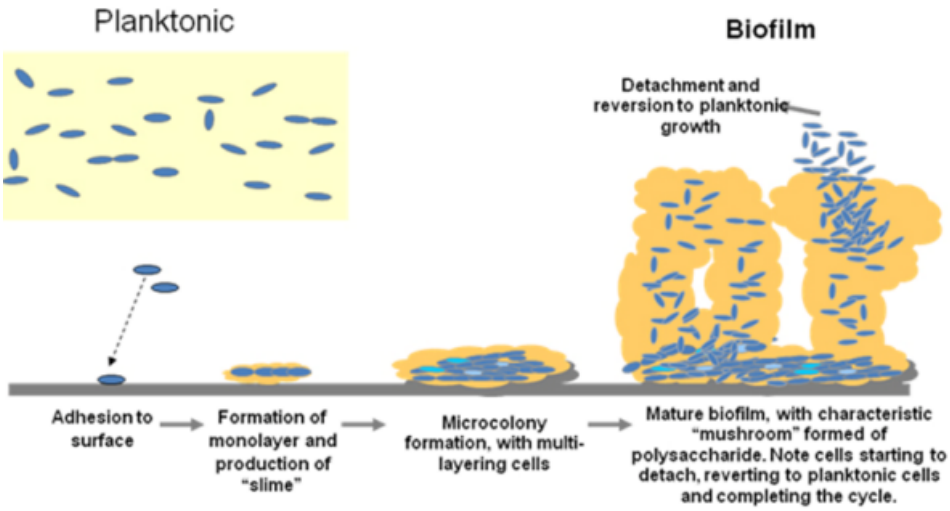

Figure 2.12: Biofilm Development, from Vasudevan (2014).

2.4.1. Components and Functions

In this section the general components of the EPS and their functions are described. It is good to keep in mind the the specific built up of EPS varies with varying bacteria in the biofilm. Each species of bacteria produces their own specific EPS, subsequently, in a mixed species colony the biofilm components can even vary locally (Flemming (2011)). Other factors, such as environmental conditions and the age of the biofilm can also influence the quantity and composition of EPS (Pan, Zhu, Chen, Qiu, and Wang (2016)).

An important function of the biofilm is the adhesion to the (solid) substratum; both in the initial phase, where a single bacterium adheres to the surface, and later when the entire biofilm is attached to the substrate. EPS is also responsible for the structural aspect of the biofilm, it forms the matrix in which the bacteria exist. Biofilm also functions as a protective barrier from substances which can harm the population of bacteria. It can absorp nutrients from its environments, which can subsequently serve as a source of nutrition for the population. Proteins in the EPS are even able to digest molecules inside the biofilm to provide the population with nutrients (Flemming (2011)).

According to Pan et al. (2016) proteins and polysacchardes make up 40 to 95% of the EPS. These two substances are also mainly responsible for the adhesive and cohesive properties of biofilm.

2.4.2. Frictional Properties of EPS

It is expected that the cohesive and adhesive properties of the biofilm are the most likely to have an influence on the frictional properties of the slime. It is generally agreed upon that the biofilms behave visco-elastically (Flemming (2011)). This is probably due to the presence of polysaccharides, which exhibit shear thinning, or pseudoplastic behaviour: their viscocity decreases as the shear strain increases. Research into the mechanical properties of biofilm is increasing and methods are being developed to determine the viscoelastic properties of the fluid (Klapper, Rupp, Cargo, Purvedorj, and Stoodley (2002), Towler and Paul (2003)).

Since the use of actual biofilms for tests is complicated, an analog is often used to approach the behaviour of EPS. This makes it possible to obtain similar behaviour during each tests. A common substitute for EPS are mass produces polysaccharides such as Xanthan and Dextran (Rosenzweig, Shavit, and Furman (2012),

Chenu (1993)). These polysaccharides are produced by bacteria and often used in the food and lotion industry because of their visco-elastic behaviour. This widespread use of polysaccharides makes them cheap and readily available for EPS imitation during tests.

Interestingly, xanthan and other biopolymers are also being investigated as a possible alternative for soil improvement methods (Chang, Im, Prasidhi, and Cho (2015)). Cabalar and Canakci (2011) found that the friction angle increased for a sand mixture with a xanthan gum content of 3 and 5%, while it decreased drastically (60%) with a xanthan content of 1%.

2.5. Geotechnical Bearing capacity

The geotechnical bearing capacity of a single pile in axial compression is the sum of the maximum base resistance and the maximum shaft friction, since shaft friction can work either positive or negative, the total bearing capacity of a pile becomes: $R_{total} = R_{base} + R_{shaft,\,pos} - F_{shaft,\,neg}$

Base capacity

The base resistance, R_{base}, of a foundation pile is determined based on CPT measurements using the Koppejan method.

$$R_{base} = A_b \times q_{b,max} \tag{2.2}$$

where:

$$q_{b,max} = \frac{1}{2} \times \alpha_p \times \beta \times s \times \left(\frac{q_{c,I,gem} + q_{c,II,gem}}{2} + q_{c,III,gem}\right) \tag{2.3}$$

R_{base} = The resistance of the pile tip [kN]
A_b = The area of the pile tip [m^2].
α_p = Factor for pile tip capacity, equals 0.7 for timber piles according to NEN 9777-1 (Normcommissie 351 006 "Geotechniek" (2016)). According to NEN 8707 (Normcommissie 351 006 "Geotechniek" (2018)) 1.0 may be used when assessing existing structures on the disapproval level or when assessing it for reconstruction if the increase of load on the structure does not exceed 15%.
β, s = Factors for the shape of the pile tip, both equal 1 for round pile tips according to NEN 9777-1.
$q_{c,I,gem}$,$q_{c,II,gem}$,$q_{c,III,gem}$ = Averages of the cone resistance 8D above and 0.7 to 4D below the pile tip

Figure 2.13 gives an example of how $q_{c,i,gem}$ can be determined from a CPT. A zone 4*D_{tip} below and 8*D_{tip} above the pile tip is defined. Going from the bottom upwards, the q_c values of the CPT are cut off at their lowest value, as shown in figure 2.13a with the black lin. $q_{c,I,gem}$, is the lowest average value of the zone between the pile tip and 0.7D to 4D below the pile tip, not taking into account the cut off q_c value.

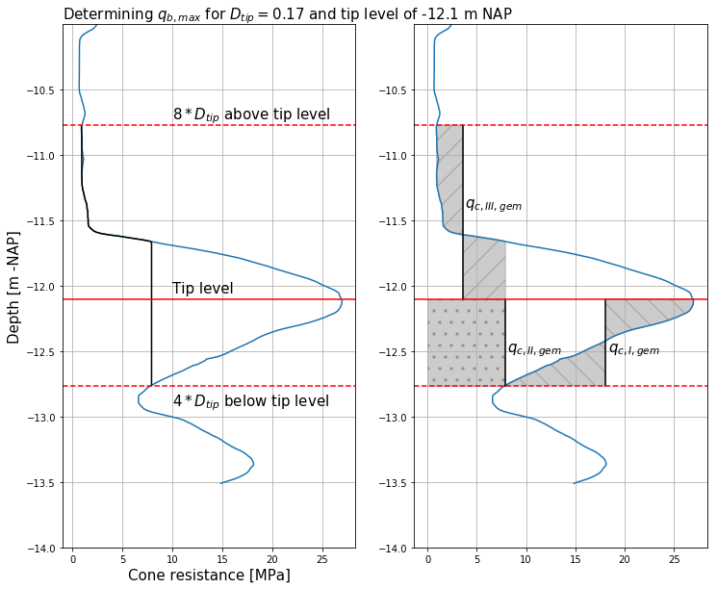

Figure 2.13: Determining $q_{b,max}$ based using Koppejan method

In figure 2.13 b $q_{c,I,gem}$ is shown, the areas of the CPT indicated by the '\\' hatch are of equal area. $q_{c,II,gem}$ is the average of the area below the pile tip, this time taking into account the cut off q_c values.

$q_{c,I,gem}$ and $q_{c,II,gem}$ must be taken at a range of at least 0.7*D_{tip} to at most 4*D_{tip} below the pile tip. The range that has to be taken is the one that results in the lowest values for $q_{c,I,gem}$ and $q_{c,II,gem}$. in the case

of figure 2.13b this range extends all the way to 4*D_{tip} below the pile tip, because this results in the lowest average q_c values.

$q_{c,III,gem}$ is the average q_c value 8*D_{tip} above the pile tip, where the equal areas left and right of q_c are shown by the '//' hatch in figure 2.13b.

The final value of $q_{b,max}$ must be cut off at a value of 15 MPa. In Amsterdam the quality of the bearing sand layer is a assessed using table 2.3 (Gemeente Amsterdam, Afdeling ruimtelijk beleid (2009)).

$q_{b,max}$ / 15	Quality
0.8 - 1.0	Excellent
0.6 - 0.8	Good
0.4 - 0.6	Reasonable
0.2 - 0.4	Mediocre
0.0 - 0.2	Bad

Table 2.3: Assessment of bearing layer based on the value of $q_{b,max}$/15 MPa determined based on a reference D_{tip} of 0.13 meters and an embedment of 0.5 meters into the bearing layer, from Gemeente Amsterdam, Afdeling ruimtelijk beleid (2009).

Shaft friction

The shaft friction can be calculated in two ways: by using a CPT based method and by using the slip method. The CPT method is often used for positive shaft friction in the bearing sand friction, while the slip method is mostly used for calculating negative skin friction in soft soil layers. They can however both be used for both purposes. Important to take into account is that the CPT method tends to overestimate shaft friction in shallow layers, while the slip method tends to do the same for deep layers, due to high effective stresses (van Tol (2006)). Calculating the shaft friction with the CPT method is done by using equation 2.4.

$$R_{shaft} = O_p \times \int_{\Delta L} p_{max,shaft} dz \tag{2.4}$$

and:

$$p_{max,shaft} = q_c \times \alpha_s \tag{2.5}$$

where:
R_{shaft} = The resistance of the pile shaft [kN].
O_p = The circumference of the pile shaft [m].
ΔL= The length over which skin friction can be generated [m].
q_c = The value of the cone tip resistance where all values must be cut off at 12 MPa, unless the thickness of the layer with cone resistance exceeding 12 MPa has a thickness of more than 1 meter. In that case the cone tip resistance must be cut off at the value which occurs over the thickness of 1 meter, with a maximum of 15 MPa.
α_s= A correction factor for the installation method and the friction between the soil and the shaft [-].

This factor depends on the soil type; values for α_s according to NEN 9777-1 are shown in table 2.4. The α_s factor for clay depends on the cone resistance in the clay layer. The value shown in the table is the α_s for clays with a cone resistance which is lower than 2 MPa, which is the case for all Holocene clay layers in Amsterdam.

Soil type	α_s
Sand	0.012
Clay	0.02
Peat	0
Silty Sand	Friction number with a maximum value of 0.025

Table 2.4: α_s for different soil types, according to NEN 9777-1 (Normcommissie 351 006 "Geotechniek" (2016)).

The slip method is based on shear stress in the soil and is computed by equation 2.4 and 2.6

$$p_{max,shaft} = K_0 \times \tan\delta \times \sigma'_v \tag{2.6}$$

where:
K_0 = 1 - sin(ϕ)
$\delta = 0.75 \times \phi$ for timber piles.
σ'_v = Average vertical effective stress over the layer for which shaft friction is computed [MPa].

$K_0 \times \tan\delta$ must be at least 0.25. For values of ϕ of soils which are present in Amsterdam $K_0 \times \tan\delta$ is always smaller than 0.25 and thus 0.25 may be used.

2.5.1. Shaft Friction and Neutral Point

Friction on a pile shaft can provide either a positive or a negative contribution to the bearing capacity. Negative shaft friction occurs when soil around the pile settles more than the pile itself, soil will then drag the pile down with it, resulting in an extra load on the pile. Positive shaft friction is mobilized if the pile settles more than the soil surrounding it, soil will stick to the pile, resulting in an upward force. From this it follows that in regular situations, where the pile tip is not allowed to settle significantly, positive shaft friction is only mobilized in the bearing sand layer. Similarly, negative shaft friction only occurs in the overlying layers, which are subject to settlement. Settlement and subsequently, the development of negative skin friction can have several causes:

- Additional loads at greenfield level such as sand fills for construction or roads.
- Lowering of the ground water table.
- Consolidation due to self-weight of soil / creep.

The point in the pile where the relative displacement between the pile and the soil is zero is called the neutral- or, reversal- point, this is also the point where positive shaft friction turns into negative shaft friction. Moreover, the neutral point is where the axial forces in the pile are greatest, thus also the location of the critical cross section when it comes to assessing the wood strength. In the previously described situation, where significant settlements are not allowed, this point is located at the boundary between the soft layers and the bearing stratum.

In the case of old timber piles, however, significant settlements often do occur. This is because negative skin friction was not recognized as an additional load until 1950 which led to structural underestimations of the necessary capacities (NF3O/SBRCURnet (2016)). When the maximum of the total bearing capacity of a pile is reached the pile will settle, thereby mobilizing additional positive skin friction until an equilibrium state is reached where: $R_{base} + R_{shaft,pos} - F_{shaft,neg} - F_{load} = 0$. Any additional load will lead to settlement of the pile reducing negative skin friction and increasing positive skin friction, thereby moving the neutral level upward, until a new equilibrium is reached.

When assessing the structural strength of the wood, it is better if the neutral point is located as close to the pile head as possible, since this is where the area of the cross section of the pile is the largest. For the assessment of the geotechnical bearing capacity however, the best case is when the neutral point is located at the interface between the soft layers and the sand layer, because this indicates that no significant settlements have occurred yet and the total bearing capacity has not been exceeded. If the interface friction between the timber pile and the soil is affected by degradation, this will probably have an effect on both the positive and the negative skin friction.

2.6. Foundation Types

In general, two types of foundations can be distinguished; shallow foundations and foundations on piles. As the top layers in the western part of the Netherlands often consist of soft clay and peat layers, it is usually necessary to use piles which reach down to sand layers from the Pleistocene. This layer is usually at a depth of -13 meters NAP in Amsterdam.

Prior to the 17^{th} century it was not possible to reach such depths and friction piles were commonly used. From the 17^{th} century on wards set ups were used where up to 40 men were needed to lift a heavy weight which was dropped on the pile head, as shown in figure 2.14. This made it possible to drive piles deeper into the ground. This was done "on stop"; a weight of 250 to 300 kg was dropped on the pile head 30 times ("een tocht") and the settlement of the pile with respect to the greenfield, or to the water table, was measured (a calendar). The required settlement per calendar was determined beforehand, once this value was reached the pile had reached the required depth (ter Linde (1990)). This is similar to driving to refusal, except that driving to refusal indicates that the pile experiences no more settlements with additional hammer blows, this was not necessarily the case for Dutch foundations.

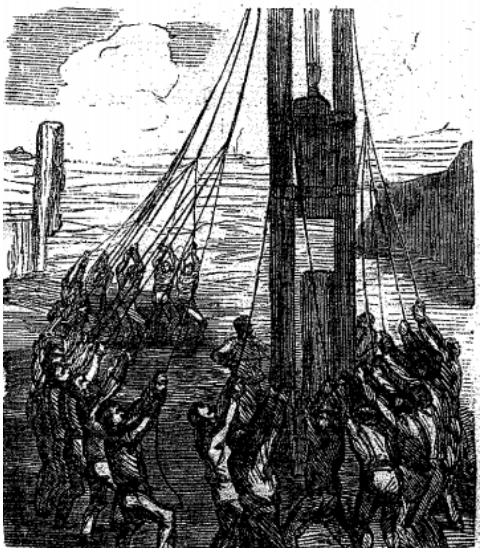

Figure 2.14: Driving piles in the 17^{th} century, from Wennekes and Grijp (2002).

It was soon realized that timber piles quickly degraded due to fungi when they were not continuously submerged. Therefore, a law was passed in 1638 that stated that pile heads had to be at least half a foot below the groundwater. Thanks to the inventions of concrete and diesel hammers in the 20^{th} century, it became possible to built higher structures with concrete foundation piles (Van der Stoel (2001)). Timber piles are still used today, especially for light weight structures and always in combination with an intermediate concrete segment to ensure the pile head remains below the groundwater table.

Generally three types of timber pile foundations are present in the Netherlands: the Amsterdam foundation, the Rotterdam foundation and a modern variety with a concrete segment as described above. The difference between the two other foundations is that the Amsterdam foundation consists of two piles with a crossbeam on top, while the Rotterdam foundation has a single pile and no crossbeam (figure 2.15). The Amsterdam foundation can mostly be found under houses and other buildings. In the case of bridges and quay walls, the piles are often placed directly under the floor of the structure.

2.6.1. Prior tests on piles in Amsterdam

For the North-South line project, several (new) timber piles have been loaded to investigate the settlement behaviour. Van der Stoel (2001) describes the tests performed on timber piles with diameters of 0.23 and 0.13 meters at the head and tip of the pile respectively. The theoretical bearing capacity here was 265 kN; 200 kN tip resistance and 65 kN shaft resistance. The test results ranged from 177 kN to 265 kN.

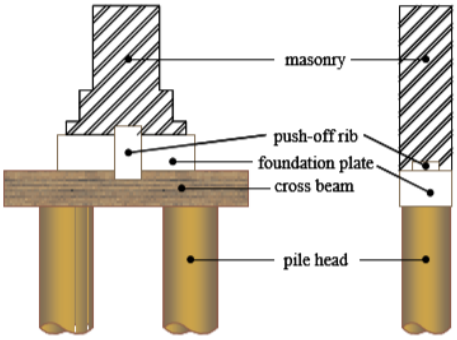

Figure 2.15: The Amsterdam foundation (left) and Rotterdam foundation (right) (Van der Stoel, 2001)

Dapperbuurt tests

In 1974 the Dapperbuurt tests were performed, this was a big testing program of the municipality of Amsterdam which had the aim of assessing the quality of the foundations in the Dapperbuurt. Two sets of tests were performed in this program (Hoekstra and Bokhoven (1974)).

Firstly, pile tests were performed on both old and new timber piles. Piles were loaded until failure in compression, then in tension and were pulled out afterwards. Since one of the new piles was installed with a casing until -11 meters NAP, it was possible to differentiate between the shaft friction in the sand layer and shaft friction in the Holocene layers. The ultimate bearing capacity for the new timber piles was 260-270 kN. Korff (2013) found that shaft friction was equal to 8.8 kN/m and 59 kN/m in the Holocene layers and in the sand layer in compression respectively. The base resistance was found to be equal to 90 - 100 kN. Comparison of the old and new piles showed that old piles had a shaft friction that was 40% lower than that of the new piles. No difference was observed between the base capacities.

Furthermore 37 piles all around the Dapperbuurt were loaded until failure in compression. Near all these tests, CPT measurements were done, which were used to accurately calculate the bearing capacity that the pile was supposed to have. Also, using the load that had been on the pile before the tests were done, the neutral point of all the piles was back calculated. This showed that there was big range in neutral points between all he piles that were tested. Some laying just above the bearing sand layer, while others were located just 1 to 3 meters below the pile head. The worst case was a pile of which the neutral point was located only 0.7 meters below the head of the pile.

Also, 1617 piles were extracted in total, of these piles the diameters at the head and the tip as well as their lengths were measured. This provides an important source of data on the dimensions of the timber piles in Amsterdam.

2.6.2. Dimensions of piles in Amsterdam

Extraction of old piles in Amsterdam was used to gain insight into the characteristic parameters of the timber piles in Amsterdam. In this analysis, two data sets have been used. Data set 1 is of the Dapperbuurt (*Dataset extracted piles Dapperbuurt* (2018)), which contains information on 1616 piles that were extracted in 1974 the eastern part of the historic centre. These piles were driven between 1876 and 1906, so had an age of 70 - 100 years. Data set 2 (*Dataset extracted piles Frans Sas* (2018)) contains information on 1110 piles, mostly from the southern district. These piles were driven from 1900 to around 1940 and were all extracted from under houses. The data sets contain information on the length of the piles, the diameter at the head and the diameter at the tip. From this data, the average tapering of the pile can be determined. Unfortunately the depth of pile head was not recorded in both data sets and it is therefore not possible to determine the embedment of piles in the sand layer.

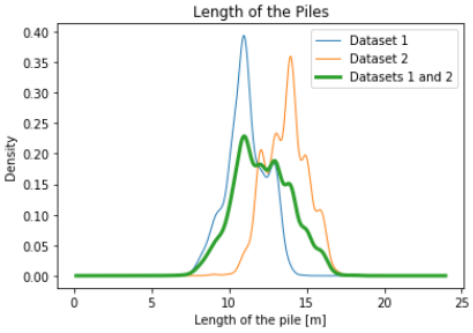

(a) Pile Lengths

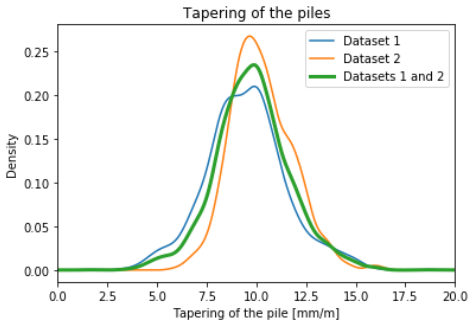

(b) Pile Tapering

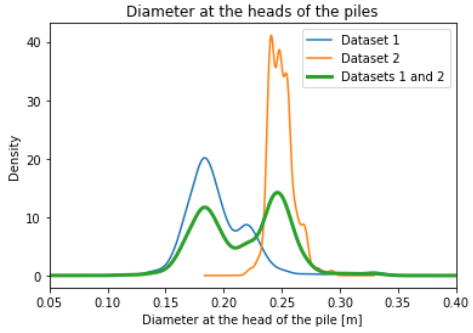

(c) Pile Head Diameters

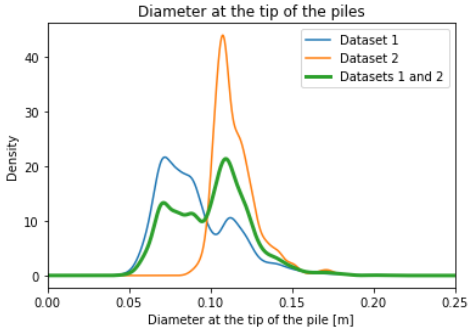

(d) Pile Tip Diameters

Figure 2.16: PDFs for pile characteristics based on two datasets *Dataset extracted piles Dapperbuurt* (2018) and *Dataset extracted piles Frans Sas* (2018).

These figures show that the data sets differ quite a lot in mean pile head and tip diameters and mean pile lengths, leading to bimodal distributions. This leads to believe that different pile types have been used in the two areas where the piles were extracted. ter Linde (1990) gives an overview of the available pile dimensions (table 2.5), the old pile types were often named after the city where they were typically used. Note that table 2.5 only shows the classification of piles that are relevant for this study; the classification continues until pile sizes with head diameters 0.32 meters, these larger piles were typically used for foundations in Rotterdam.

Classification	Diameter at 1 meter below the pile head [m]	Diameter at pile tip [m]	Length [m]
50/30	0.16 - 0.18	0.1 - 0.11	6 - 11
55/30	0.18 - 0.19	0.1 - 0.11	6 - 13
60/32	0.19 - 0.21	0.1 - 0.11	7 - 15
65/35	0.21 - 0.22	0.11 - 0.12	7 - 16
70/35	0.22 - 0.24	0.11 - 0.13	8 - 17
75/35	0.24 - 0.26	0.11 - 0.13	8 - 16
75/40	0.24 - 0.26	0.13 - 0.14	10 - 23

Table 2.5: Overview of available pile types according to NEN 3180-6.1.1.4, after ter Linde (1990)

The 70/35 types was known as the 'Amsterdam' size, so was probably the most used pile size in Amsterdam. This corresponds to the size of the piles that were extracted for data set 2. However, smaller pile diameters have been found on piles extracted from the Dapperbuurt, these sizes correspond better with the 50/30 size piles, which were known as 'Zaanse' sizes.

ter Linde (1990) describes several causes for uncertainty in pile dimensions. The required depth and dimensions of the piles were often determined beforehand and captured in the construction drawings. This, however, does not mean that these were also used by the construction crew; in case of lacking supervision, thinner piles were often used. Furthermore, since the piles were installed on stop, the necessary length of the pile was not known beforehand, the excess piece of pile was cut off after the pile had reached the required

depth. It was customary that this left over piece of wood would be given to the crew members, who therefore benefited from larger pieces of excess wood and thus smaller embedments in the bearing layer.

As mentioned previously, piles were usually driven 'on stop' into the first sand layer. The embedded length of the pile is a very important parameter for a pile's bearing capacity: the base capacity and the shaft friction in the sand layer are based on this parameter. Unfortunately. this is a parameter which is highly uncertain, it is currently assumed that the embedment of the pile is approximately 0.5 meters, with an uncertainty of 0.25 meters. This assumption is based on the given that piles were typically driven 2 calendars deep into the sand layer.

The definition of one calendar has however changed over the years. Previously, a calendar was equal to the additional settlement that a pile showed after 30 drops of a weight of 250 to 300 kg. Currently, one calendar is equal to the number of hammer drops that are needed for a settlement of 25 cm. So the assumed depth of 0.50 cm is probably based on the current definition of calendar. Using the old definition, 2 calendars does not correspond to a certain depth in the sand layer.

The types of wood that were most often used for timber piles are spruce (Dutch: vuren) and pine (Dutch: grenen). Sometimes firs (Dutch: Dennen) were also used, but not nearly as often as spruce and pine wood. Often, different types of wood can be found under a single bridge. Under several quay walls and bridges in Amsterdam, analysis of the state of the wood have been performed (*Database Amsterdam houtmonster analyse* (2018)). The piles under one bridge were often installed in different years and were made from different species. This allowed for an analyses of the degradation per wood species, the data set contains data of 257 spruce, 65 pine and 26 fir pile heads. Since the data is obtained from quay walls and bridges, it can be assumed that the pile heads have been submerged for their entire life span. Therefore degradation is most likely only due to bacteria.

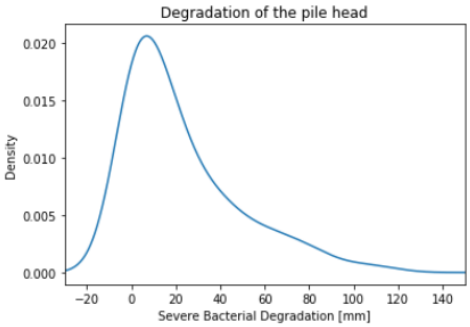

(a) Thickness of the soft shell due to bacterial degradation overall

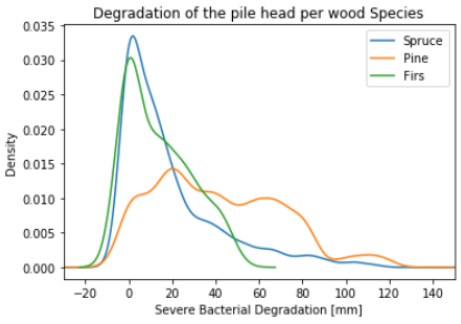

(b) Thickness of the soft shell due to bacterial degradation per wood Species

Figure 2.17: PDFs for wood degradation, after *Database Amsterdam houtmonster analyse* (2018)

Overall, the thickness of the soft shell is distributed log-normally, with the highest amount of pile heads showing no severe degradation. When the data is grouped per wood species, a different picture arises. Where spruce and firs are indeed log-normally distributed, but with a smaller standard deviation, and where pine wood appears to be a normally distributed. This shows that pine wood is more susceptible to bacterial degradation. For this reason pine wood piles have not been allowed to be used as foundation piles since at least 1983 (R. Klaassen et al. (2000)).

2.7. Current Assessment Method for Timber Pile Foundations

It is often hard to assess the remaining capacity of old timber piles. Mainly because most of them were constructed before extensive knowledge of geotechnics was present. Before 1950, the phenomena of negative skin friction had not been recognized as additional load on piles, which led to the structural underestimation of the necessary capacity. This underestimation leads to timber piles which often settle continuously. This is something that is hard to account for in the current calculation model. The fact that piles that were installed before 1950 have been placed on stop increases the amount of uncertainty and therefore the difficulty of assessing old piles (NF3O/SBRCURnet (2016)).

The code that is currently used in the Netherlands to assess the quality of timber pile foundations is the F3o guideline. The F3o assesses the piles bearing capacity on five aspects: the stability of the overall construction, the wood strength of the pile, cross beams and foundation plate and the geotechnical bearing capacity. In this thesis, only the geotechnical bearing capacity will be regarded. According to the F3o, the geotechnical bearing capacity can be determined in one of two ways. Method 1 is based on the proven strength of the foundation, this strength is determined based on the total settlement, settlement speed and the differences in settlement. The second method is based on the calculated bearing capacity according to NEN 9997-1. This method uses CPT measurements in addition to the total settlement. The focus in this thesis will only be on the method which uses CPT measurements.

Since the city of Amsterdam has quite a lot of structures which are founded on old timber piles, there is a set of assumption specifically for the city.

- The used tapering of all timber piles is equal to 8 mm/m (Gemeente Amsterdam, Afdeling ruimtelijk beleid (2009)).
- If the diameter at the head of the pile is unknown, a diameter of 0.25 meter may be assumed (Kalt and Dusseldorp (2018)).
- If the tip level is unknown it is assumed to be equal to 2 to 3 calenders (=0.5 - 0.75 m) into the bearing sand layer. In thinner sand layers the depth at which the bearing capacity is largest may be assumed (Gemeente Amsterdam, Afdeling ruimtelijk beleid (2009)).
- The length of the pile is based on the top of the sand layer as determined from CPTs and the embedment of 0.5 - 0.75 meters (Kalt and Dusseldorp (2018)).
- If the diameter at the tip of the pile is unknown, it may be calculated using the diameter at the head of the pile, the assumed tapering of 8 mm/m and the length of the pile (Gemeente Amsterdam, Afdeling ruimtelijk beleid (2009)).
- Bacterial degradation does not influence the geotechnical bearing capacity (Kalt and Dusseldorp (2018)).
- The geotechnical bearing capacity in the first sand layer can be assumed to be 100 kN per pile (Kalt and Dusseldorp (2018)).
- The bearing capacity is mostly made up of the pile's base capacity and only a limited contribution is provided by the shaft friction (Kalt and Dusseldorp (2018)).

Some of these assumptions regarding the pile parameters are not in accordance with those from the two datasets that are shown in figures 2.13 a through d. The tapering of the piles for instance is assumed to be 8 mm/m for all piles, while the mean value of the tapering in both datasets is around 10 mm/m. Using 8 mm/m instead of 10 mm/m results in larger values for the tip diameters, and thus in an overestimation of the bearing capacity.

The head diameter of 0.25 m that may be assumed is indeed found often in dataset 2 (reference), but the mean head diameter of dataset 1 equals 0.195 meters. This assumption also leads to overestimation of the pile. Luckily, pile head inspections are often performed so this assumption does not have to be used as often.

Calculating the tip diameter as a function of the diameter at the head and the tapering of 8 mm/m is a good approach. But when both these parameters are overestimated to begin with, the diameter at the tip of the pile will also be an overestimation of the true value.

Bacterial degradation is taken into account when determining the structural strength of the pile itself at the critical cross section. The thickness of the soft shell is then not included in the area of the cross section

that bears the load. In practice, something similar is sometimes done when assessing the geotechnical bearing capacity. A reduction in the piles effective diameter is then used in the calculation, so a reduced shaft capacity is found. This is however not described in any documents, nor does it make any physical sense, since the outer area of the pile does not reduce due to degradation. Therefore this reduction of the effective diameter is not used in this thesis.

3

Interface friction Tests

In order to determine the effect that wood degradation has on the interface friction properties, shear tests have to be performed. However, since the irregular shape of the pile sections does not allow the use of a regular direct shear box, an alternative test set up was constructed. In this chapter the test set-up will first be described. The different variations in tests and their purposes are mentioned. Next, the samples and the used soil will be described. Then, the tests results will be given and lastly the test results will be interpreted and recommendations will be made.

3.1. Tests

In order to properly identify the differences in friction between old and new piles several different variations have to be made, while certain parameters have to be kept constant. Based on the main question, three sub questions could be identified on which the different variations are based.

The first sub question is related to the influence of degraded wood structure on the shaft friction. For this purpose, tests are performed on both old and new samples. No slime is applied in these tests so only the effect of wood structure is studied.

The second sub question is based on the effect that the bacterial slime has on the shaft friction. To investigate this, wood samples are tested with and without a layer of slime. It was studied what could serve as a suitable imitation of the bacterial slime. As discussed in chapter 2, polysaccharides such as Xanthan gum are often used as a model slime in lab tests.

Lastly, the actual difference between old and new piles has to be studied. This will be done by comparing the results of old samples with slime, to new samples without slime. These results should be similar to the results found in the Dapperbuurt tests, where old and new piles have been loaded in tension and compression.

The tests will be performed using only one type of sand. Parameters of this sand such as the minimum and maximum void ratio and the grading curve have been studied using several other lab testing methods. The test will be displacement-controlled, meaning that a constant speed of displacement is applied and the resulting forces are measured. In this case the applied displacement will be set to 1 mm/min.

As described earlier all the tests have to be performed at at least three different normal loads. Due to the relatively large area that is sheared, compared to a regular shear box, it is not possible to reach stresses that are similar to those in the first sand layer in Amsterdam. The biggest limitation to the amount of normal force that could be applied is the surface on which the weights have to be stacked. For safety reasons, only one layer of 5 kg weights could be used. The surface area was large enough to fit 4 of these blocks onto the wood sample. Therefore. normal loads of 5, 10, 15 and 20 kg (excluding the weight of the wood sample) were used.

Furthermore, tests FW1 and FW2 will be used to verify that this alternative set-up can be used to measure the interface friction angle. Since these wood specimens are not degraded and are not treated with a layer of slime, the interface friction angle should be similar to the one which is reported in literature.

3.1.1. Set-Up

Interface friction tests are usually performed in a regular direct shear box, however, this test only has a thin horizontal shear plane. Which only makes it suitable to test flat pieces of materials. Since the purpose of

Tests	New wood	Degraded wood	No Slime	Slime
FW1 and FW2	x		x	
FWS1 and FWS2	x			x
DW		x	x	
DWS		x		x

Table 3.1: Overview of performed tests and their conditions

these tests is to test the interface of the shaft of a timber pile, which has a very irregular shape, it is impossible to perform these tests in a shear box. For this reason, an alternative set up was used, which will be described below.

Similar to a direct shear test the sample is sheared horizontally with a normal load applied to the sample. In this case the normal load is put directly on top of the wood sample. By performing the test with different normal loads, a value for the apparent cohesion and the friction angle can be obtained.

Due to the irregular shape of the wood sample it is nearly impossible to determine the exact area which is sheared during this test, so an important assumption is made. Which is that the area which transfers the normal load from the wood to the soil is exactly the same as the area which generates the friction between the wood and the soil. This makes it possible to determine the friction angle without knowing the exact area. The next problem is that the area is also needed to determine at what stresses the tests are performed and to get an indication of the amount of apparent cohesion that occurs during the tests. For these purposes the average of minimum and maximum estimate surface of each sample is used. These areas will be described below.

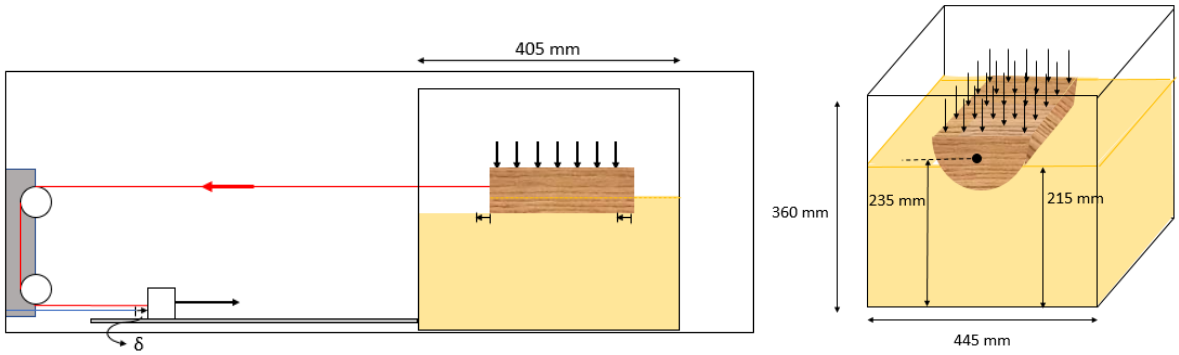

(a) Test Set-Up schematisation

(b) Inner Dimensions of box

Figure 3.1: Schatisation of the test set-up

A schematic picture of the setup is shown in figure 3.1a. It consists of a box which contains the sand and wood sample and a motor which moves along a rails. A rope (red line in the figure) connects the motor to the wood sample, as the motor displaces, the wood sample is pulled over the sand sample. Between the rope and the motor is a device which measures the force; which in this case is the force which is necessary to apply the displacement to the wood sample. Furthermore, a displacement meter measures the actual displacement of the motor (blue line in the figure).

Figure 3.1b shows the inner dimensions of the box which is used for the tests. The box is made of 18 mm thick timber plates which are connected by screws and finished with sealant to ensure it is watertight. On the front side of the box a hole is drilled with a diameter of 10 mm through which the rope goes to connect the wood to the motor. The sand sample is made up to 15 mm under the bottom of the hole, or 215 mm from the bottom, so only the bottom of the wood sample is sheared by the sand.

3.2. Wood Samples

The wood samples have a big influence on the result of these tests, their weight, but more importantly; the shape of their surface is responsible for behaviour which can deviate strongly from what can be expected. For this reason, the wood samples and their properties will be discussed in this section.

3.2.1. Fresh wood

To be able to compare frictional behaviour of new wood to old wood, a fresh log is also tested. This piece is a pine wood log, with a diameter of approximately 16 centimeters.

Surface

This log was cut in half to be able to test two fresh wood samples, FW1 and FW2, shown in figures 3.2 and 3.3 respectively. Using CT-scan data, an elevation figure is made to help describe the surface of the samples. The lighter regions in figures 3.2b and 3.3b indicate more elevated surfaces, whereas the red areas are lower.

The surface of FW1 over which the sliding occurred is quite symmetric. The centre of the surface is located lower than the left and right edge of the sample. Located in the centre and in the back of the sample is node of approximately 2.5 cm in diameter. The two lower lying areas on either side of the node are not expected to be in contact with the soil while the shear tests are performed. Meaning that the area which is actually sheared during the tests consists of the two elevated areas, left and right of the centre, and of the node itself.

Thanks to the symmetric surface of FW1, it did not tilt a lot throughout the tests. If tilting did occur during a test, it was often towards the right (the bottom of FW1 in figure 3.2). This side is less elevated and has a relatively flat surface, thanks to the flat surface no unexpected behaviour was observed during the tests on FW1.

(a) Photo of Sample FW1

(b) Height profile FW1

Figure 3.2: Wood Sample FW1

The surface of FW2 is much less symmetric than that of FW1. The left side (bottom in figure 3.3) is more elevated than the right side of the log. The left side is relatively flat but FW2 tilted onto its right side during every test. This side is very irregular and contains sudden changes in elevation and a node of 2 cm in diameter. This caused an occurrence of less consistent behaviour during the tests; for example multiple peaks in a single test, or a sudden drop in resistance after the supposed constant volume strength had been observed. Examples of test series where this behaviour is observed are the FW2 tests at 10 and 15 kg, shown in figures A.27 and A.28 in Appendix A.4.3. This behaviour made it difficult to determine the true value of the constant volume friction. FW2 contains two more nodes on either side of the sample, one has a diameter of 2.5 cm and the other of 3 to 3.5 cm.

(a) Photo of Sample FW2

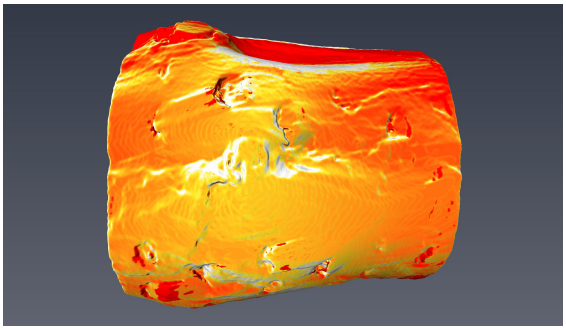

(b) Height profile FW2

Figure 3.3: Wood Sample FW2

The wood samples both have a surface with a very irregular shape, from which is was hard to determine which parts of the area were actually in contact with the sand sample. It was attempted to visualize this area by applying a layer of slime which was stained with blue colorant to the surface and then performing a single shear test. The expected manner of sliding of sample FW1 is confirmed by the results from the blue stain test, from which it can be seen clearly that the centre of the imprint of the log is not stained blue, see figure 3.4.

Figure 3.4: Blue stain test on FW1

It is not possible to know the exact area that was sheared in each test, but it is possible to establish an upper and lower estimate of the area that was in contact with the soil. With this information it can be estimated at what stress range the tests are performed. In the case of FW1 the minimum area is considered to be the area of the two elevated sides, not including the lower area in the centre, the maximum area includes the lower laying area as well. With a length of the sample of 18 centimeters the minimum and maximum area of FW1 are 0.0216 and 0.0252 m^2 respectively. For FW2 the minimum area is taken for an embedment of approximately 1 cm and the maximum is taken at 2 cm. This leads to a minimum and a maximum area of 0.018 and 0.0252 m^2 respectively.

Weight

The old wood samples were completely saturated when they arrived and they had to remain submerged in water in order to prevent fungal degradation. Since the piles are also in a saturated condition in situ, the shear tests are also performed on saturated wood samples. This meant that the new wood had to be saturated before performing the tests.

A few days before the start of the tests the samples were submerged in water. However, since the samples were completely dry before they were submerged, the weight of the logs increased over time from 0.883 and 0.913 kg to 1.481 and 1.443 kg for samples FW1 and FW2 respectively. The weight increase occurred logarithmic as shown in figure 3.5. Since the weight of the samples is an important parameter to determine the normal load, this figure is used to determine the weight of the logs on the days of testing.

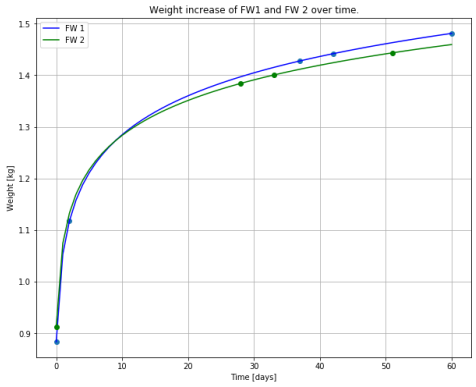

Figure 3.5: Increase in weight overtime

3.2.2. Old Wood

The old wood samples are from piles which have been extracted from the quay wall at the "Oudezijdse Achterburgwal" in Amsterdam. The quay wall was estimated to have been built between 1870 and 1920, so the piles have an age of between 100 and 150 years old. More information on the quay wall and about the extraction of the piles is given in Appendix A.1. The weight of wood sample DW 1 was equal to 4.66 kg. Since the wood sample was already fully saturated from being the the soil for the past 100 years, the weight did not change with time. Interestingly, CT images that were taken when the wood sample was still wet showed that the the core of the sample actually did not contain water, even though the sample had remained submerged after extraction. This can be seen in the centre of the slice of sample in figure 3.6b, which is coloured much darker than the surrounding wood. A darker colour represents a lower density in this image.

(a) Piece of old pile from which sample DW was extracted

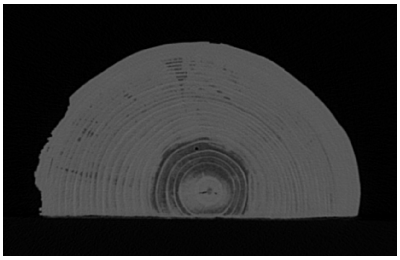

(b) Wet CT image of DW

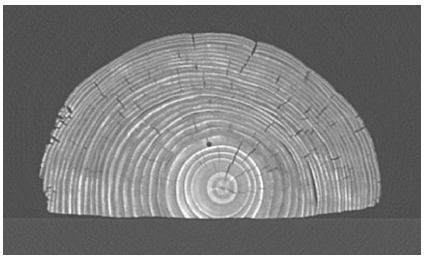

(c) Dry CT image of DW

Figure 3.6: Wood Sample DW

Species

The wood species had to be determined using light microscopy images, the wood can be classified by looking at the shape of the cross field pits, as was discussed in chapter 2. The microscopy image showed that the shape of the crossfield pits correspond to the genus pinus, or the pine family. Oddly, this particular species of pine is not the same as the type of pine that is usually found as foundation pile in the Netherlands. The common species of pine wood used as foundation piles is the *pinus silvestris*, a species of pine which is native to the Netherlands and has windowlike crossfield pits. The microscopy images show that the crossfield pits have a pinoid shape, most of the pines with pinoid pits are native to North America. There are two species with pinoid pits from Europe, but both are from the Mediterranean. The literature which is known to the author has never mentioned piles being imported from that far away, only from European countries such as Belgium and Germany (ter Linde (1990), R. Klaassen et al. (2000)).

Surface

The surface of DW is actually most similar to what one would expect from half a log, it is almost a perfect semicircle. The surface is mostly flat, especially in the centre part. On the sides there are some irregularities

which are mostly caused by damage to the bark of the sample and by a node of 2.3 to 3 cm. Moreover, the microscopy analysis has shown that there is most likely still a layer of bark present on the sample. Unfortunately this sample was also not very stable throughout the tests. It often experienced a sudden tilt as resistance was building up, leading to a peak in the test results even though the actual peak had not been reached yet. Such behaviour can be seen in some tests in all the test series of DW and in some of the 5 kg tests of DWS. All of these are shown in the figures in Appendix A.4.5.

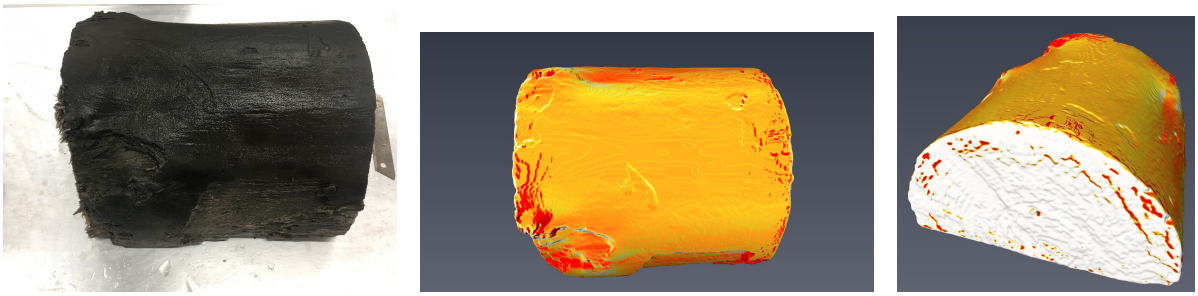

(a) Photo of Sample DW (b) Height profile DW (c) Height profile DW from front

Figure 3.7: Wood Sample DW

It is not possible to know the exact area that was sheared in each test, but it is possible to establish an upper and lower estimate of the area that was in contact with the soil. With this information it can be estimated at what stress range the tests are performed. The minimum and maximum circumference that was in contact with the soil during a test are equal to 10 cm and 23 cm. With a length of the sample 22.5 cm this leads to a minimum and maximum estimates area of 0.0225 $m^2$and 0.05175 m^2.

Degradation

The degree of degradation of the wood sample is determined in three ways; by determining the thickness of the soft shell using IML measurements, by determining the moisture content of the wood and by studying a slice of the wood under a light microscope.

A parameter which is often used to describe the degradation of a timber pile is the thickness of the soft shell. The thickness of the soft shell of sample DW was measured using a drilling resistance measurement system (IML-RESI PD300), which is shown in figure 3.8a.

(a) ML-RESI System (b) Locations of IML measurements

Figure 3.8: IML tests on DW

The device inserts a drilling needle into the sample at constant speed and rotation while measuring the resistance. The result of the test is a graph of the drilled distance versus the drilling resistance that was measured. From this resistance, the thickness of the soft shell can be determined.

The test was performed at two times; first when it was still wet, and later after it had been dried in the oven. In total, 8 measurements were done, 5 when the sample was wet and 3 when the sample was dried. All these tests were performed at a feed speed 500 mm/min and a needle speed of 3000 rpm. Figure 3.8b shows the locations of all the measurements that were performed.

The results of the one dry and one wet drilling test that were taken close to each other are shown in figure 3.9. From both these tests it seems that the sample has a soft shell of about 7 mm. Going deeper into the sample the drilling resistance remains approximately constant. At a depth of 70 mm the resistance increases, possibly because the core of juvenile wood is reached. The results of all the other IML tests are shown in Appendix A.1.1.

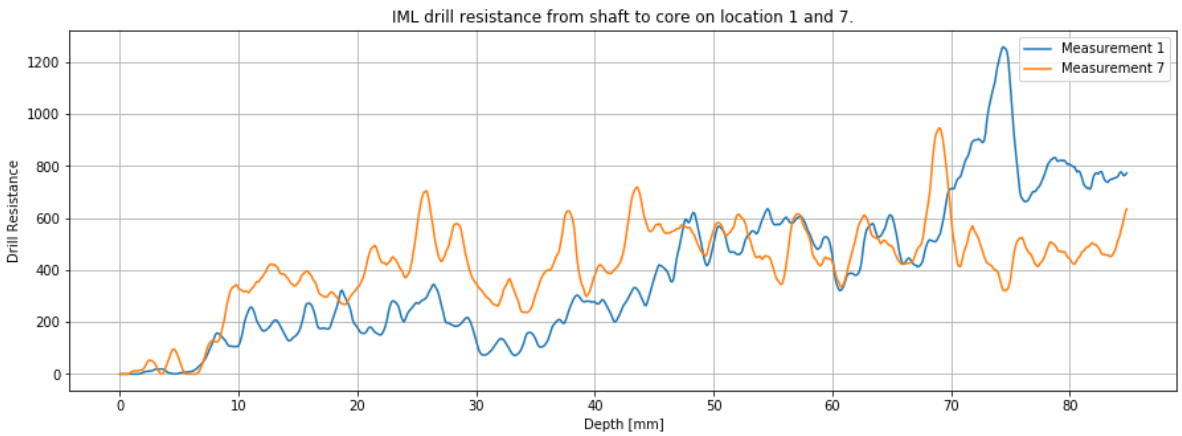

Figure 3.9: Result of two drilling resistance tests near each other

Moisture content of wood (ω(%)) is determined by $(M_{wet}-M_{dry})/M_{dry}$. The wet weight of the sample was equal to 4.66 kg. After drying the sample in the oven at 67 °C for several days, the dry weight was equal to 1.46 kg, leading to a moisture content of $\omega = 219\%$. Normally, when the moisture content of wood is determined, blocks of 10 mm x 10 mm x 15 mm are used. In this case the sample was dried as a whole. CT data showed that the core of the wood sample was not fully saturated before drying it. This leads to the expectation that if blocks were cut, the moisture content would have been higher. According to R. K. Klaassen (2008) a moisture content higher than 200 % is found at more severe degrees of degradation. So the moisture content that is found does indicate that the wood is degraded.

The degree of degradation is also determined by taking a slice of 30 μm thick and studying this under a light microscope. Using this method no degradation was found on the slice that was studied.

Overall, the three methods do not agree on whether sample DW showed degradation or not. The moisture content and IML measurements did seem to show that the sample was degraded, but microscopy imaging did not confirm this. Perhaps the slice that was studied on the microscope happened to not be degraded, but this seems unlikely.

3.3. Soil Description

The sand that is used for these tests is similar to the sand that is present in the first sand layer in Amsterdam. North-South line measurements, shown in Korff (2013), show that this sand layer has a D_{50} of 125 μm and a friction angle of 33°.

The sand which is used for the tests is a fine grained sand which has a D_{50} of 117 μm. The sand is uniformly graded with a Uniformity Coefficient (C_u) of 1.55 and a Coefficient of Curvature (C_c) of 1.24 (figure 3.10). The friction angle of the sand is equal to 36°. The minimum and maximum void ratios are 0.64 and 1.07 respectively. The results of the soil lab testing are reported in Appendix A.2.

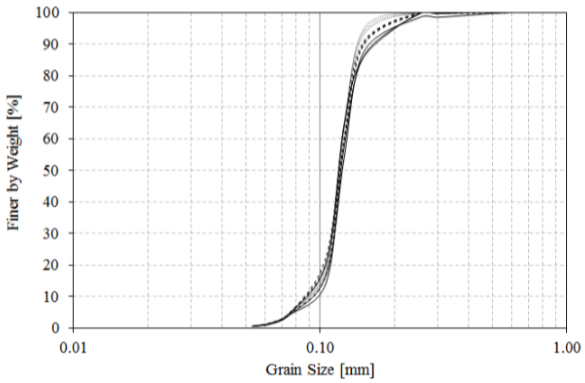

Figure 3.10: Grain size distribution of the sand, from Maghsoudloo, Galavi, Hicks, and Askarinejad (2017)

To determine the relative density and the moisture content of the sand sample that was used for the tests, core samples were taken after the tests were finished. The test procedure and results are described in Appendix A.3.

3.4. Method

Using a piece of Plexiglas which is sawn in the shape of the sample, a trench is made in the centre of the box (figure 3.11). The water level cannot reach all the way to the surface of the sand sample, because then it would not be possible to make a trench in the shape of the sample without it collapsing before the sample is placed. To make sure that the sand is fully saturated in the zone where the shear between the wood sample and the sand occurs, the water level reaches up to at least 1 cm above the bottom of the trench.

The rope is then attached to the hook which has been screwed into the wood sample. The sample is placed in the trench in such a way that the rope goes through the hole in the box, without touching any of the edges of the hole. Preferably, the rope is positioned slightly to the top of the hole, in order to correct for settlement which occurs during the test.

Next, the required amount of normal load is put on top of the log, after which the vertical displacement meters are set in place.

Before starting the test, sand which is in front of the sample is removed, to prevent (as much as possible) the formation of sand heaps during the test. Furthermore, the embedment of the log in the sand is noted, as well as a the manner of tilting of the log (forward, backwards or sideways).

During the test a camera is set up, making a time lapse of the vertical displacement meters. Before, during and after the test pictures are taken to capture the behaviour of sand around the sample.

After completion of the test, the tilting of the sample is noted again. Also any tilting in the rope, and the height and state of the sand which has accumulated in front of the sample is noted. Next, the displacement meters, the loads and the sample are removed from the box.

To prepare the box for the start of a new test, the sand and water which were removed from the box to make the trench are put back. Then the surface of the sand is made flat again using a plastering tool. To somewhat approach the same density for each test, the box is tapped on each side approximately 50 times with a hammer, tapping from the bottom upwards. This method, however, does not provide any guarantee that the exact same density is reached in every test. That is one of the reasons why the constant volume friction angle was used instead of the peak friction angle.

Figure 3.11: The plexiglass tool and the trench

3.4.1. Slime

As mentioned previously, Xanthangum powder mixed with water is used to imitate the bacterial slime layer. In this study the amount of xantangum was chosen as 1% of the weight of water, so 200 grams of water was mixed with 2 grams of the powder. Since the powder tends to flock together when it is mixed in with the water, the mixture is left on magnetic stirrer for 15 minutes on the fastest stirring setting at room temperature.

For each test, about 20 grams of slime was used. The slime was poured onto the part of the wood sample that was sheared and was spread evenly, so the shaft was covered with a 1 to 2 mm thick layer of slime.

When placing the wood sample into the trench, it was attempted to pry the wood sample as little as possible, this to prevent the layer of slime from being disrupted by the sand or dissolved in the water before the start of the test.

3.5. Observations

Failure plane

During almost every test, a failure plane was observed forming around the sample. For test number 176, the photo's that were taken during the test in combination with the measurement will be shown. Test number 176 was part of the FWS2 test series; tests with slime on sample FW2, the additional load in the test was 20 kg. Photo's were taken at 5 moments during the test; before the start, at 13 mm displacement, at 23.5 mm displacement, at the end of the test and after sample FW2 had been removed.

(a) Before start of test

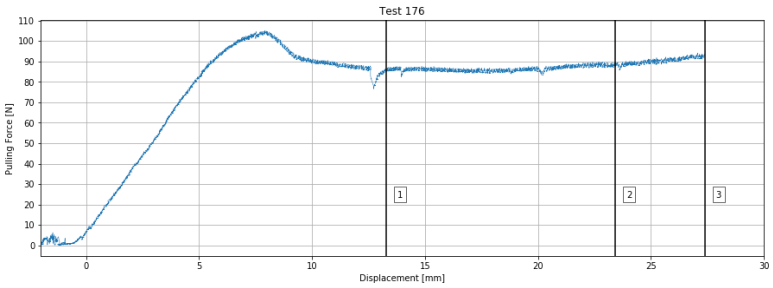

(b) Load displacement curve of test 176

Figure 3.12: Load displacement curve of test 176 and photo before the start of the test.

The numbers of the vertical lines in figure 3.12b correspond to the numbers of the pictures in figure 3.13. The figures below show that the failure plane originates at the front of the sample and moves further back as the sample is displaced further. From other tests it seemed that the failure plane did not start forming until after the peak. It is expected that the cause of the failure plane is that a heap of sand forms in front of the log, which is pushed forward, causing failure around the sides. The observed plane looks similar to what is observed during vertical penetration. If this is indeed the cause then the measured resistance must increase as the failure plane progresses, and more sand heaps up. This idea is confirmed by comparing figures 3.13 a to c to figure 3.12, where it can be seen that there is indeed and increase in the pulling force as the displacement increases and the failure planes progresses.

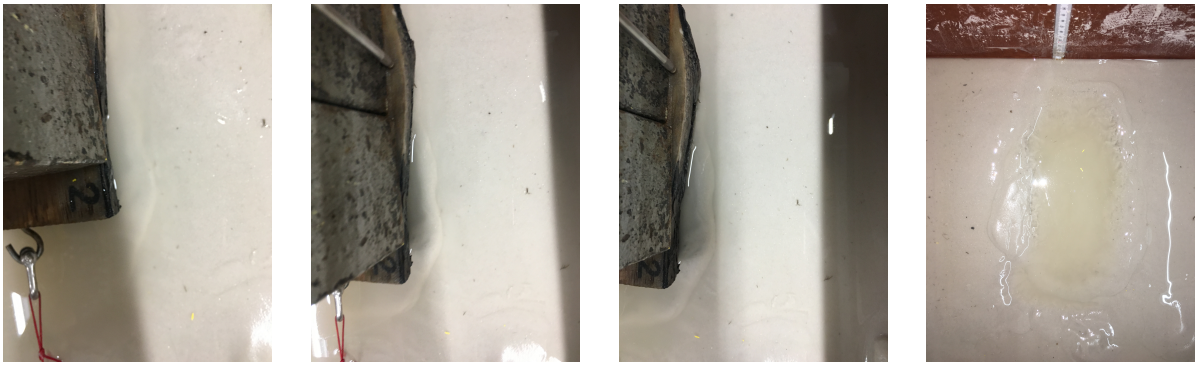

(a) 1 (b) 2 (c) 3 (d) After test

Figure 3.13: Photo's taken during test 167.

Due to the increased resistance caused by the sand heap, it was important to take the residual shear strength value as close after the peak as possible. Otherwise the measured resistance would not only be due to the friction, but also due to the passive failure of the sand. In the case of test 167 the residual shear strength was taken at a displacement of 15 mm, just after photo 1 was taken. It is expected that the results are not influenced by the heap of sand yet.

Suction

During some tests, not enough water was present in the box. This was the case in test 188. Test 188 was part of test series DW; tests without slime on the old wood sample. The additional load during this test was equal to 15 kg. Figure 3.14 shows the load displacement curve of test 188 and the situation before the start of the test. The vertical lines in figure 3.14b again correspond to the numbers in figure 3.15.

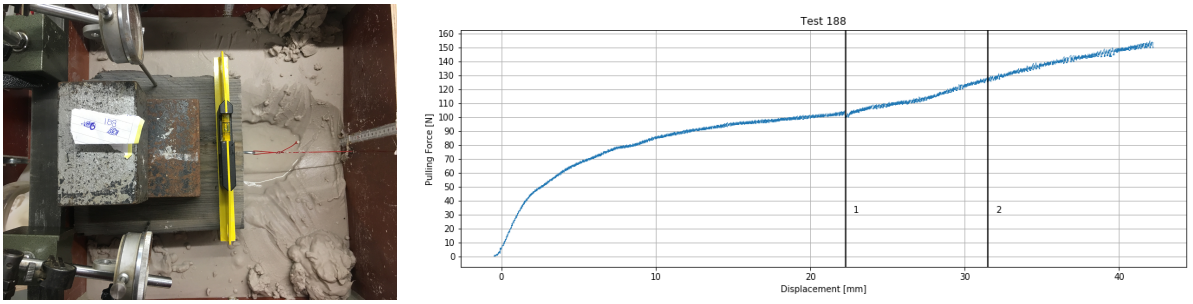

(a) Before start of test (b) Load displacement curve of test 188

Figure 3.14: Load displacement curve of test 188 and photo before the start of the test.

In figure 3.14a it can already be observed that there is only a small puddle of water in front of the sample. Then, in figure 3.15a, a heap of sand can be observed, which still seems moist. But in picture 3.15b no moisture can be observed anymore and the sand seems completely dry. It is expected that this loss of moisture happens due to dilation occurring in the sand sample. The moment at which the sand seems to have lost its moisture can be seen in the load displacement as a sudden increase in the measured pulling force. This happens because the sand is no longer saturated; suction forces arise in the sand, increasing the resistance.

Whenever this drying out of the sand was observed during a test, the results of this tests were not used. Especially during the tests on the old wood it was difficult to maintain the right amount of water in the test. If there was too much water before the test, it was not possible to make the trench. But if there was not enough water, the sand dried out, causing suction and making the results of the tests useless.

(a) 1 (b) 2 (c) After test

Figure 3.15: Photo's taken during test 188.

Slime

Especially when several tests with slime had been performed, it was observed that the slime was affecting the behaviour of the sand. A consequence of this was that the re-densification of the sample using the taps was not as effective and the sand sample remained soft at the location of the trench. This softer material generally caused bigger settlements during the test, which caused the rope to be under a downward angle at the end of the test. Once it was observed that the trench was not densified properly anymore, usually after around 5 tests with slime, the sand sample was fluidized and densified again. This was done as follows; first, the hole in the box was closed off using a piece of cling film. Then, around 1.5 liters of excess water was added to the sand sample and the top few centimeters of the sand were tossed loose. Next, using the same tapping method, the sand was densified and the excess water was removed from the box. After this, the regular preparation method was used, first using the plastering tool to equalize the sand level in the box, and then performing the tapping again. Using this method resulted in a sand sample which had the same density everywhere.

Indentation

After wood sample DW was dried is was studied with a magnifying glass to see if any traces of indentation of sand grains into the wood structure could be observed. Figures 3.16a and b show photos that were taken through the magnifying glass.

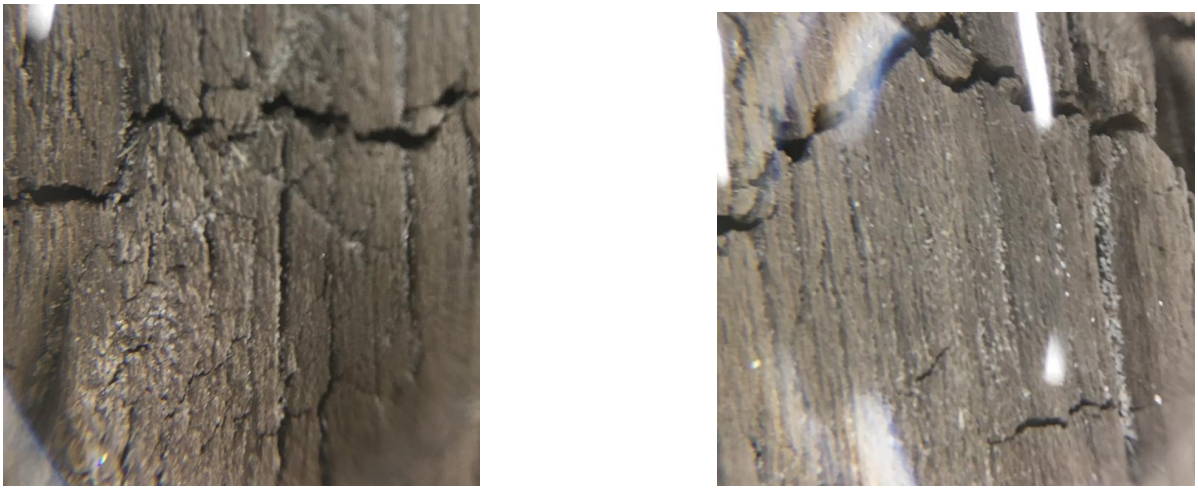

(a) (b)

Figure 3.16: Sand grains in cracks of the dried wood

From the pictures it can clearly be seen that there is some sand present in the cracks of the wood, this was not observed in samples FW1 or FW2. Whether this indented sand has actually influenced the measured

friction angle is questionable. The friction angle that was measured from the DW sample was indeed higher than what was expected, but literature describes that the effect of indentation was only seen in the friction angle at high normal loads. Since the loads at which these tests were performed were extremely low it is uncertain whether the effect could have been measured. But this observation does strengthen the suspicion that indentation of sand into the wood can occur at lower stresses when the wood is more degraded.

3.6. Evaluation

Since new slime is applied to the sample in every test, the concentration of slime which is left behind in the sand sample inevitably increases with every passing test. A solution to this for further research is to mix the slime directly into the sand sample, instead of applying it to the wood sample. This way the concentration of slime is controlled better in every test, and the effect of variations in the amount of slime which is present can be studied as well.

Due to the settlement of the log, that occurs during the test, the rope is often situated under an angle at the end of the test. This has probably caused some deviation in the measured pulling force. It was therefore attempted to have the rope situated at the top of the hole at the start of the test. A possible solution to this problem in further research could be to increase the size of the hole, or to make a slit instead of a hole.

The constant volume resistance for each test has now been taken at a set displacement, for example at 50% or 75% of the total displacement, while this is not necessarily the best approach. For example; in test series FWS1 with normal loads of 5 kg; taking all values at a displacement of 10 mm results in the values: 34,30,30 and 31 N. If the test results are examined more closely, it becomes apparent that the two test that are not equal to 30 N at 10 mm displacement, do appear to show constant volume friction of 30 N at other displacements; at 5 mm and 15 mm for tests 148 and 146 respectively (figure 3.17). This suggests that taking the values at a set displacement may not be the best approach. Instead, every test should be assessed individually.

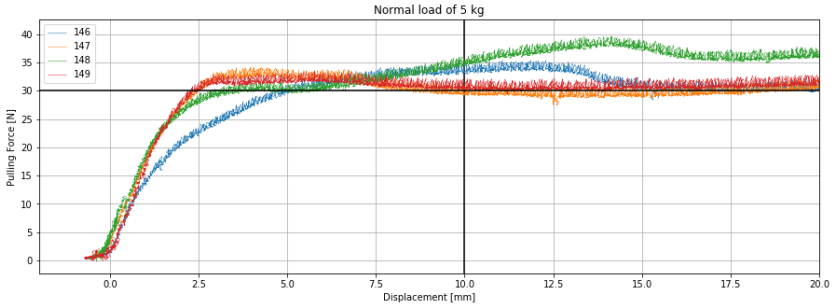

Figure 3.17: FSW1 tests on 5 kg normal load

It was observed during almost every test that tilting of the sample occurred. A consequence of this is that the area that was in contact with the soil, and thus the normal and shear stresses, might not have been constant during a single test. Also, due to the shape of the samples, the normal stress will probably not be constant over the area that is sheared. Moreover, since more settlement occurred in the tests with higher normal loads, it is likely that the area that was sheared during these tests was also larger.

Due to the relatively large area, the normal stresses on which the tests are performed are extremely low, corresponding to the in-situ conditions at 1 meter below the greenfield at most. It is usually recommended that shear box tests are performed at normal loads which represent 50%, 100% and 150 - 200% of the in-situ conditions. Since the sand which is used represents that of the first sand layer, where stresses of between 70 an 80 kPa typically occur, these normal loads are nowhere near the recommendation.

3.7. Results

In this section the results of one set of tests is first shown and described. Firstly, to show that the results that were found are reproducible and secondly, to explain how the values were found that are used in the interpretation of each test series. Then the overall result of each test series is given. In interpreting the results an assumption is made that the sheared, and loaded area is equal to the average of the lower and upper estimates of the area of the samples. This has no effect on the friction angle that results from the tests, as this is independent of the area. Some apparent cohesion was measured during the tests, but since the values are

very small (between 0.01 and 0.51 kPa) and there is no physical reason for cohesion to occur, all the intercepts are forced through zero. The measured apparent cohesion are most likely due to measuring inaccuracies.

3.7.1. Reproducibility of results

In order to be able to draw conclusions from this alternative test set up, it is important to confirm that the results of the test are reproducible. This paragraph will show this for one of the set of tests, the graphs of all the other sets of tests are shown in appendix A.4. Moreover, it is described where the values of each residual strength is taken from the tests.

Figure 3.18 shows the load displacement curve of 4 tests that were performed on wood sample FW1 with a normal load of 5 kg placed on top. As can be seen from this figure, all the tests show the same behaviour, having similar stiffness and reaching the same peak values at approximately the same displacements. This proves that the alternative set up is able to provide consistent results for the same tests. For some test series, such as FW2 and DW, the results do not coincide this nicely, but this is usually due to the shape of the wood sample.

The black line in the graph indicates where the values for the residual shear strength is taken. This is done at 50% displacement in the tests at 5 and at 10 kg additional normal load, and at 75% displacement in the tests at 15 and 20 kg additional normal load. These values have been chosen because in the latter two tests a larger displacement was needed to reach the peak friction. The numerical results of each test, and the average values at the different loads are given in tables A.3 until A.26 of Appendix A.4. As will be described later, some of the test series required more displacement before reaching their peak shear strength. Therefore it was sometimes necessary to deviate from the criteria mentioned above. The displacement at which the values were taken for each set of tests is shown in the figures in Appendix A.4. From this picture the effect of the failure plane that was described in the observations section becomes clear. After 10 mm displacement, the pulling force slowly increases. This is due to the forming of a heap of sand in front of the sample. This makes it difficult to determine a good location to take the residual shear strength, especially for the tests which require more displacement.

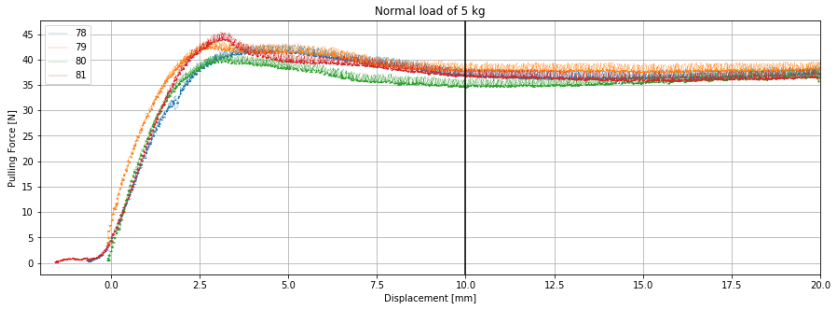

Figure 3.18: The results from test series FW1 at 5 kg additional load

3.7.2. FW1 tests

The FW1 test series was performed on wood sample FW1, no slime was applied in this test series. The tests were performed over a period of 3 days, when FW1 had been submerged in water for 7 to 9 days. The weight of the sample itself was taken from figure 3.5 at 8 days, leading to a self weight of 1.26 kg. The average area of the sheared surface is 0.0234 m^2, so additional loads of 5, 10, 15 and 20 kg lead to normal stresses of 2.6 kPa, 4.7 kPa, 6.4 kPa and 8.5 kPa.

At least 4 tests were performed on each normal load. In case it was found that there was a large scatter additional tests were performed. This was the case in the tests that were performed with 15 and 20 kg of additional load. The FW1 test series resulted in an interface friction angle of 30° as can be seen from figure 3.19. The results of all the test from series FW1 can be found in Appendix A.4.1.

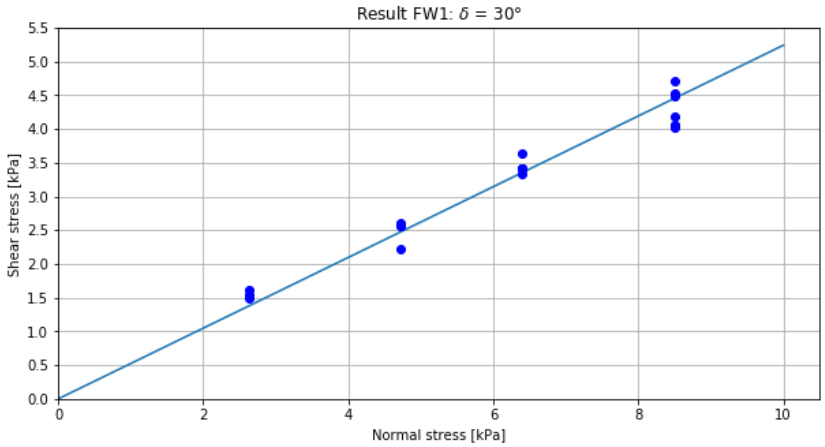

Figure 3.19: Interface friction angle resulting from FW1 test series

3.7.3. FWS1 tests

The FWS1 test series was also performed on wood sample FW1, with a layer of slime applied to the sheared area. Most of the tests were performed within a time span of 3 days, except for tests 130 and 131, these tests were performed 20 days prior. The weight of FW1 for these two tests is 1.34 kg, while for the other tests the weight is equal to 1.43 kg. The additional loads which are used in all tests and the average area of 0.0234 m^2 lead to normal loads of 2.7 kPa, 4.8 kPa, 6.9 kPa and 9 kPa. The tests with different normal loads in the 10 kg additional loads series have been averaged to find the friction angle. Similar to test series FW1 a minimum of 4 tests were performed for each normal load, additional tests were done where necessary. The FWS1 test series resulted in an observed interface friction angle of 25.2°.

One outlying value can be observed in the 15 kg normal load tests, see figure 3.20. It is mentioned in the notes that prior to the start of this test, the wood sample was shifted to ensure the rope would go through the centre of the hole. Possibly this has disrupted the slime, which would explain why this value is more similar to the tests performed without slime. Not including this value in the determination of the interface friction angle would results in a decrease of 0.3°.

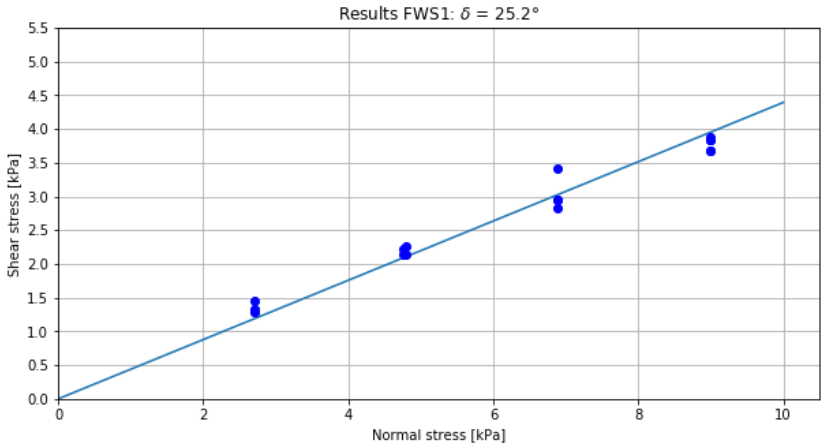

Figure 3.20: Interface friction angle resulting from FWS1 test series

3.7.4. FW2 tests

The FW2 test series were performed on wood sample FW2, no slime was applied during these tests. All tests were performed in a time span of 5 days, when the sample had been submerged between 1 and 6 days. The 10 kg test series was done after one day, the other series were done between four and six days. Since the increase of weight in time is larger in these first days, the weight for the 10 kg test series is assessed seperately, for the other tests an average is used. The weight of the block for the 10 kg test series is equal to 1.05 kg, while the

weight for the rest of the tests is equal to 1.2 kg. With an average area of 0.0216 m^2 the normal stress at which the tests are performed are equal to 2.8 kPa, 5 kPa, 7.4 kPa and 9.6 kPa.

The results of the tests are shown in figure 3.21 and in Appendix A.4.3., the load displacement curves that are found from the FW2 tests are less consistent than those found from the FW1 test. This is most likely due to the irregular shape of the sample which led to tilting during the tests. As can be seen there is again a large scatter in the results that were found from the test series that were performed at higher normal loads. Overall, the tests on FW2 resulted in an interface friction angle of 27.3°.

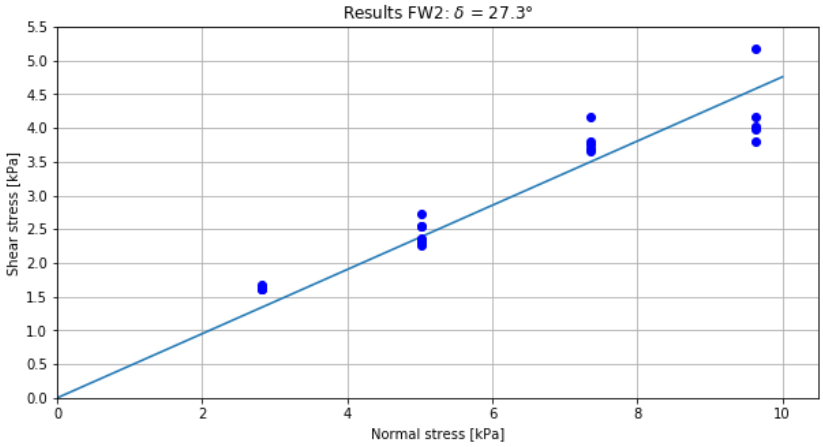

Figure 3.21: Interface friction angle resulting from FW2 test series

3.7.5. FWS2 tests

The FWS2 test series were performed on wood sample FW2 with a layer of slime applied before each test. The tests were all performed in a time span of 4 days, so all test were performed at approximately the same weight of the sample, which is 1.42 kg. With an average area of 0.0216 m^2 the normal stresses were equal to 2.9 kPa, 5.2 kPa, 7.5 kPa, 9.7 kPa. The scatter from the FWS2 tests is much smaller than of the FW2 tests, with the exception of one outlying value in the 20 kg test series. The results of the tests are shown in figure 3.22 and appendix A.4.4. The resulting interface friction angle is equal to 24.7°.

If the one outlying value is disregarded, the resulting interface friction angle would be equal to 24.1°. The value is taken into account, since the range of the values is not much different from the other test series and so there is no good reason to disregard the value.

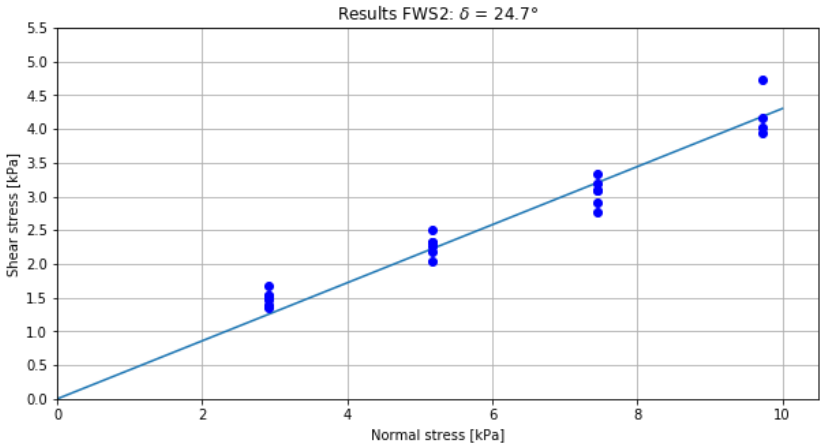

Figure 3.22: Interface friction angle resulting from FWS2 test series

3.7.6. DW tests

The weight of the DW wood sample did not change over time, so the time span in which the tests were performed is not important. With a weight of 4.66 kg and an average area of 0.037 m^2 the normal stresses at

which the tests have been performed are 2.5 kPa, 3.9 kPA, 5.2 kPa and 6.5 kPa. These normal stresses are even lower than those of the fresh wood samples. This is due to the fact that the area of DW is bigger.

The results of the DW tests are shown in figure 3.23 and in Appendix A.4.5. The resulting interface friction angle is equal to 29°. When the individual test in Appendix A.4.5 are regarded, the tests do all show irregular behaviour, but do converge to the same shear stress.

Most of the tests show multiple peaks while going to the residual shear stress, after each peak the stiffness seemed to decrease. This is something that was not observed in any other tests.

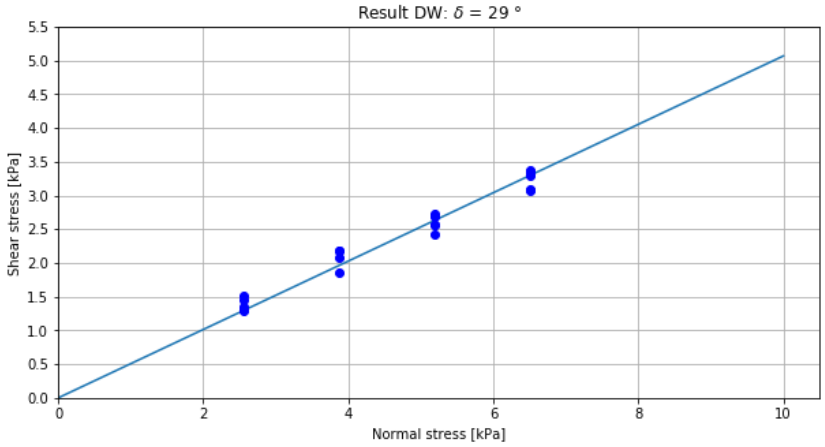

Figure 3.23: Interface friction angle resulting from DW test series

3.7.7. DWS tests

Due to time constraints all the tests of this series were repeated three times instead of four. The tests show good convergence so it is not expected that performing additional tests would have changed the results much. Since the weight and the area of the sample have not changed the normal stresses at which the tests are performed are the same as in the DW tests. Unlike the DW tests, the DWS tests did not show multiple peaks or changes in the stiffness.

The results of the DWS tests are shown in figure 3.24 and in Appendix A.4.6. The resulting friction angle is equal to 28.1°. The range of results for each test series shows a very small range, especially at the 20 kg additional loads tests, where all three tests resulted in 120 N.

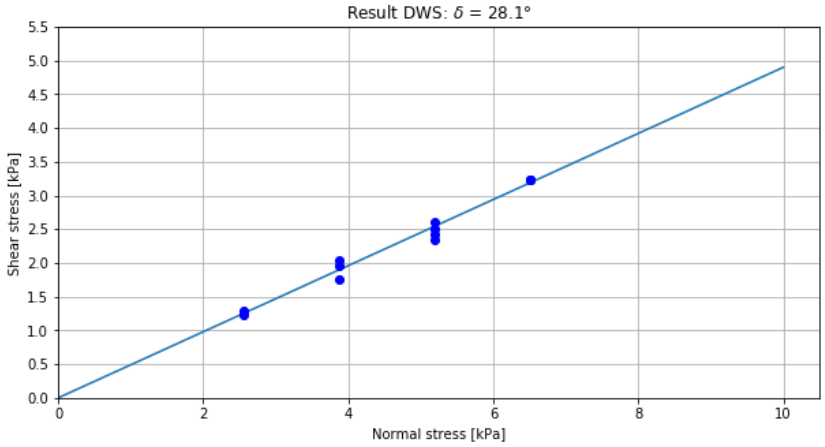

Figure 3.24: Interface friction angle resulting from DWS test series

3.8. Conclusions

In this section the results of the test series are compared to each other, and conclusions are drawn , thereby answering the three research questions regarding the effect of slime, the effect of degradation and the difference between old and new piles.

First it has to be verified that the results that are found here correspond to those found in literature. The interface friction angles, δ, are summarized in table 3.2. If the FW1 test series is regarded, an interface friction angle of 30° is found. Using the residual friction angle $\phi_{residual}$ from Maghsoudloo et al. (2017) of 36°, the ratio between the two becomes: $\delta_{FW1} = \frac{5}{6} \times \phi$. Test series FW2 results in a friction angle of 27.3°, which results in: $\delta_{FW2} \approx \frac{3}{4} \times \phi$. δ_{FW1} Agrees well with the factor that Potyondy (1961) found for dense saturated sand, which was 0.85 $\times \phi$. The value found for FW2 is equal to the value that is used in NEN 9777-1 (Normcommissie 351 006 "Geotechniek" (2016)). This shows that the found results are similar to those that can be expected.

In conclusion, the results of the test set up have been verified and the set up can now be used to perform shear tests on materials which are irregularly shaped and thus not suitable to be tested in a direct shear box. The test set up gave results that were reproducible and that were in agreement with what could be expected from literature.

Test	Interface friction angle
FW1	30.0°
FWS1	25.2°
FW2	27.3°
FWS2	24.7°
DW	29.0°
DWS	28.1°

Table 3.2: Summary of results from all test series

Effect of degradation

The first sub question regarded the effect that a degraded wood structure has on the interface friction, for this purpose tests FW1, FW2 and DW are compared. Interestingly, when comparing FW1 to FW2 the results are quite different, with FW2 resulting in a friction angle which is 2.7° lower than FW1 (figure 3.25a). An explanation could be that the FW2 sample had a more irregular shape, leading to tilting during the tests, which influenced the results. When the results of the degraded wood sample without slime are compared to the fresh samples without slime (figure 3.25b), it is observed that the results are all very similar. DW has a friction angle that lies between that of FW1 and FW2.

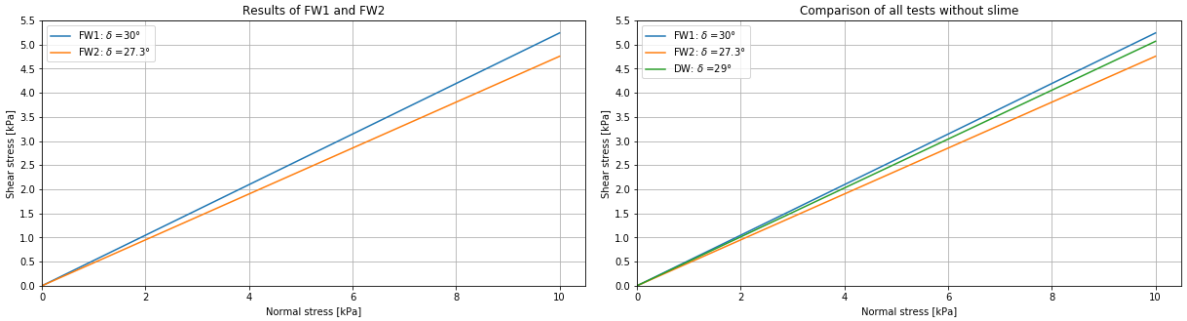

(a) Results of test series FW1 and FW2

(b) Results of test series FW1, FW2 and DW

Figure 3.25: Comparison of test series on samples FW1 and FW2 and DW

A reason for the similar results of three tests could be that the DW sample was actually not very degraded, as is also suggested by the microscopy images. Another reason can be that a higher value of the interface friction is measured due to indentation of sand grains into the wood sample. According to literature, indentation occurs under higher normal stresses, but since the degraded wood has a soft shell it might already occur under smaller normal loads. Also, the fact that sample DW still had its bark might have an effect on the softness of the shell.

Effect of slime

The second sub question is about the effect that a slime layer has on non degraded wood, test series FW(S)1 and FW(S)2 are regarded for this purpose. To see if this effect is also seen in degraded wood, DW and DWS are also compared to each other.

Contrary to the FW1 and FW2, FWS1 and FWS2 give nearly exactly the same results, with a difference of only 0.5°. The irregular shape that might have influenced FW2, however, would not explain why the FWS1 and FWS2 results do match well. Perhaps the difference in friction angle between FW1 and FW2 is due to the roughness of the wood sample and that the application of the slime has cancelled this effect out.

To determine what the influence of a slime layer is on fresh wood the results of FW1 and FWS1, as well as FW2 and FWS2 are compared. Both comparisons show a decrease in the interface friction angle when slime is applied. In the tests on samples FW1 this is a decrease of 4.8° and in the tests on sample FW2 this is a decrease of 2.6° (figure 3.26).

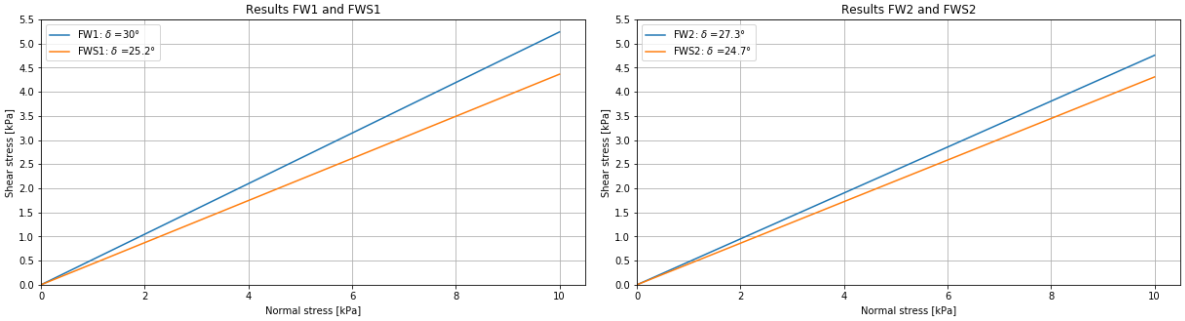

(a) Results of test series FW1 and FWS1

(b) Results of test series FW2 and FWS2

Figure 3.26: Comparison of the effect of slime on both FW1 and FW2

When DW is compared the DWS (figure 3.27), it can be seen that the slime has less influence on this wood specimen than is did on the fresh samples. DWS has a friction angle that is only 0.9° smaller than DW, this is a much smaller difference than between the fresh specimens.

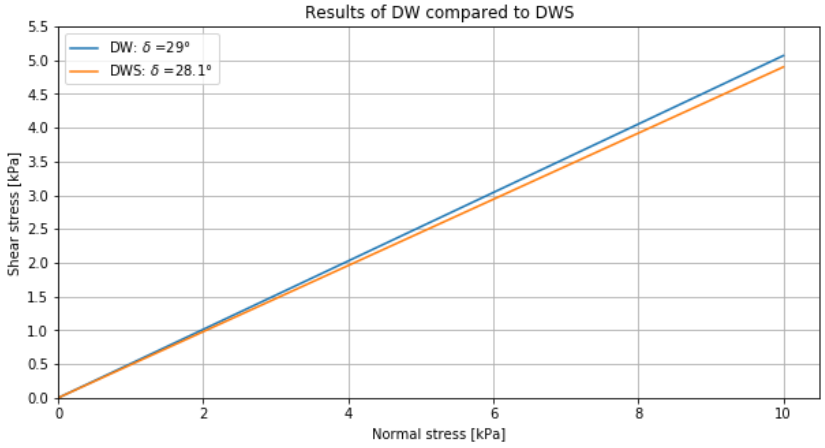

Figure 3.27: Results of degraded wood with and without slime

All in all, a layer of slime reduces the interface friction between fresh wood and fine sand. Due to unknown reasons, this effect of slime is not seen in the tests on the degraded wood samples.

Possible explanations of this are that the effect of slime disappears when indentation of particles occurs instead of regular sliding. Another explanation for the lack in difference between DW and DWS is that sample DW still contained slime from actual bacterial degradation so the application of additional slime did not cause any more difference.

Old and new wood

Now for the last sub-question which aimed at finding the difference between old and new piles, tests FW1 and DWS are compared in figure 3.28a and tests FW2 and DWS are compared in figure 3.28b. The first comparison does show a small decrease (1.9°) in interface friction of the degraded specimen with slime. The comparison between FW2 and DWS however, does not confirm this as an increase in the interface friction angle is found. In any case the difference between old and new wood, as measured here is nowhere near what was expected from the results of the Dapperbuurt tests, which predicted a decrease of 40%.

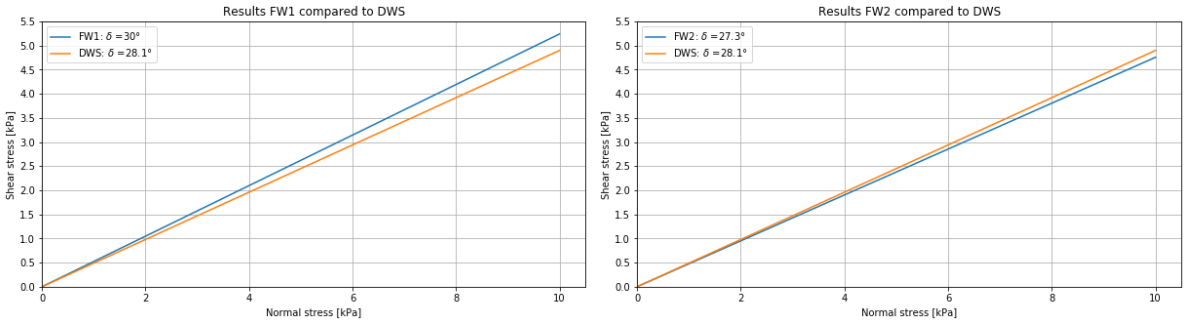

(a) Results of test series FW1and DWS

(b) Results of test series FW2 and DWS

Figure 3.28: Comparison old and new wood

The degree of degradation of sample DW was not very severe, so it is possible that the expected 40% does occur in more degraded samples. Another possibility is that the 40% will only be found in tests on clay, as these particles are not able to indent into the wood structure. It is concluded that additional research is necessary before this question can be answered. Especially concerning whether indentation occurs at lower stresses if the wood is degraded, and what the effect of it is on the skin friction is worthwhile to investigate.

3.9. Recommendations

Since this was the first attempt of determining the frictional properties between wood and sand using the alternative set up, there is much more research which can be conducted.

In this research, only one timber pile was tested which had been in the ground for approximately 100 years. Compared to certain existing structures in Amsterdam, the quay wall was not extremely old. Also, it did not become fully clear from the three methods whether the pile was degraded or not. It would be interesting to investigate the difference in friction between this pile and more degraded specimens, possibly also differentiating in the wood species.

As mentioned in the evaluation, the normal loads at which the tests have been performed were too low to represent the in-situ conditions in the first sand layer. Therefore it would be useful to conduct the same experiments on higher normal loads. Another reason to perform additional tests on higher normal loads is because Potyondy (1961) reported that, at higher normal loads, the interface friction between wood and sand increased due to indentation of the sand particles into the soft wood structure. The high loads at which signs of indentation were observed were 143.6 kPa, these kinds of stresses do occur in the soil around piles in Amsterdam in vertical directions, but not in horizontal directions, working on the pile's shaft. It would be interesting to see what effect degradation has on indentation, as this has never been investigated but observations during these tests already seemed to show some signs of indentation. Since the structure of the degraded wood is softer, indentation might occur at lower normal loads. Another possibility is that the wood structure has such a low strength that it will be completely demolished by the indenting sand. Moreover, if indentation does play a role in the shaft friction of old timber piles, this would probably only be the case in sandy layers, as clay particles cannot indent into the wood. This would have a positive effect on the shaft friction in the first sand layer and thus on the total bearing capacity.

The main focus for this research has been to determine what effect degradation has on the positive shaft friction that is generated in the first sand layer. It is expected that the same effect will be found in negative skin friction. To verify this, a similar study can be done into the effects of degradation on the negative skin friction. As mentioned in chapter two, negative skin friction is generated in the soft soil layers that overlie the

first sand layer in Amsterdam. To test this, the sand would have to be swapped by clay and the direction in which the wood sample are sheared would have to be changed too.

In the tests that are performed here, the main goal was to see *if* the presence of slime between the wood and the soil would make a difference for the interface friction. Now that it is established that there is indeed an influence from slime, it can be investigated more precisely. To do this it first has to be investigated what amount and concentration of slime are actually produced by the bacteria that colonize the timber piles in Amsterdam.

Tests can also be performed on a larger scale, for instance by placing a pile into a tank filled with soil and pulling it out. It is then important that the horizontal pressure in the tank can be regulated, so tests can be performed at different normal loads. Another possibility is to test piles in situ. Piles from existing structures such as quay walls and bridges are sometimes removed, as was also the case with sample DW. If, during the extraction, the load and displacement is measured, this can be compared to load tests on fresh piles, which are tested in the same soil profile. This is similar to what has been done in the Dapperbuurt tests.

4

Sensitivity Analysis

The aim of this sensitivity analysis is to study the effect that the different pile parameters have on the geotechnical bearing capacity of timber piles.

4.1. Monte Carlo Analysis

For this sensitivity analysis, a Monte Carlo analysis is performed. In a Monte Carlo analysis, probability density functions are defined for all relevant parameters. During each simulation, parameters are picked randomly from their distributions, using these parameters the bearing capacity is computed. This is repeated 50.000 times to create a probability density function of the geotechnical bearing capacity. In this specific sensitivity analysis, two different locations are studied in order to compare bearing capacities in different soil profiles. Therefore, two separate Monte Carlo analyses with each a different CPT, are performed. It has to be born in mind that the aim of this analysis is to study the uncertainty associated with pile parameters and degradation, *not* to study the uncertainty associated with soil profiles throughout Amsterdam. If this were the case, many more CPTs would be needed for each location.

The problem will be analysed as the assessment of an existing structure on disapproval level or for reconstruction, assuming that the load has not increased with more than 15%. For this reason an α_p of 1.0 may be used according to NEN 8707 (Normcommissie 351 006 "Geotechniek" (2018)). Since only one CPT per location is used, ξ_3 equals 1.39. The partial factors, γ_s and γ_b, are both equal to 1.2, both in accordance with NEN 9997-1 (Normcommissie 351 006 "Geotechniek" (2016)).

Furthermore, the bearing capacities of the tip, the shaft capacity in the sand layer and the shaft capacity in the soft (Holocene) layers are reported separately. By doing this, the effect that parameters have on the various contributions to the total and ultimate geotechnical bearing capacity can be studied. In the analysis, both total and ultimate capacity will be regarded. Total capacity is defined as the bearing capacity of the tip plus the shaft capacity generated in the first sand layer. Since in Amsterdam, piles often show continuous settlement, ultimate capacity is also studied. As this indicates the amount of additional bearing capacity that can be generated once the load on the pile has exceeded the total bearing capacity. Ultimate capacity is defined as the total bearing capacity plus all of the shaft friction that can be generated in the soft soil layers overlying the first sand layer.

4.1.1. Locations

The sensitivity analysis will be performed for multiple locations in an attempt to cover the most important variations in the Amsterdam soil profile as discussed in paragraph 2.1.2. One location will be chosen which is representative for the largest part of the city. Then a variation will be made for the part of the historic city centre, where the Amstel and the Oer-ij were located. This extra location is chosen because this part of the historic city centre still contains many structures on timber piles. So it is important to study how a variation in the soil profile, mainly in the Holocene layers, can affect the bearing capacity. The two locations are shown in figure 4.1 and 4.2.

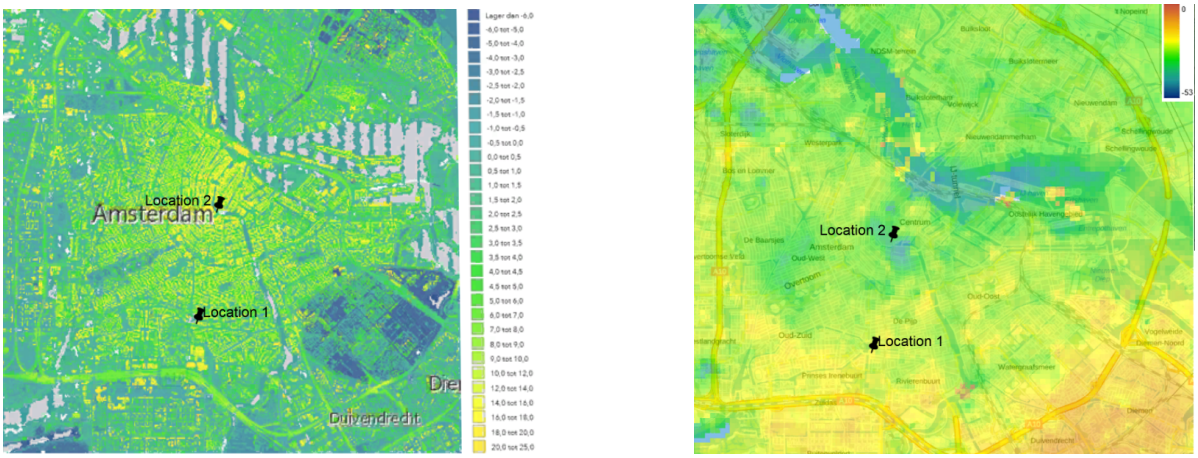

(a) Level of the greenfield

(b) Depth of the first sand layer

Figure 4.1: Locations picked for sensitivity analysis

Figure 4.2 shows a cross section through the city of Amsterdam, showing the most likely lithoclass according to the Geotop model of Dino loket (*DINOloket* (2019b)). This cross section shows that the soil profile on location 1 is indeed representative for most locations along this cross section. From 2.2 to 2.6 km into the cross section the profile is slightly different, with the first sand layer located deeper and the top peat layer being absent.

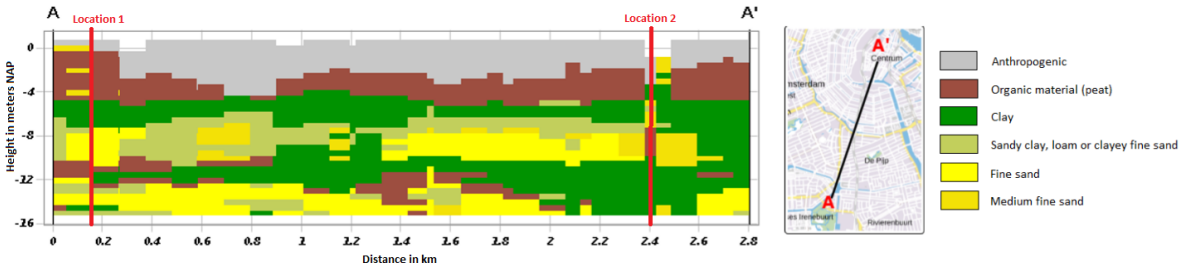

Figure 4.2: Cross section through Amsterdam, after *DINOloket* (2019b)

The first location can be considered as the reference situation for most of the city. The greenfield is located at a height of between 0.5 and 1 meter NAP. Directly under the greenfield is a man-made sand fill of several meters thickness. Underlying this is the layer of Hollandveen peat. The first sand layer is at a depth of -11 to -12 meters NAP, overlying this is another thin layer of peat. There is a slight increase in the cone resistance between -7 and -10, where the wadsand layer is located. An indication of the quality of the first sand layer is given based on the classification as shown in table 2.3. $p_{r,max}$ / 15 = 0.73 for the reference embedment of 0.5 meters and tip diameter of 0.13 meters, which classifies the sand layer as good according to table 2.3.

The second location is different from the typical Amsterdam profile, as it is from a location where the Amstel and the river IJ have left their marks. Due to erosion, the first sand layer is located deeper than is typically the case: at -14 meters NAP. Erosion also caused the peat layer and the wadsand layer to both be absent ,they have been replaced by a peaty clay layer. Overlying this are river deposits from the Amstel, on top of this is a sandy top layer reaching up to surface level, which is at 1.5 meters NAP. The area where the Oer-IJ has been can be seen well in figure 4.1a, the blue areas are where the first sand layer is located deeper and has thus been eroded by the Oer-IJ. On this location $p_{r,max}$ / 15 = 1 for the reference pile, classifying the sand layer as excellent according to table 2.3.

Since the sensitivity analysis mainly focuses on the influence of the pile parameters, and not on the influence of the exact soil profile, only one CPT is used for each location. To take into account the uncertainty in the soil profile from using only one CPT, NEN 9997-1 prescribes a safety factor ξ_3 of 1.39.

4.1.2. Parameters

Before elaborating on the parameters and their distribution, the used equations will shortly be described, after which it will be mentioned how the parameters that will be varied in this analysis influence the components of the bearing capacity. The parameters that will be varied are the diameter at the tip D_{tip}, the diameter at the head , D_{head}, and the embedment of the pile tip in the sand layer. The depth of the pile head will be kept constant, as will the top of the sand layer, which will be determined based on CPT data. Since the tapering is a function of the length of the pile and the diameters it will automatically also vary. Where possible, the distributions that are used for the parameters are based on the two data sets that were described in paragraph 2.2. It is assumed here that similar piles were used under bridges and under houses. The distributions will be described in more detail later. As mentioned in paragraph 2.3 the bearing capacity is made up of two components; shaft resistance and base resistance. The shaft resistance can be further divided into shaft resistance in the sand layer and shaft resistance in the soft layers overlying the sand layer.

Base resistance

The base resistance is determine using equations 4.1 to 4.2. The variation of D_t will influence both the area A_b and $q_{b,max}$, the variation of the depth of the pile tip will only affect $q_{b,max}$.

$$R_{base} = A_b \times q_{b,max} \tag{4.1}$$

Where :

$$q_{b,max} = \frac{1}{2} \times \alpha_p \times \beta \times s \times (\frac{q_{c,I,gem} + q_{c,II,gem}}{2} + q_{c,III,gem}) \tag{4.2}$$

R_{base} = The resistance of the pile tip [kN]
A_b = The area of the pile tip [m^2].
α_p = Factor for pile tip capacity, equals 1.0 because an existing structure is regarded.
β, s = Factors for the shape of the pile tip, both equal 1 for round pile tips according to NEN 9777-1.
$q_{c,I,gem}$,$q_{c,II,gem}$,$q_{c,III,gem}$ = Averages of the cone resistance 8D above and 4D below the pile tip, as explained in paragraph 2.3.

Shaft resistance

The shaft resistance is calculated using equations 4.3 to 4.5. The shaft friction in the sand and in the soft layers is calculated using the same formulas, for the shaft friction in the sand layer the integral goes from the top of the sand layer to the tip of the pile, while for the shaft friction in the soft layers the integral goes from the head of the pile to the top of the sand layer. Since the pile is tapered, the circumference of the pile, O, is also a function of the depth. The variation of the embedment of the pile will only influence the shaft capacity in the sand layer, the shaft capacity in the soft layers will be independent of the embedment of the pile. The diameter at the tip of the pile influences both shaft frictions, while the diameter at the head of the pile will mostly influence the shaft friction in the soft layers. There will be a small effect of the diameter at the head of the pile noticeable in the shaft friction in the sand layer, mostly due to the tapering and therefore the area of the pile in the sand layer.

$$R_{shaft} = O_{s,z} \times \int_a^b q_{s,max,z} dz \tag{4.3}$$

where:

$$q_{s,max,z} = q_c \times \alpha_s \times \alpha_{red} \tag{4.4}$$

and:

$$O_{s,z} = \pi(D_{head} - \int_a^b T dz) \tag{4.5}$$

a,b = The range from the pile head to the top of the sand layer, or the range from the top of the sand layer to the pile tip in the case of friction in the soft layers and friction in the sand layer respectively. Where 0 is the head of the pile, and L is the tip of the pile.

D_{tip} = The diameter at the tip [m].
T = Tapering of the pile in mm/m
q_c = The value of the cone tip resistance where all values must be cut off at 12 MPa, unless the thickness of the layer with cone resistance exceeding 12 MPa is more than 1 meter. In that case the cone tip resistance must be cut off at the value that occurs over the one meter with a maximum of 15 MPa.
α_s = The factor for shaft resistance, varies for different soil types. The values for α_s according to NEN 9777-1 are shown in table 2.4. It is assumed here that enough displacement occurs to mobilise the full shaft friction in each soil type.

Figure 4.3 shows the parameters that are used in the Monte Carlo analysis and from which parameters can be determined (dotted lines). Due to the tapering, three dimensions are needed to describe the shape of a timber pile: the length, the area at the head or at the tip and the amount of tapering. The relation between these parameters will be described later.

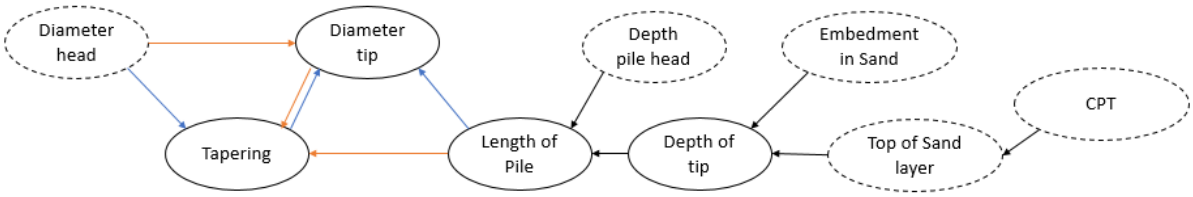

Figure 4.3: Pile Parameters

Length of the pile
The top of the sand layer can easily be determined based on CPT data. This, minus the embedded length in the sand layer results in the depth of the pile tip. The embedment in the sand layer will be picked randomly from a distribution, which will be described later. The depth of the pile head will be kept constant since it is not expected to have a major influence on the piles bearing capacity as it only influences the shaft friction in the Holocene layer. The depth of the pile head is set to 2 meters below the greenfield, which is equal to the required depth below the groundwater table. From these parameters the length of the pile can be determined. The data for pile lengths in Amsterdam from chapter two is not used here, because randomly picking a length from the distribution would likely result in unrealistic values for embedment of the piles in the bearing layer.

Embedment in First Sand layer
As described in chapter two, the embedment in the sand layer has unfortunately not been captured during the extraction of the piles in the data set. Therefore, it is necessary to make some assumptions regarding the distribution of this parameter. It is assumed that all values for the embedment lie between 0.25 and 0.75 meters with the peak lying at the value of 0.5, which is the value which the municipality of Amsterdam uses for all piles. It is assumed that the embedment cannot be more than 0.75 meters because the technology of the time did not allow for deeper pile driving. It is also assumed that no piles have a smaller embedment than 0.25 meters, because these piles would have such low bearing capacities that they would have failed over the years. All in all, a truncated normal distribution (figure 4.4) with boundaries set at 0.25 and 0.75 is used.

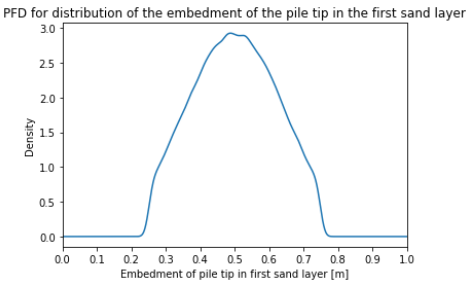

Figure 4.4: Probability Density Function of pile embedment in the first sand layer

Diameters

Next, the diameter at the head and the tip and the tapering have to be determined. There are two ways to describe the parameters, shown by the orange and the blue arrows in figure 4.3. Either a correlation is used to determine the tapering from the diameter at the head and subsequently calculate the diameter at the tip using equation 4.6, or the other way around.

$$D_{tip} = D_{head} - T \times L \tag{4.6}$$

Where:
D_{tip} = Diameter at the tip of the pile in mm
D_{head} = Diameter at the head of the pile in mm
T = Tapering of the pile in mm/m
L = Length of the pile in m

To determine which of these two relations show the strongest correlation the pearsons number, or correlation coefficient, was calculated. This coefficient was equal to 0.45 for the relation between the tapering and the head diameter and is 0.73 for the relation between the tip and head diameter. This indicates that relating the two diameters to each other and subsequently calculating the tapering would give the most accurate results. Figures 4.5a and b show both parameter relations and the linear regression fit line of the two data sets. Data set 1 is the data which was gained from extracted piles from the Dapperbuurt test (*Dataset extracted piles Dapperbuurt* (2018)) and data set 2 are the piles that are extracted in the southern district of Amsterdam *Dataset extracted piles Frans Sas* (2018). From the figures it is already visually apparent that the two diameters show the better correlation. Therefore, this is used for the generation of random pile parameters.

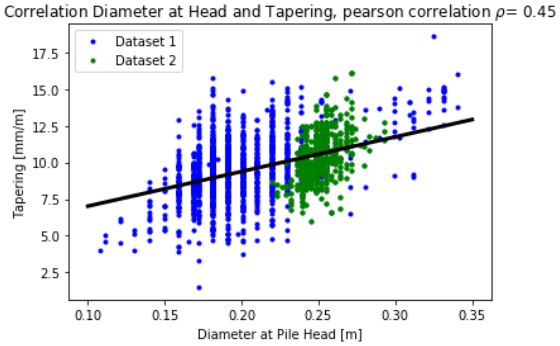

(a) Relation between Diameter at the Head and the Tapering

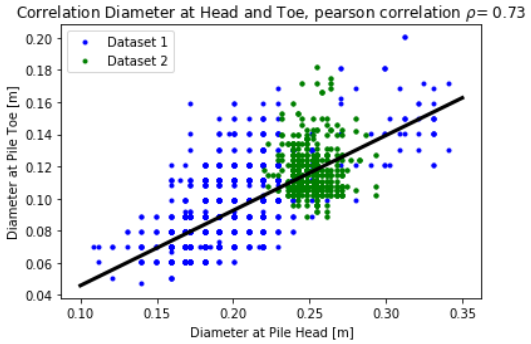

(b) Relation between Diameter at the Head and Diameter at the tip

Figure 4.5: Analysis of the relation between the parameters

Since the diameter at the head and at the tip are multivariate random variables, a generating method has to be used which ensures that the generated diameters show the same correlation as the one that is found in the data sets. Therefore it is decided to make use of Cholesky Decomposition as described in Thomopoulos (2012). Using two independent normal distributions, X_1 and X_2, both with $\mu = 0$ and and $\sigma = 1$, the random values of both the tip diameter and the diameter at the head are computed using equations 4.7 and 4.8 . Note that random value X_1 is the same for both equations.

$$D_{head} = \sigma_{Dhead} \times X_1 + \mu_{Dhead} \tag{4.7}$$

$$D_{tip} = \sigma_{Dtip} \times (\rho \times X_1 - \sqrt{(1-\rho^2)} \times X_2) + \mu_{Dtip} \tag{4.8}$$

Where:

D_{head} = The randomly picked value of the tip diameter
μ_{Dhead} = Mean value of the head diameter from the data set, equal to 0.2175 m
σ_{Dhead} = Standard deviation of the head diameter from the data set, equal to 0.03595 m
D_{tip} = The randomly picked value of the tip diameter
μ_{Dtip} = Mean diameter at the tip of the pile from the data set, equal to 0.100 m
σ_{Dtip} = Standard deviation of the tip diameter from the data set, equal to 0.0230 m
ρ = The correlation coefficient (pearsons correlation) found from the linear regression, equal to 0.73

Using this method leads to generated data which matches quite well with the data from the data set. The distributions of both the data sets and the generated data are shown in figure 4.6a. The tapering that corresponds to each data point is calculated using the length that is determined based on the embedment and the depth of the sand layer. Since this differs for each location, the distribution of the tapering also differs per location. Figure 4.6b, shows the distribution of the tapering from the data set and that is generated for locations 1 and 2. It shows that the tapering matches slightly better with the data set on location 2 than on location 1, this has to do with the fact hat the length of the piles differ on both locations. On location 1, the generated lengths of the piles range between 10.34 and 10.84 meters. Since the first sand layer is located deeper, while the greenfield is at a similar height, the length of the piles on location 2 range between 11.61 and 12.11 meters. Since the generated values for tip and head diameters doesn't change between the two locations, the smaller length causes the tapering on location 1 to be slightly larger.

Figures 4.6a and b have also been computed for the case where tapering and the head diameter are generated, and the tip diameter is calculated. These are shown in appendix B and show that the chosen approach has better results.

Some random numbers are generated with a tip diameter which is smaller than 0. Since this is physically impossible it is necessary to disregard all the randomizations which have tip diameters which are smaller than 0 cm. Logically, data points are also generated which have extremely low tip diameters, for example those ranging between 1 mm and 2.5 cm. It is decided to not consider generated points with a tip diameter smaller than 2.5 cm. This because it is likely that if such small diameters did occur, these piles would have failed already due to extremely low bearing capacities, also the smallest diameter that is encountered in the data sets has a tip diameter of 5 cm.

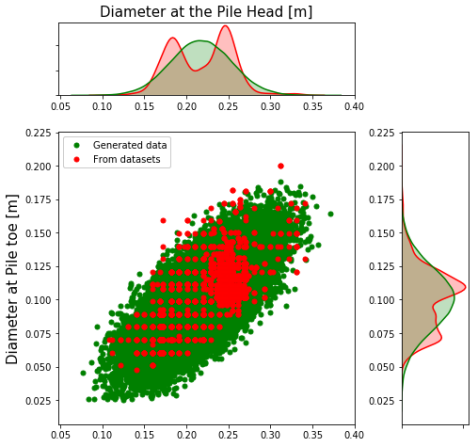

(a) Distributions of generated data and dataset

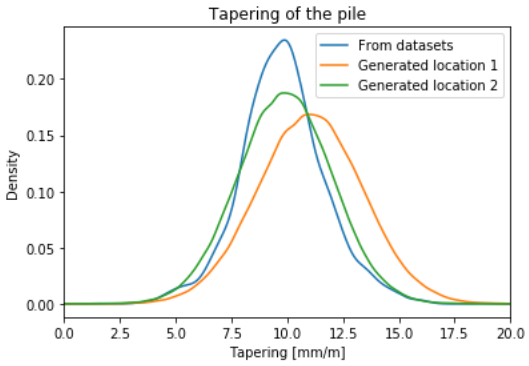

(b) PDF for tapering on two locations and from dataset

Figure 4.6: Results from Cholesky decomposition

4.1.3. Pile Degradation

To study the impact that pile degradation has on the bearing capacity, an extra variable was added to the analysis. The lab tests, described in the previous chapter appeared to show that degradation of the wood structure caused no clear reduction in shaft friction, but the presence of a slime layer did. Since, however, many more tests have to be performed on various degrees of degradation, soil types and stresses, the results from the Dapperbuurt tests are used to base the reduction factor on.

From the Dapperbuurt tests it became apparent that wood degradation of timber piles only led to a decrease in the pile's shaft resistance. Based on load-displacement curves this was quantified to be a reduction

of 40%. Therefore the factor α_{red}, which ranges from 1 (no reduction) to 0.6, was introduced. This factor was applied to both the shaft resistance in the sand layer and in the soft layers for positive as well as negative skin friction. Since nothing else is known about this reduction, a uniform distribution is assumed.

In practice, a reduction of the diameter is sometimes used to account for a reduction in skin friction due to bacterial degradation. This has not been done in this analysis, as is makes no physical sense that the shaft area of the pile would reduce due to bacterial degradation. Note that this reduction of the diameter is also used when assessing the wood strength of a cross section. In this case a reduction of the effective diameter is justified as this part of the cross section is unable to contribute to the material strength of the cross section.

4.1.4. Calculation of the maximum geotechnical bearing capacity

As described in chapter two the maximum geotechnical bearing capacity consists of two components; the base resistance and the shaft resistance. The total bearing capacity consists only of the base resistance and the shaft resistance which is generated in the bearing sand layer. If the load on the pile exceeds the bearing capacity generated by the tip and the friction in the sand layer, the pile will settle. Due to the settlement, the location of the neutral point will move upward, leading to additional shaft friction being generated in the soft soil layers. Settlement will continue to occur until a new equilibrium is reached. If the load is increased again, the neutral point will shift further upwards, this can continue to occur until the neutral point has reached the pile head, and the shaft friction in the soft layers is fully mobilized. This resistance is referred to as the ultimate bearing capacity. In practice this situation should never occur, because the pile would have failed.

In this analysis both cases are regarded, so for each pile a calculation is made of the base resistance, shaft resistance in the sand layer and shaft resistance in the holocene (soft) layers. The base resistance is calculated using the Koppejan method and the shaft friction in the sand layer is calculated using the CPT based method, both in accordance with NEN 9777-1 (Normcommissie 351 006 "Geotechniek" (2016)). The results of these have been verified using the D-foundations program.

CPT interpretation in the soft layers

The shaft friction in the soft Holocene layers is determined in two ways. Firstly, using the slip method and secondly using a cpt based method. The interpretation of the layering and the corresponding unit weights are given in Appendix B. The CPT based method uses the α_s factors for peat, clay and silty sand as given in NEN 9777-1 (Normcommissie 351 006 "Geotechniek" (2016)). The determination of the various soil types is done using the CPT data, the normalized IC-method by Robertson (2009) and the Robertson (1990) $Q_t - F$ chart. Even though the $Q_t - F$ chart has 9 different soil type zones, it is decided that in this case the only soil types that are distinguished are sand, clay, peat and silty sand. Which is in accordance with the soil types for which α_s factors have been defined in the NEN.

Since it was found that the method does not perform well on identifying peat Holocene peat layers, as is also reported by Młynarek, Wierzbicki, and Bogucki (2015). It was decided to use an additional criterion, where if Fr>5 a layer is also identified as peat. Table 4.1 gives an overview of the interpretation and the corresponding α_s factors.

Soil type	Identification	α_s
Sand	IC < 2.05	0.012
Silty Sand	2.05 > IC > 2.6	Friction number with a maximum value of 0.025
Clay	IC > 2.6	0.02
Peat	Fr > 5 or IC ≥ 3.5	0

Table 4.1: α_s and identification criteria for the different soil types

Figure 4.7 shows the cone resistance, the friction number and the IC number with interpretation of the soil layers on the left, and the expected lithography from the GeoTop model (*DINOloket* (2019b)) on the right. Figure 4.8 shows the same for location 2. Both interpretations show good agreement with the expected lithography from the GeoTop model.

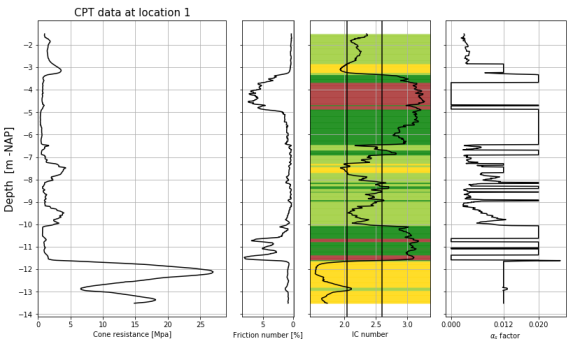

(a) CPT data and interpretation on location 1 with deviation from the IC method

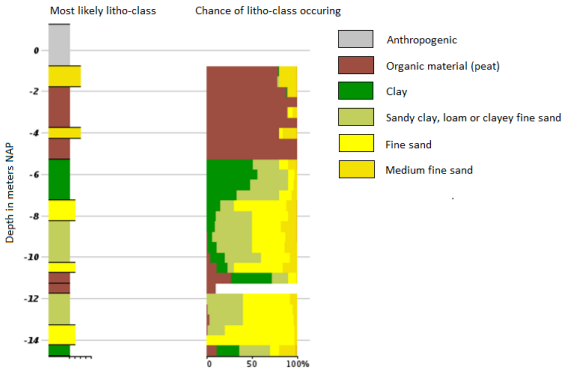

(b) Lithography according to the GeoTop model, after *DINOloket* (2019b)

Figure 4.7: Lithography according to the GeoTop model and CPT interpretation using IC method

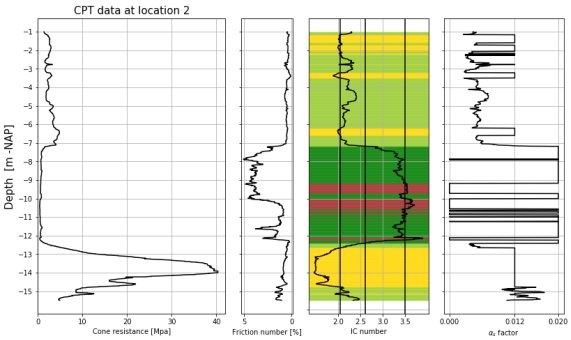

(a) CPT data and interpretation on location 2 according to the IC method on location 2

(b) Lithography according to the GeoTop model, after *DINOloket* (2019b)

Figure 4.8: Lithography according to the GeoTop model and CPT interpretation using IC method

Slip vs. CPT method

First, a choice has to be made on whether to use the slip method, the CPT method or an average of the two to describe the shaft friction in the soft layers. On location 1 the slip method and the CPT method give very similar results, as can be seen from figure 4.9a. Since the two methods do not differ a lot, it is chosen to use the results of the CPT method in the analysis. This is done because this method is based on in-situ data, which is considered more reliable than the data which is used as input for the slip method.

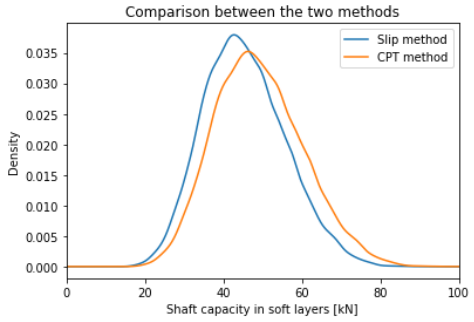

(a) Location 1

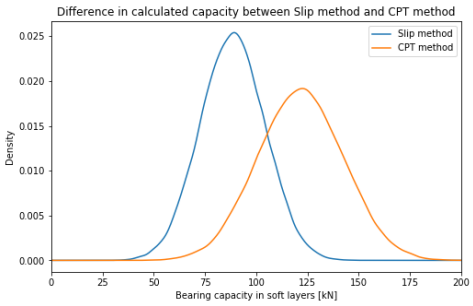

(b) Location 2

Figure 4.9: Difference in resulting shaft capacity using the slip method and the cpt method on location 1 and 2

On location 2 the difference between the two methods is much bigger than on location 1, as can be seen from figure 4.9b. This might be because, as mentioned in chapter 2, the CPT based method tends to overes-

timate the bearing capacity in the shallow layers, while the slip methods tends to overestimate the resistance in the deeper layers. On location 1 the two methods balanced each other out because sandy layers which provide resistance occurred over the whole depth (figure 4.10a). On location 2 however, all the layers which provide some resistance are located very shallow, while the deep layers hardly provide any resistance (figure 4.10b). Due to this, the overestimation of the CPT method might be more pronounced. Furthermore, since the tapering of the pile causes it to have most of its area in the more shallow layers, this is even more exaggerated. It is decided to use an average value of the two methods. This is chosen because it is acknowledged that the CPT method might have resulted in an overestimated value, but since it does take into account the shallow sand layers better it will not be disregarded.

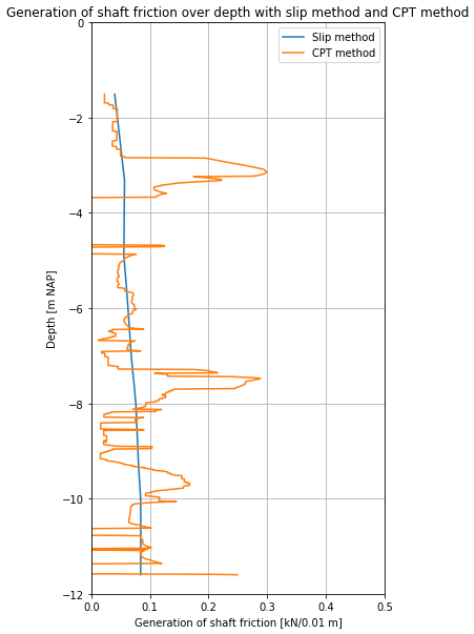

(a) Location 1

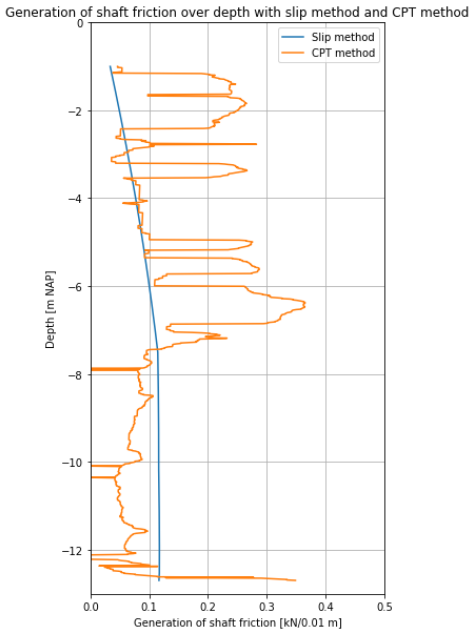

(b) Location 2

Figure 4.10: Generation of shaft friction over depth using the slip method and the cpt method on location 1 and 2

Neutral Point and axial load

For both locations a calculation based on the set of assumptions that the municipality uses is made. For this reference pile the development of the axial load and the neutral level in the pile is shown. This is done purely to give an idea of what happens on the different locations and when α_{red} factor is applied.

Since the purpose of this is only to get a crude idea of what happens, some simplifications have been made. The calculation of the location of the neutral point is only based on the equilibrium between the forces that work on the pile (equation 4.9).

$$R_{base} + R_{shaft,sand} + R_{shaft,pos} - F_{shaft,neg} - F = 0 \tag{4.9}$$

Where:
R_{base} = The base Capacity in kN
$R_{shaft,sand}$ = The shaft capacity generated in the bearing sand layer in kN
$R_{shaft,pos}$ = The shaft capacity generated in the soft layers below the neutral point in kN
$R_{shaft,neg}$ = The shaft capacity generated in the soft layers above the neutral point in kN
F = The external load on the pile head

The pile is assumed to be infinitely stiff, so no deformations occur in the pile itself. No calculations have been made regarding the settlement of the pile that has to occur to move the neutral point upwards. Also, only the maximum positive and negative skin frictions are used, the transition zone where positive skin friction turns into positive skin friction is not regarded. Furthermore, the time dependency of the processes is not taken into account. In reality, both the negative skin friction and bacterial degradation develop over time, the way these two develop relative to each other also influences the location of the neutral point.

4.2. Results

In this section the results of the Monte Carlo analysis will be discussed, in this first part the α_{red} factor is not included yet. First, all the components and how they vary with depth and tip diameter are discussed. Next, their relative contribution to the total and ultimate capacities and how this is influenced by the depth of the pile tip and the tip diameter is shown in figures 4.15 and 4.16. Lastly, it is shown how knowing the value of one parameter can influence the uncertainty of the outcome. This is first done for location 1, after which the differences between location 1 and 2 are highlighted. Besides the Monte Carlo analysis, calculations have been made using the assumptions that are used by the municipality of Amsterdam. These are then compared to the findings from the analysis to see how the assumptions and their outcomes compare to the values found from the analysis. All the reported values are calculation values, meaning that both safety factors ξ and γ have been applied.

Some of the results are shown in box and whisker plots, the upper half of the box plot shows the shaft resistance in sand and the base resistance, which make up the total resistance. The lower half shows the shaft resistance in the soft layer and what changes when this is also taken into account. The box and whisker plots show 5 data points; the line in the centre of the box signifies median value, the left and right edges of the box are Q1 and Q3 meaning that 50% of all the values fall within the range of the box. The whiskers signify the minimum and maximum values that occur, these are defined as 1.5 * IQR - Q1 and 1.5* IQR + Q3 respectively. The data may contain outliers, which are not shown in the figures below to make them more clear, the box and whisker plots which do include the outliers are shown in Appendix B.

4.2.1. Location 1

Figure 4.11 shows the difference in total and ultimate bearing capacity on location 1 if every parameter is unknown. Figure 4.11 shows how the three components contribute to the total and ultimate bearing capacities. Of the three components, the base capacity is able to contribute most to the bearing capacity of the pile.

The amount of base capacity that can be generated, however, is very uncertain if nothing is known about the diameter and the embedment. Depending on these parameters, the minimum and maximum base capacities are equal to 4.5 kN and 151 kN. It has to be noted that this smallest base capacity occurs in the case where the tip diameter is equal to 2.5 cm, such small diameters have not been encountered yet. The base capacity for the smallest encountered tip diameter (4.7 cm) is 15.6 kN.

The shaft resistance in the sand layer has a much lower contribution: ranging from 1.6 kN to 31.8 kN, with the mean value lying at 12.9 kN. The shaft friction in the soft soil layers can provide quite a lot of additional resistance once the total bearing capacity of a pile is exceeded, as can be seen from 4.11. The additional shaft friction that can be generated from the soft soil layers lies between 12.6 and 63 kN.

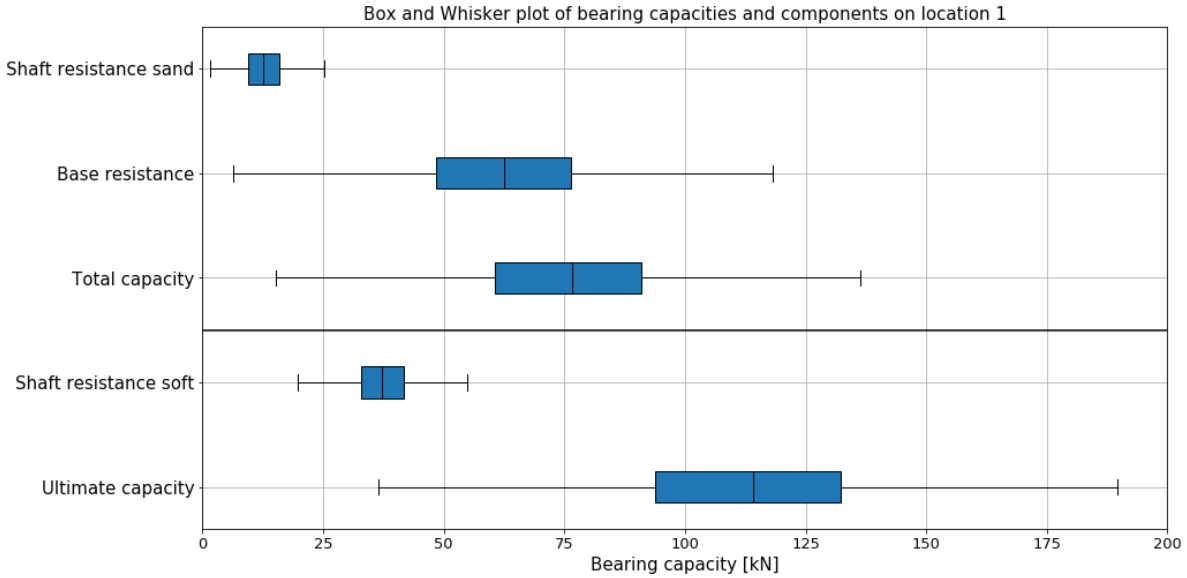

Figure 4.11: Box and whisker plots bearing capacity components on location 1

Figure 4.12 shows how the embedment of the pile and the diameter at the tip influence the two com-

ponents of the total bearing capacity. The highest resistance in the sand layer is mobilised by a pile with a large tip diameter with a large embedment. This makes sense as a pile with a larger area in the sand layer can generate more resistance. The base resistance is obviously also influenced by the diameter at the pile tip. Furthermore, the higher base capacities are found at smaller embedments of the pile tips. This is due to the small thickness of the bearing sand layer. If the tip of the pile is lowered, the 4D range of the koppejan method falls below the bearing sand layer, causing the capacity to drop dramatically.

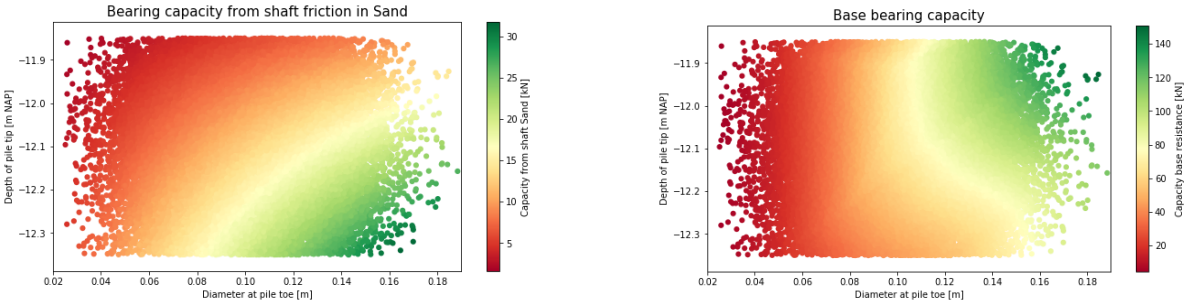

(a) Shaft resistance from sand layer

(b) Base resistance

Figure 4.12: Shaft resistance in sand and base resistance for all tip levels and tip diameters

Since the shaft capacity in the soft layers is not influenced by the depth of the pile tip, these results are shown by the diameters at the head and at the tip (figure 4.13). As can be expected the highest capacities are from piles with large tip and head diameters, again because these have most area.

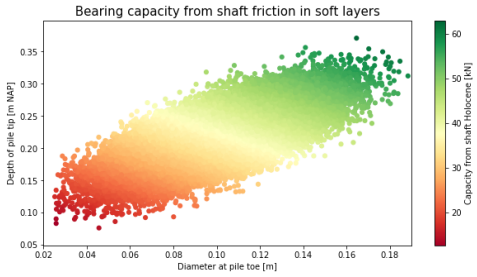

Figure 4.13: Shaft capacity from the soft layer for all head and tip diameters

Since the base capacity and the shaft capacity in the sand both have either the minimum or the maximum embedment as an advantage, these are more or less balanced out, with the tip resistance having a slightly larger influence. This is shown in figure 4.14a, leaving the diameter at the tip as the most crucial parameter. In figure 4.14b, the same can be seen, as well as the influence of the shaft capacity in the soft layers.

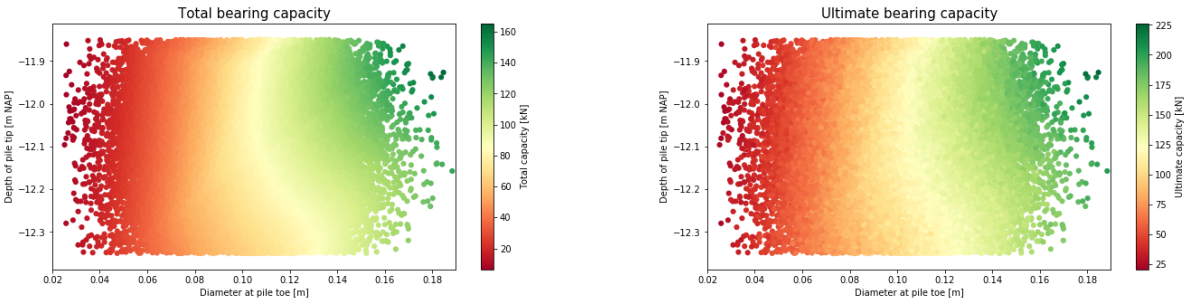

(a) Total capacity

(b) Ultimate capacity

Figure 4.14: Total and ultimate capacities for all tip levels and tip diameters

In figure 4.15 the contributions of the three components to the total (left) and ultimate (right) bearing

capacity are regarded at a depth of -12.1 meters NAP. Figures are given for both the total and the ultimate bearing capacity, and as a percentage thereof. The results are sorted by the diameter at the tip, which leads to an increase in resistance with increasing tip for the base capacity and the shaft capacity in sand. But since the diameter at the head has a large influence on the shaft friction in the soft layers, an increasing tip diameter does not always lead to an increasing bearing capacity. This is the reason for the blur that can be seen in figures b and d.

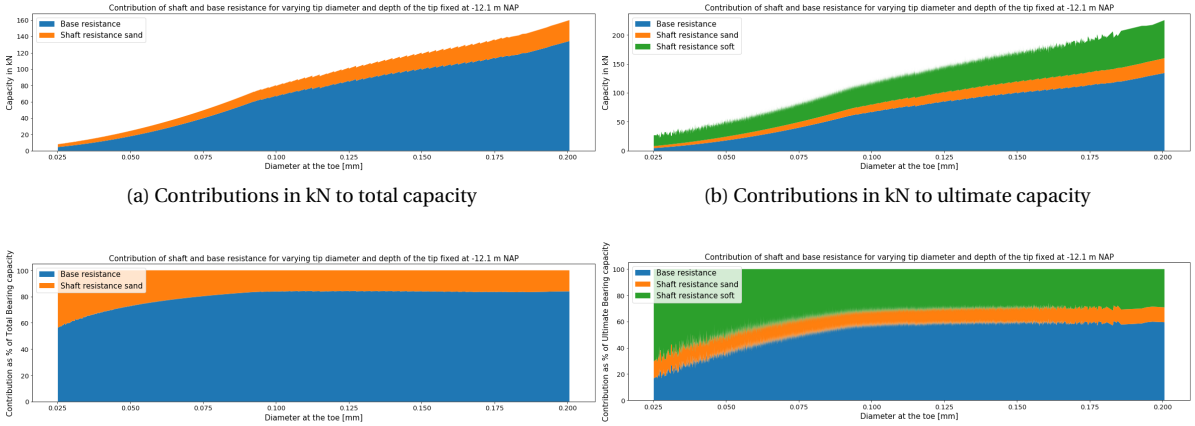

(a) Contributions in kN to total capacity

(b) Contributions in kN to ultimate capacity

(c) Contributions as percentage of total capacity

(d) Contributions as percentage of ultimate capacity

Figure 4.15: Contributions of the components for a fixed depth of -12.1 meter NAP and increasing tip diameter

Figures a and c show that the total capacity depends highly on the diameter at the tip of the pile. From the smallest to the largest diameters the total capacity increases from 8 kN to 160 kN. Both the shaft resistance in the sand layer and the base capacity increase with increasing tip diameter, leading to a constant contribution of approximately 20% shaft capacity and 80% base capacity for all pile tip diameters from 0.1 to 0.2 meters. From 0.025 to 0.1 the contribution of the shaft capacity is larger than that of the base capacity.

More or less the same can be seen from figures b and d. The ultimate capacity increases linearly with increasing diameter and from 0.1 m tip diameter on wards all components deliver a constant contribution of 30% shaft friction in the soft layers, 60% base resistance and 10% shaft friction from the sand layer.

The same can be done for varying embedment depths while the diameter of the tip is kept at a constant diameter of 0.1 meters (figures 4.16 a to d).

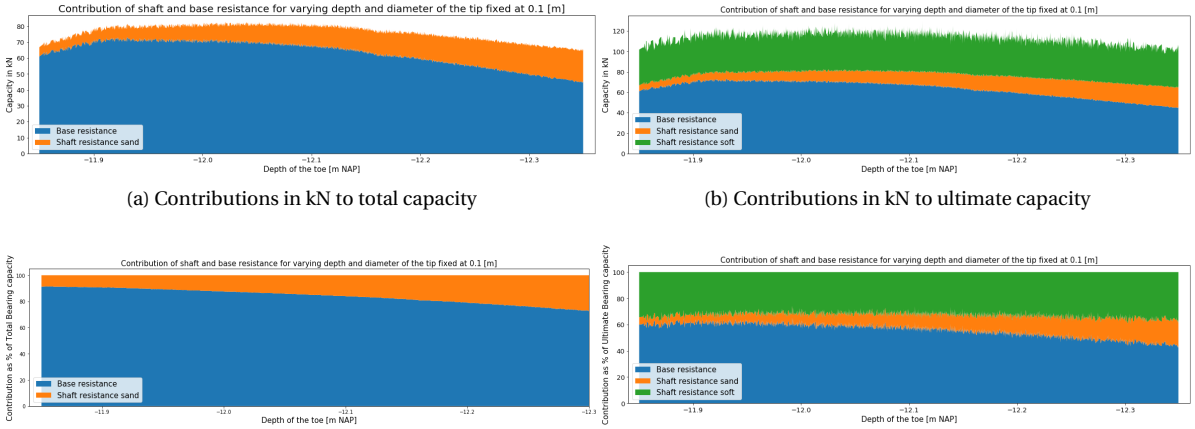

(a) Contributions in kN to total capacity

(b) Contributions in kN to ultimate capacity

(c) Contributions as percentage of total capacity

(d) Contributions as percentage of ultimate capacity

Figure 4.16: Contributions of the components for a fixed tip diameter of 0.1 m and varying depth

Since the sand layer on this location only has a small thickness, piles with more embedment have a smaller base capacity due to the 4D range of the koppejan method falling below the sand layer. Since the shaft ca-

pacity in the sand layer increases with depth, while the base capacity decreases with depth, the percentage of the total capacity that is generated from the shaft friction in the sand layer becomes bigger with depth, going from 10 % to 30%.

Influence of knowing variables on uncertainty

It is studied what the effect on the uncertainty is if certain pile parameters are known. The three parameters that are regarded are the depth of the pile tip, the diameter at the head and the diameter at the tip of the pile. Due to the manner at which data is generated in this Monte Carlo analysis, looking at a fixed value for the diameter at the head of the pile, still results in a range of diameters at the tip of the pile. This is shown in figure 4.17 where the blue data points show the range of tip diameters that occur when the diameter of the head is set to its mean value. The yellow data points show that range of head diameters that occur when the diameter at the tip is set. This range is purely to show the difference in effect between knowing the head versus the tip diameter. It is realised that it is not realistic that one would know the value for the tip diameter while not knowing the head diameter.

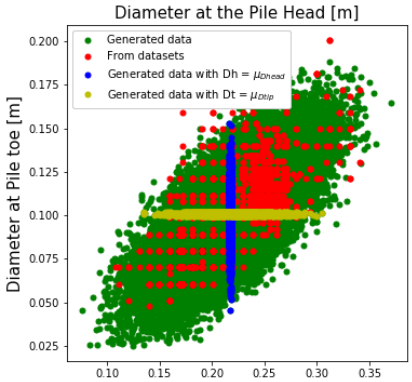

Figure 4.17: Data points of the tip and head diameter for when D_h or D_t are fixed

Figure 4.18 shows box plots of all the three components plus the total and ultimate capacities for the case where all the parameters are uncertain in blue and for the case where the depth of the pile tip is set at -12.1 meters NAP in green. From this figure it can be seen that knowing the exact depth of the tip of the pile does not significantly decrease the range of outcomes of the total bearing capacity. The range of the shaft friction in the sand layer and base capacity decrease slightly. The uncertainty of the shaft resistance in the sand layer has slightly decreased, the value of the mean remains at 12.9 kN. The distribution of the base resistance has become more narrow since all the highest and lowest base resistances occur at most deep and most shallow depths. The mean value has increased from 62.6 to 64.7 kN. The shaft resistance in the soft layers is not affected at all by the depth of the pile tip. A slight increase in the total and ultimate capacities are observed, mostly due to the increase in base resistance.

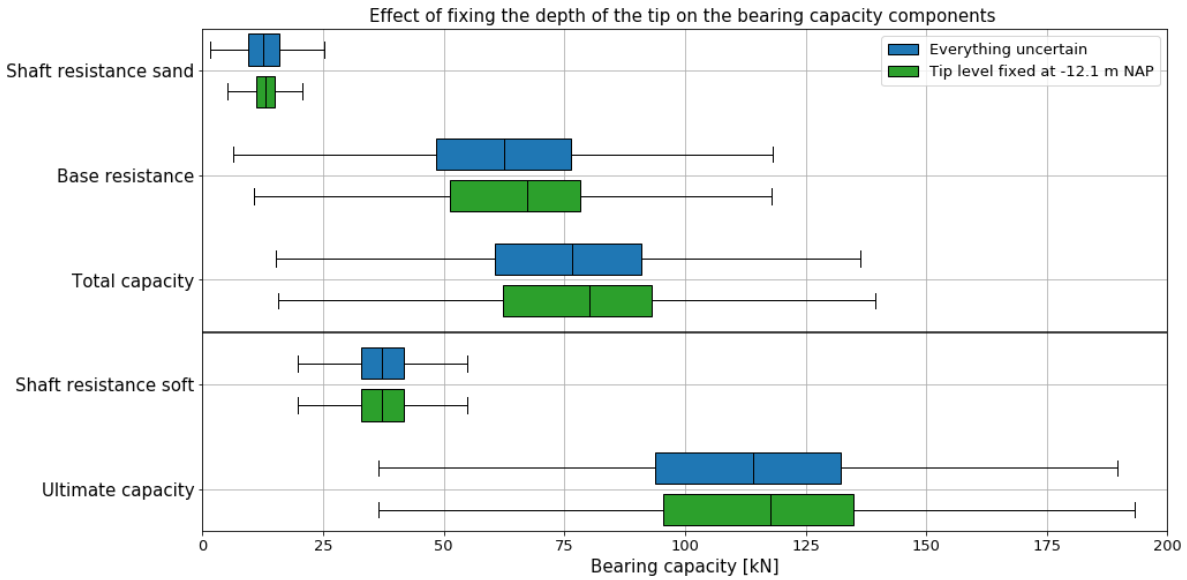

Figure 4.18: Box and Whisker plots for all bearing capacity component with all parameters uncertain and with the tip level set to -12.1 m NAP

Next, the diameter at the head of the pile is fixed at its mean value of 0.217 meters, the effect of this is shown in figure 4.19. It immediately becomes clear that this parameter has a much bigger effect than fixing the depth of the tip had. All components show at least some decrease in the range of results when the diameter at the head of the pile is fixed. There is a slight decrease in the range of the resistances in the sand layer, the reason for the decrease in uncertainty is that fixing the head diameter causes a limitation in the values that are generated for the tip diameter. So the decreasing range of tip diameters is actually responsible for the smaller range in capacities. The same applies to the much smaller range in base resistances. The effect on the resistance in the soft layers is much bigger because this component is affected directly by the diameter at the head of the pile. Both the total, and the ultimate capacities show a smaller range when the diameter at the head is set. The range of the ultimate capacity decreases more than that of the total capacity, due to the resistance in the soft layer which has now become more certain.

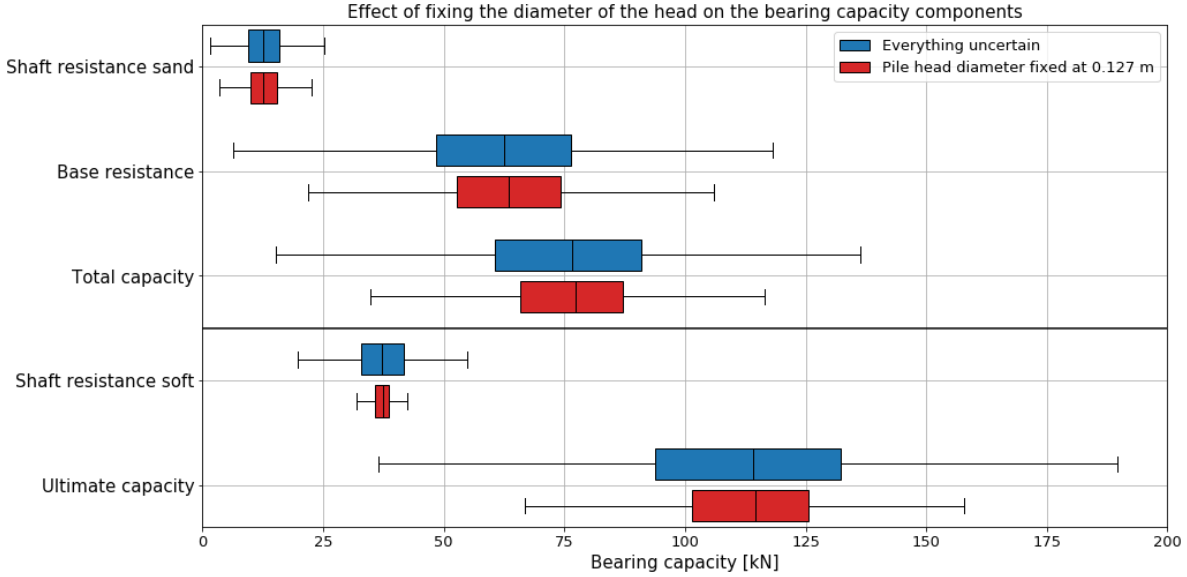

Figure 4.19: Box and Whisker plots for all bearing capacity component with all parameters uncertain and with the head diameter set to 0.217 m

Figure 4.20 shows the effect that fixing the value of the tip diameter has. Obviously, this is the parameters

that has the largest impact on all the components and thus on the total and ultimate capacities.

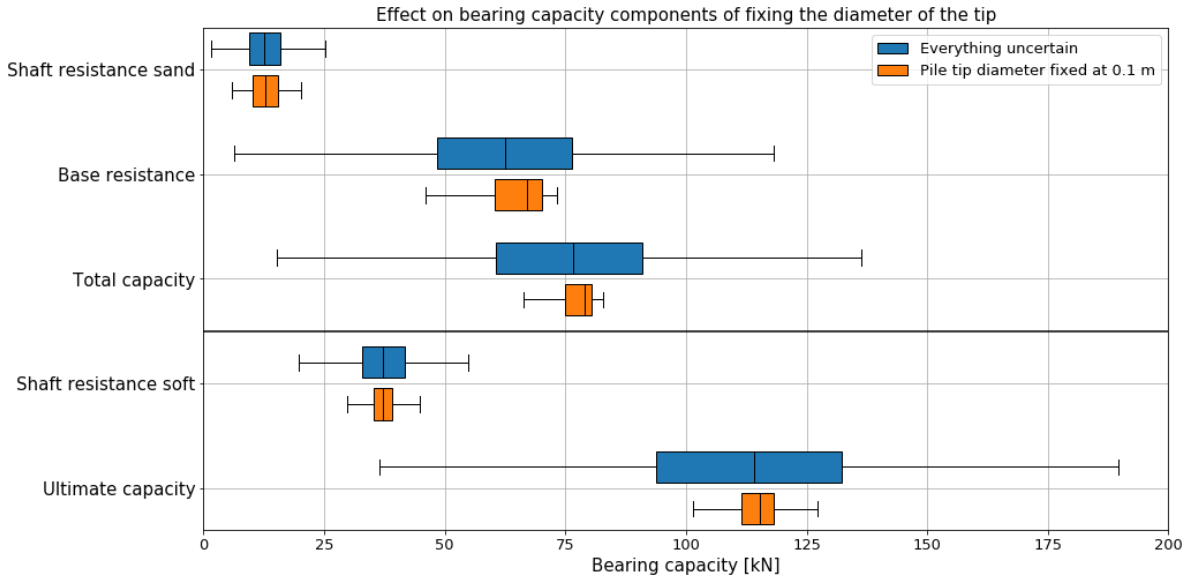

Figure 4.20: Box and Whisker plots for all bearing capacity component with all parameters uncertain and with the tip diameter set to 0.1 m

It also shows that knowing the diameter at the head of the pile is not nearly as effective as knowing the diameter at the tip of the pile in this case. Unfortunately, it is just not possible to measure the diameter of the pile tip without extracting the pile. Knowing the head diameter would, however, add much more value if the relationship between the diameters at head and tip is defined better. This would narrow down the range of tip diameters for a certain head diameter even more and therefore also decrease the amount of uncertainty.

Interestingly, the uncertainty of the shaft friction in the sand layer decreased more when the tip level was fixed than when the diameter is fixed. This shows that this component is affected more strongly by the embedment of the pile than by the diameter.

Reference Pile

The municipality of Amsterdam uses a set of pile parameters for calculation in the case that no pile and soil parameters are known, these were described in Chapter 2. The reference pile has an embedment of 0.5 m into the bearing sand layer, a head diameter of 0.25 m and a tapering of 8 mm/m. With the length of the pile being 10.6 meters, the diameter of the tip becomes 0.165 meters on this location. A calculation is made for this reference pile, which is checked against the other assumptions that are made.

The reference pile has a total bearing capacity of 137 kN, made up of 107 kN base resistance and 30 kN of shaft capacity from the sand layer. The assumed allowed bearing capacity of 100 kN is a safe assumption compared to the calculated value. Figure 4.21 shows the neutral level and axial load in the pile for loads equal to 100, 120, 140 and 160 kN. It can be observed that the neutral level shifts upwards about 1.5 meters between 100, 120 and 140 kN, while between 140 and 160 kN of load, the neutral point shirts upward 3 meters. This is explained by the two layers of wadsand, from which more resistance can be generated and the the three meters of relatively low cone resistances between -4 and -7 meters NAP from which little resistance is generated.

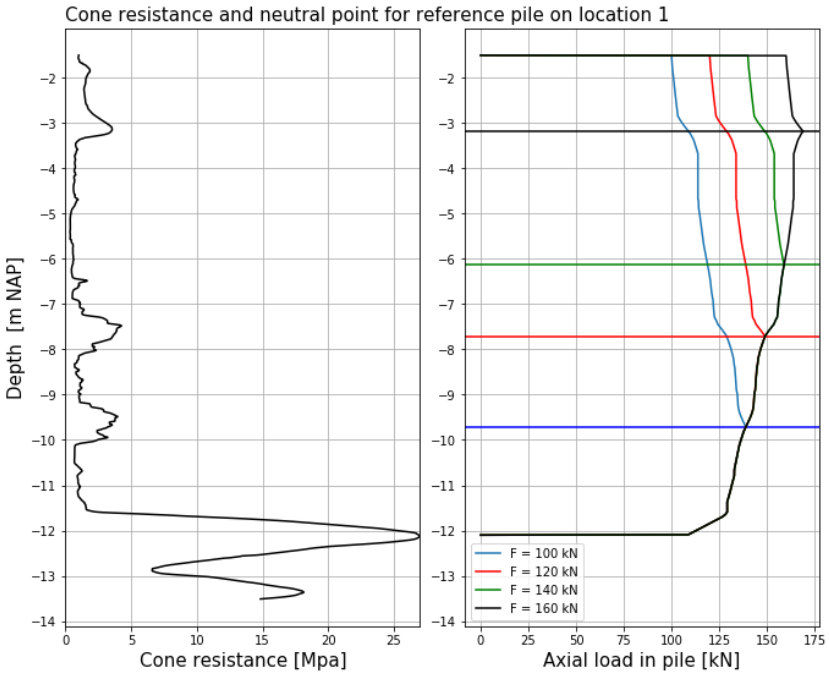

Figure 4.21: Neutral level and axial load in the reference pile on location 1

The calculated total capacity based on the set of assumptions from the municipality is much higher than the mean value that is calculated from the generated data which was equal to 75.5 kN (figure 4.11). This is due to the very large tip diameter that follows from the assumed pile parameters. The tip diameter of the reference pile is 0.165 meters, while the mean tip diameter from the data sets and the generated data equals 0.1 meters. For the mean tip diameter of 0.1 meters and embedment of 0.5 meters the total bearing capacity would have been 79.6 kN, in that case the 100 kN assumption would not be safe anymore.

4.2.2. Location 2

Since some aspects are the same for locations 1 and 2, the emphasis will be put on the main differences between the locations and what causes these differences. Figures that are similar on locations 1 and 2 will not be shown here, but are included in Appendix B.

Figure 4.22 shows the differences in the capacities of all the components between locations 1 and 2. The shaft friction in the sand increases slightly between locations 1 and 2, even though the amount of embedment into the first sand layer has remained constant. This slight increase is due to the thickness of the first sand layer; according to NEN 9777-1 (Normcommissie 351 006 "Geotechniek" (2016)) the value for q_c has to be cut off at 12 MPa, except when the layer has a thickness of over 1 meter, then the value of q_c may be cut off at a maximum of 15 MPa. The first sand layer on location 2 exceeds one meter and has a maximum q_c occurring over a full meter of 20 MPa, which is cut off at 15 MPa. While on location 1 the first sand layer has a thickness of only 0.75 meters at a qc of 15 MPa and has a maximum q_c over a thickness of 1 meter of 10 MPa.

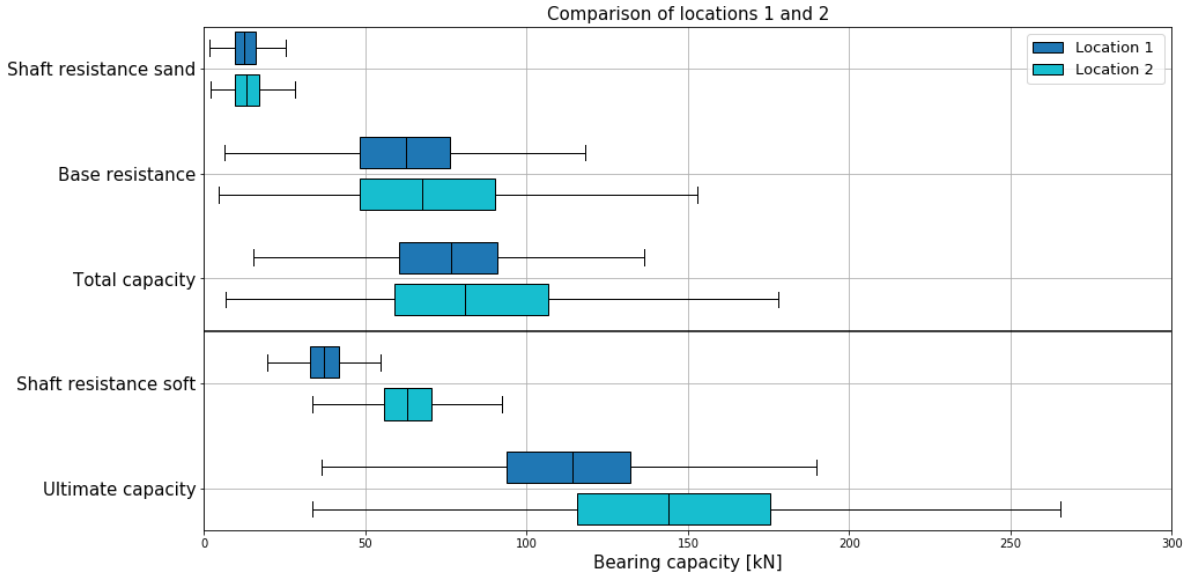

Figure 4.22: Box and Whisker plots for all bearing capacity component comparing locations 1 and 2

The increase in base resistance on location 2 is also due to this thick sand layer with high q_c values, this causes the $q_{b,max}$ to exceed 15 MPa more often than on location 1. This can best be expressed by figure 4.23 where the value for $q_{b,max}$ is shown for all tip diameters and embedments on both locations.

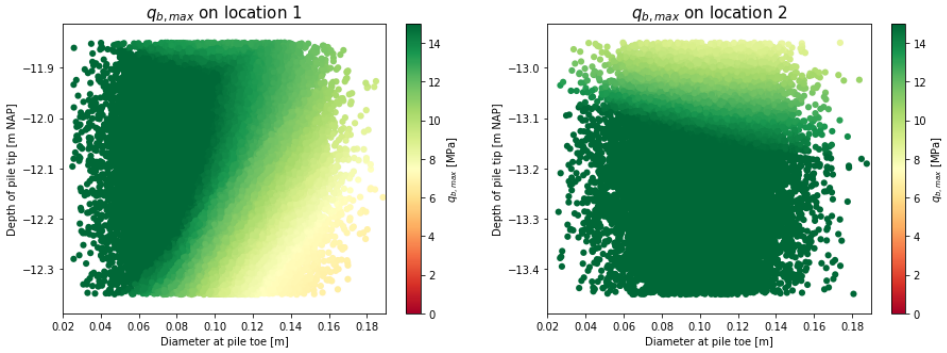

Figure 4.23: $q_{b,max}$ on both locations for all tip diameters and embedments

Due to the thin first sand layer on location 1, only piles with small diameters reach values for $q_{b,max}$ which exceed or equal 15 MPa, since these are all small diameters, this does not result in high values for the base capacity. Similarly, the lower $q_{b,max}$ values mostly occur at high embedment and large tip diameters, causing low values for the base capacity. This combination causes the relatively small spread of base resistances on location 1.

On location 2 however, the thickness of the first sand layer causes the $q_{b,max}$ values to become higher with depth, regardless of the diameter at the pile tip. So high and low $q_{b,max}$ values occur for both large and small tip diameters, leading to a bigger spread on location 2 compared to location 1. Since the value for $q_{b,max}$ has to be limited at 15 MPa according to the NEN, the base capacity does not increase anymore over the last 0.3 meters, as is also shown in figure 4.24a. In this case, the base resistance remains constant at about 70 kN.

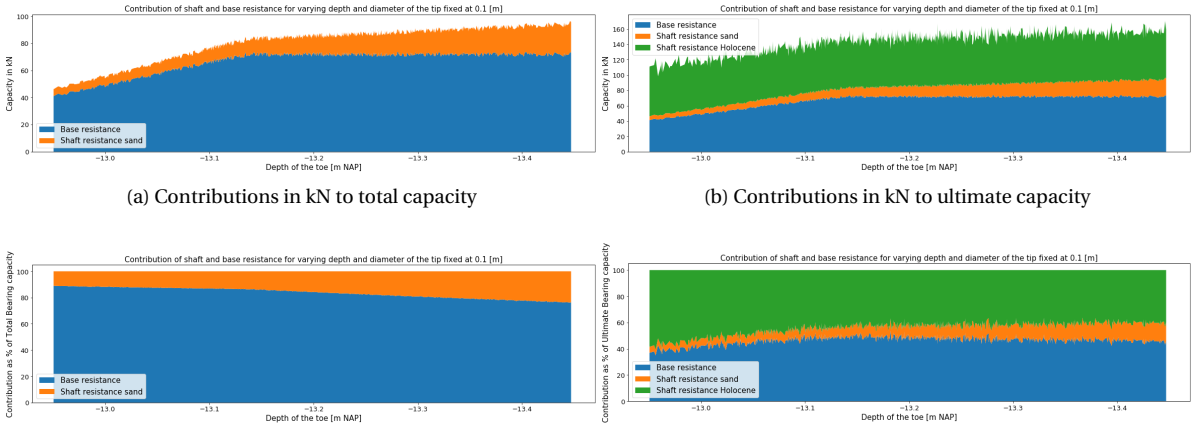

(a) Contributions in kN to total capacity

(b) Contributions in kN to ultimate capacity

(c) Contributions as percentage of total capacity

(d) Contributions as percentage of ultimate capacity

Figure 4.24: Contributions of the components for a fixed tip diameter of 0.1 meter and increasing depth of the tip on location 2

Since the $q_{b,max}$ remains constant at a depth of -13.2 meters NAP, the quadratic increment of the base capacity is more clear on this location than it was on location 1, as can be seen from figure 4.25. Both shaft resistances increase linearly with increasing tip diameter. Therefore the relative contribution of the base resistance becomes bigger with increasing tip diameter.

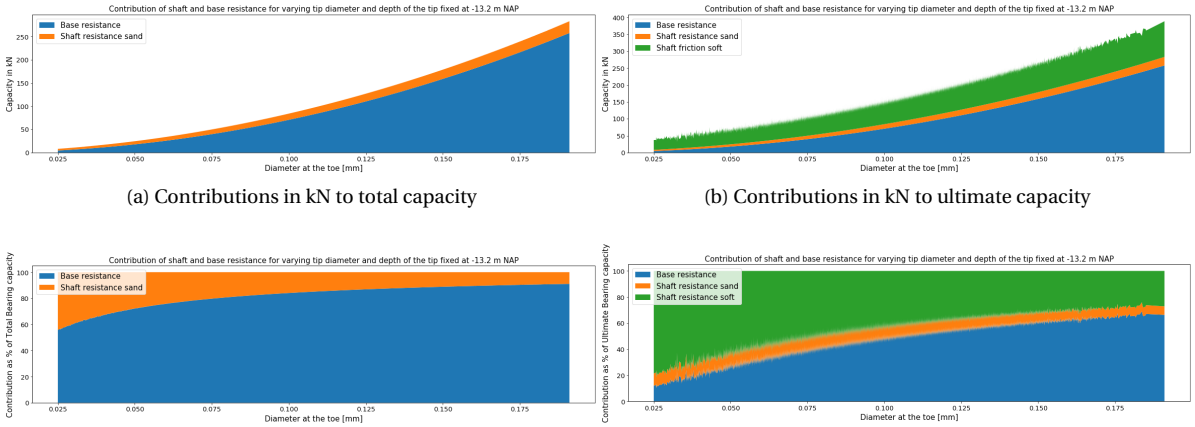

(a) Contributions in kN to total capacity

(b) Contributions in kN to ultimate capacity

(c) Contributions as percentage of total capacity

(d) Contributions as percentage of ultimate capacity

Figure 4.25: Contributions of the components for a fixed depth of -13.2 meter NAP and increasing tip diameter on location 2

The shaft resistance in the soft layers is also much higher on location 2 than on location 1, this has multiple reasons. Firstly, the length over which shaft friction can be mobilized in the soft layers is higher, because the first sand layer is deeper. This length is equal to 10.1 meters on location 1 and 11.3 meters on location 2. Secondly, location 2 has more and thicker layers that can provide shaft friction due to the (silty) sand layers. Lastly, most of the resistance is generated in the top layers on location 2, this is also where the piles have a larger area due to their tapering. On location 1, these layers are more evenly distributed over the depth of pile, leading to an overall smaller area in the layers which provide more resistance. Due to this much higher resistance from the soft layers, the ultimate bearing capacity is also much larger, and has a larger range than on the first location.

Influence of knowing variables on uncertainty

For location 2, parameters have been fixed exactly the same as on location 1. The embedment is fixed at 0.5 meters into the sand layer, and the diameters are set to their mean values (figure 4.17).

When the depth of the pile tip is set, the only major difference with location 1 is that the value of the base resistance overall becomes larger instead of smaller. The spread also becomes larger, this is both seen back

in the total capacity as well. The reason for this is that the base resistance on location 2 has a larger spread to begin with, and the larger values lie at a larger embedment. The rest of the components show similar behaviour on both locations.

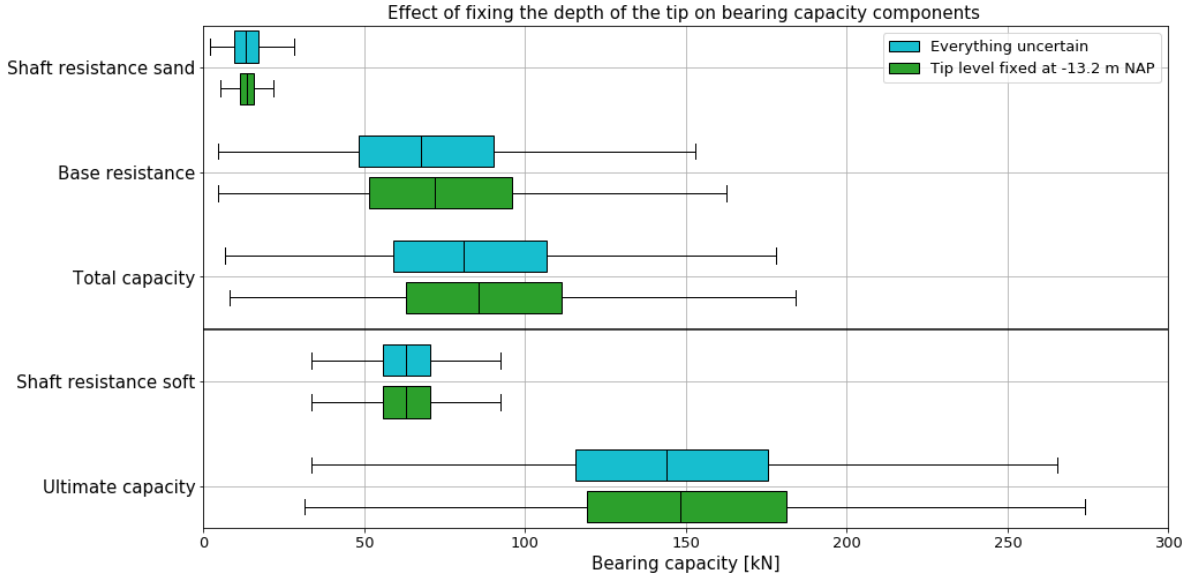

Figure 4.26: Box and Whisker plots for all bearing capacity component with all parameters uncertain and with the tip level set to -12.1 m NAP

When the diameter at the head of the pile is fixed, no real differences are observed between locations 1 and 2. On both locations, the spreads all become smaller while the mean values remain the same. Since nothing changes, this box plot is not shown here, it is shown in Appendix B.

Fixing the diameter of the tip does not make the same impact on location 1 as on location 2. The main reason for this is that the spread of the base capacity decreases more than on location 1. This shows that on location 1, the embedded depth has a relatively bigger impact on the base capacity than it does here.

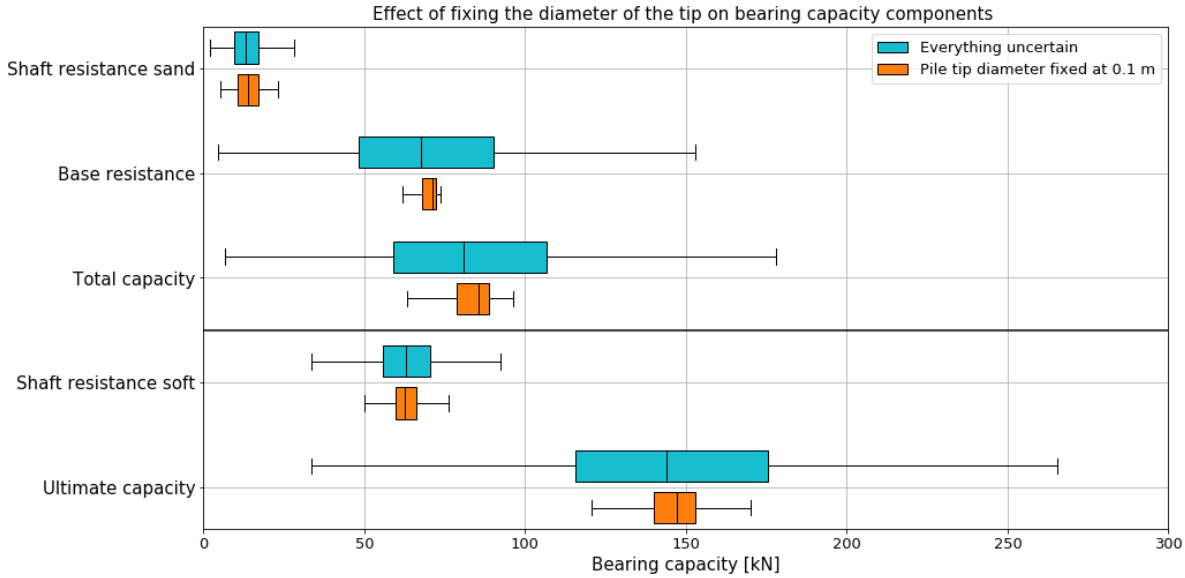

Figure 4.27: Box and Whisker plots for all bearing capacity component with all parameters uncertain and with the tip diameter set to 0.1 m

Reference pile

On this location, a calculation is also made for the reference pile. Here, the set of assumptions in combination with the length of the pile leads to a tip diameter of 0.155 m. The reference pile has a total capacity of 190.5 kN, made up of 170 kN of base capacity and 20.5 kN of shaft capacity from the sand layer. The shaft friction from the sand layer is similar to that on location 1. The base resistance is much larger than on location 1. In this case the 100 kN of assumed bearing capacity is also a safe value. But since the shaft friction in the soft layers is also much bigger on this location, leading to a higher value for the negative/ positive skin friction, the pile would still settle under a load of 100 kN and would have to mobilize additional shaft friction in the soft layers as shown in figure 4.28. In this figure the location of the neutral point is shown for four different loads; 120, 140, 200 and 220 kN. In the deeper part in the cone resistances measured in the CPT are very low, because of this the neutral point shifts upwards over 2 meters when the load is increased from 120 to 140 kN. The more shallow layers have higher cone resistances and can thus generate more friction. That is why the neutral point only shifts less than one meter upward under the additional load of 20 kN.

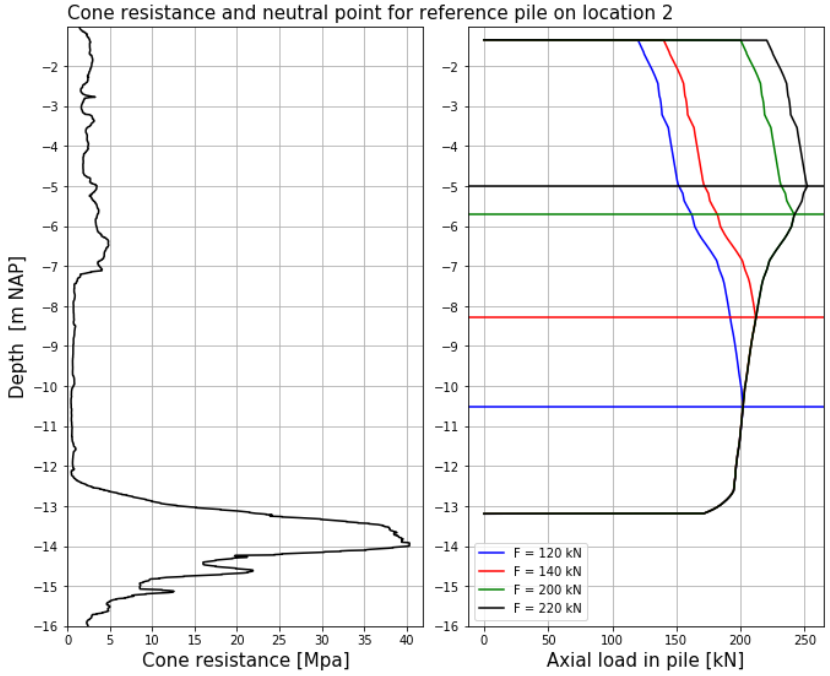

Figure 4.28: Neutral point for four loads on the pile head for the reference pile on location 2

On this location the pile parameters that are based on the assumptions of the municipality also lead to too high values for the total bearing capacity. Due to length of the pile being larger than on location 1 while the assumed head diameter and tapering remain the same, the tip diameter of 0.155 is smaller than on location 1. This is, however, still much larger than the mean value of the tip diameter from the dataset. Using the mean diameter of 0.1 meters, the total capacity would be equal to 84.4 kN instead of 190 kN. In this case using the assumptions would lead to a serious overestimation of the total bearing capacity.

4.3. Impact of degradation on geotechnical bearing capacity

The next step is to study what happens when the α_{red} factor is introduced. This factor is assumed to be the same for the shaft resistance in the sand layer and in the soft layers. Figure 4.29 shows box and whisker plots for the case where there is no α_{red} and where α_{red} varies between 1 and 0.6, 1 being no reduction and 0.6 being a reduction of 40% of the shaft capacity. Figure 4.30 shows stack plots of how the three components contribute to the total and ultimate capacities, both in kN and as a percentage. These figures are only shown for location 1 because location 2 shows the exact same behaviour.

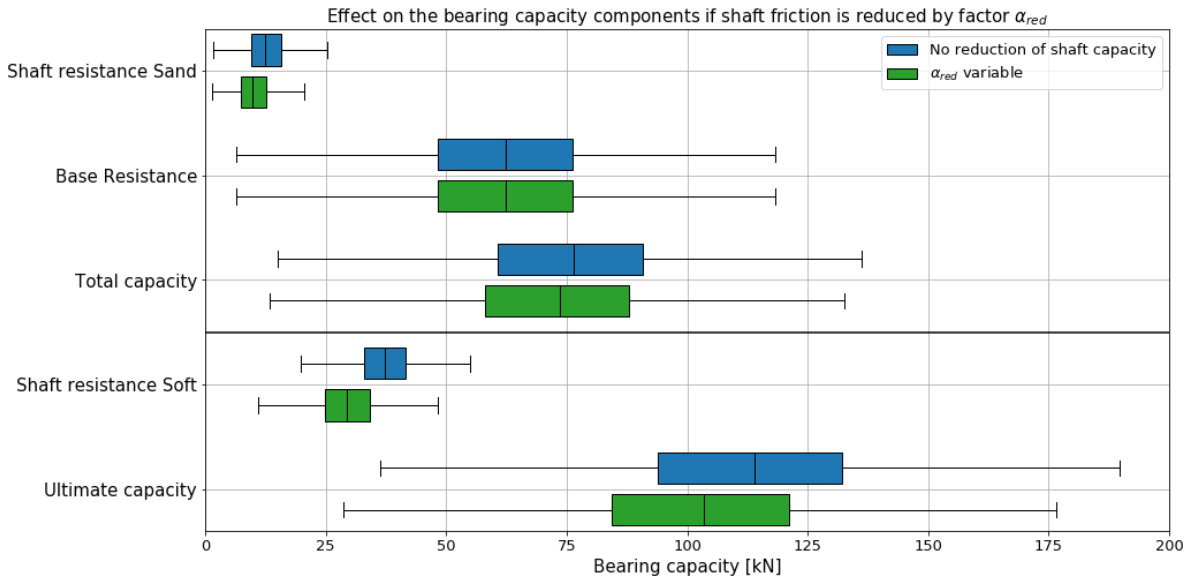

Figure 4.29: Box and Whisker plots for all bearing capacity components with and without factor $\alpha_+ red$ on location 1

The figure shows that potential reduction of the shaft capacity ranging from 0 to 40% does not have a very big effect on the total capacity. This is because the total capacity is mainly made up of the base resistance, which is not affected by the α_{red} factor. This can also be seen from figures 4.30 a and c, where the contributions of base capacity and shaft capacity in the sand layer are shown for a fixed depth, tip and head diameter. without the reduction factor the total capacity is equal to 80 kN, made up of 67 kN base capacity and 13 kN shaft capacity. With a maximum α_{red} of 0.6, the total bearing capacity decreases to 75 kN.

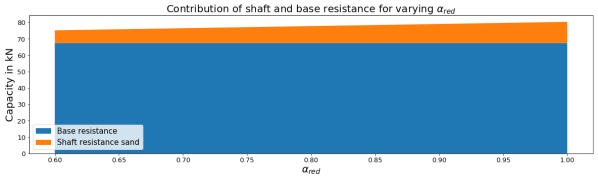

(a) Contributions in kN to total capacity

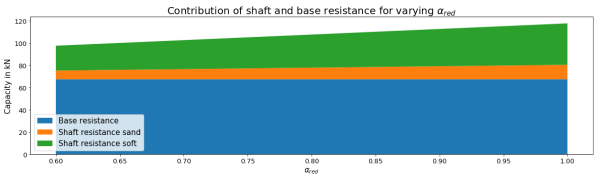

(b) Contributions in kN to ultimate capacity

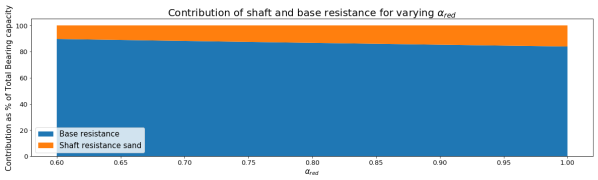

(c) Contributions as percentage of total capacity

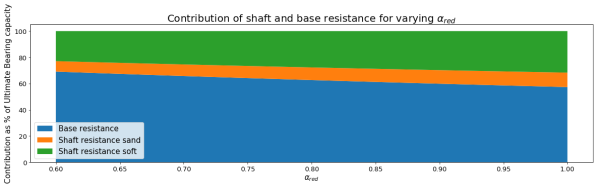

(d) Contributions as percentage of ultimate capacity

Figure 4.30: Contributions of the components for a fixed tip diameter, head diameter and depth, with varying α_{red} on location 1

The ultimate bearing capacity is impacted much more from the reduction factor. This is due to the bigger relative contribution of shaft resistance, which can be seen from figures 4.30 b and d. The ultimate capacity decreases from 117.5 kN to 97.5 kN.

It seems likely that if a slime layer is the cause of the reduction of the skin friction, this same alpha factor would also influence the negative skin friction working on the pile. This would mean that the reduction factor would also have a positive influence on the bearing capacity of the pile, since the additional load from the negative skin friction would decrease. This would also influence both the location of the neutral level in the pile and the maximum axial load in the pile. Figures 4.31a and 4.31b show the axial load and neutral level in the pile for α_{red} =1 and for α_{red} = 0.6 on both locations under a load of 140 kN on the pile head.

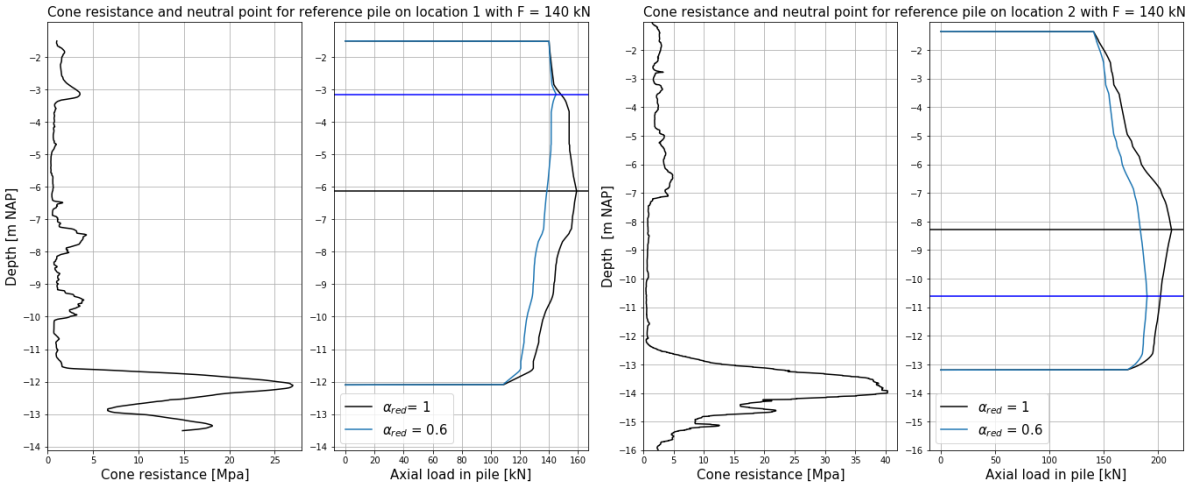

(a) Location 1

(b) Location 2

Figure 4.31: Effect of α_{red} on axial load and neutral point

It becomes clear from this figure that the axial load in the pile decreases for both cases. On location 1 the neutral level of the pile where α_{red} = 0.6 lies higher than α_{red} = 1, while on location 2 it is the other way around. This is due to where the layers which generate more friction are located relative to the neutral point, since α_{red} has a bigger effect on these layers. On location 1 there are the two wadsand layers which generate friction. Since these are located lower, and fall within the positive friction zone, less positive skin friction is generated when α_{red} = 0.6, leading to a more shallow depth of the neutral point. On location two, where the layers with friction are located more shallow, the α_{red} factor causes the negative skin friction to be reduced, lowering the neutral point.

4.4. Conclusion

The conclusion will reflect on the findings of this study in comparison to the assumptions that are currently being made. New findings will also be described.

4.4.1. Parameters

Concerning the parameters for this Monte Carlo analysis it was found that using the Cholesky decomposition resulted in generated data which fitted well with the two datasets with pile parameters. It was also found that using the relation between the diameter at the tip and the diameter at the head worked better than using the correlation between the tapering and the head diameter. The reason for this is firstly that the data shows the better correlation: a pearson correlation value of 0.73 versus 0.45. Secondly, the remaining parameter has to be calculated based on the length of the pile. This leads to a shift in the mean of the calculated parameter for different length piles. Since the tip diameter has a larger effect on the total bearing capacity than the tapering, it is less desirable that this shift occurs in the mean tip diameter than in the tapering.

The pile tip diameter that results from the set of assumptions of the municipality is too large and results in unrealistically large values. The total capacities on locations 1 and 2, using the assumptions, results in 137 and 190.5 kN for tip diameters of 0.165 and 0.155 meter respectively. The mean tip diameter from the combined datasets equals 0.1 meters. Using this tip diameter on locations 1 and 2 would result in total capacities of 79 kN and 84 kN respectively. Using the set of assumptions from the municipality could therefore result in extremely overestimated values for the total bearing capacity. The reason for this overestimation in the tip diameter is that both the assumed value for the tapering and the assumed value for the head diameter are larger than the parameters from the data sets. The datasets both clearly show that the mean of the tapering lies on 10 mm/m, instead of 8 mm/m (value that is used as assumption). The mean head diameters of the two datasets differed, dataset 2 indeed has a mean value of 0.25 m, but dataset 1 had a mean of 0.195. This leads to a mean value of the combined datasets of 0.217 m. It is expected that only dataset 2 has been taken into account to come to the assumed value that the municipality uses. It is advised to also take dataset 1 into account and to determine a new value to assume for the head diameter.

4.4.2. Pile Capacity

One of the assumptions of the municipality is that the piles get most of their capacity from the base resistance. This is true if total capacity is regarded. However, since piles in Amsterdam often show continuous settlement due to having been under designed (NF3O/SBRCURnet (2016)), it is likely that the neutral point is shifting upwards, also mobilising some of the shaft friction in the soft layers. If the neutral point has shifted up to the head of the pile, the base capacity can in some cases contribute less than half of the ultimate capacity.

Another assumption is that 100 kN per pile can be used as the calculation value. This will be compared to the results from this analysis where α_{red} = 1.It must be noted that it was no clarified on which method the 100 kN assumption was based, and which safety factors are included. It is assumed that it is based on the assessment of an existing structure with a partial factor of 1.2. What is not known is the amount of CPT's on which this value of based. The amount of CPTs determines which factor should be used for ξ. Since in this analysis, only one CPT was used per location, the highest ξ factor had to be applied. Table 4.2 shows the (mean) calculation value of the capacities when different parameters are used.

Location		Calculation value [kN]
1	Everything variable	75.5 (Mean)
	Tip diameter of 0.1 m and embedment of 0.5 m	79.6
	Using set of Assumptions	137
2	Everything variable	85 (Mean)
	Tip diameter of 0.1 m and embedment of 0.5 m	84.4
	Using set of Assumptions	190.5

Table 4.2: (Mean) Calculation value of the total bearing capacities in different situations on both locations

Table 4.2 shows that the assumption of 100 kN is indeed a safe assumption on both locations when the set of assumptions of the municipality is used. When, however, the pile parameters from the data sets, and the embedment of between 0.25 and 0.75 meters is used the 100 kN is an overestimation on both location 1 and 2. However, as shown in figure 4.23 location 2 has high values for $q_{b,max}$ in its bearing sand layer and its thickness allows the maximum q_c that can be used for shaft friction in the sand layer to be cut off at 15 MPa instead of 12 MPa. The quality of both sand layers according to the classification system (table 2.3) are very good. It has to be examined how representative the sand layers on these two locations are for the rest of the city in order to determine if the 100 kN value is too low everywhere. It seems likely that the 100 kN assumption is based on more CPTs, so a comparisson will also be made using the ξ factor of 1.25, which corresponds to using 10 CPTs. When this factor, instead of 1.39 is used, the total bearing capacities on location 1 and 2 with a tip diameter of 0.1 meters and an embedment of 0.5 meters are equal to 88.5 kN and 93.9 kN respectively. Both values are still smaller than the 100 kN assumption.

It has to be born in mind that the soft layers are able to provide a lot of additional bearing resistance if the total capacity is exceeded. The total amount of additional shaft friction from the soft layers can in some cases almost equal the amount of total bearing capacity. Of course it is not desirable to mobilize all the skin friction in the soft layers, because this would mean the pile would have settled at lot and there would be no safety margin left in the pile. Important in this case is where the pile is able to mobilize the additional shaft friction, and how fast the neutral point moves upward under a given load. This depends on where the sandy layers, which generate more shaft resistance, are located. Figures 4.21 and 4.28 show how far the neutral point moves upwards for an additional 20 kN of load on the piles head on locations 1 and 2. On location 1, this is equal to 1.5 meter per 20 kN in the softer layers. On location 2 the shallow layers provide most of the shaft capacity, therefore a lot of additional load on the pile head is needed before this can is mobilized. So, in total the shaft capacity of the soft layers is more on location 2, but it is less useful because a lot of settlement has to occur before this part of the shaft friction is mobilized.

4.4.3. Effect of Degradation

The potential reduction of 40% of the shaft friction due to a slime layer does not show to have a big influence on the total bearing capacity of a pile, because the total bearing capacity is mostly made up of base capacity, which is not affected by α_{red}. The effect is bigger on the ultimate shaft friction, due to the addition of the shaft capacity in the soft layers.

The most important difference that α_{red} makes is on the axial load and on the location of the neutral

point. If it is assumed that α_{red} works on negative as well as on positive skin friction, the reduction of shaft friction can have a positive effect on the piles bearing capacity, as the additional load from negative skin friction is decreased. Also, the axial load on the pile is always smaller if α_{red} is smaller than 1, this is positive for the calculation of structural strength of the wood itself. What happens to the location of the neutral point when α_{red} is smaller than 1 depends largely on the soil profile. If the layers that generate more friction are located near the head of the pile, they will usually work as negative skin friction. When α_{red} is applied in this case, the negative skin friction will be reduced and the neutral point will be lower than when $\alpha_{red} = 1$. When the layers with more friction lie closer to the tip of the pile, they will be more likely to be mobilized as positive skin friction. When α_{red} is applied in this case, the neutral level will be located higher than when $\alpha_{red} = 1$, because α_{red} will mostly impact the positive skin friction. The latter case is the most optimal for the calculation of the wood strength in the pile, because the higher the neutral point, the larger the cross section of the pile. This in combination with the lower axial load leads to a more beneficial situation for the calculation of the wood strength.

4.5. Recommendations

This analysis shows that some of the assumptions that the municipality makes regarding the pile parameters can be improved. The mean tapering from the data sets is not the same as the assumed value, resulting in tip diameters which are often too large. The assumed head diameter should be reïnvestigated as well, the assumed value of 0.25 meters agrees with one of the datasets, but the other dataset shows that this can vary significantly.

The assumption of using a 100 kN as calculation value for the geotechnical bearing capacity should be revisited as well. This value is safe and makes sense when the set of assumptions is used, but since these have shown to be optimistic, the values that were found for these locations and parameter distributions often lie below 100 kN.

In general it would be beneficial to perform additional pile extractions. The two datasets show that there can be a lot of variability in the dimensions of the piles that are used. A more in depth study into the pile parameters might provide more information on when and where certain pile types were used. These extractions would also need to be performed under bridges to verify that similar piles were used under houses and under bridges.

The relationship between the tapering, pile head and pile tip should be studied further as well. When better correlations have been established it would provide more certainty between for instance the head and tip diameter. From these datasets it became clear that using the correlation between the head and tip diameter resulted in the best generated data. Perhaps studying the data more closely and differentiating also in the length of piles would give a different result.

Also relationships can probably be found between a pile's parameters and its location and/or age. This can already be seen in the two datasets that were used here. The datasets have different means, probably due to the fact that they were extracted on different locations from structures that had been built in different years. It is possible that at certain moments in time, different piles were cheaper. Perhaps it is beneficial to have a different set of assumptions for each district or year of construction.

Additional pile extractions are also necessary to give more information on the embedment of the pile in the sand layer. The current assumptions are based solely on the given that a pile was driven two calendars into the sand layer. Since, however, the definition of one calendar varies in time, this assumption might be wrong. Once data of embedment of piles is available, it might be possible to determine a correlation between the cone resistance in the top of the sand layer and the embedment of the pile tip.

The effect of pile groups is not regarded here. Since the Amsterdam pile foundation always has two piles next to each other, this might make an important difference. Moreover, since the piles in Amsterdam often show continuous settlement, redistribution of loads between the piles in a pile group must also be taken into account when a whole structure is regarded.

5

Conclusions and Recommendations

In this chapter the conclusions and recommendations from the laboratory tests and from the Monte Carlo analysis will be summarized. Furthermore, some additional recommendations, which do not necessarily result from the two investigations, are made as well.

5.1. Conclusions and recommendations from the interface friction tests

The following conclusions are drawn from the interface friction tests on old and new wood samples sheared with and without a layer of slime.

- The alternative set up that was used to conduct the interface friction tests gave consistent results which resulted in values similar to those described in literature, and can thus be used for further research on this topic.
- No significant difference in interface friction was observed between the fresh samples and the old sample.
- A decrease in interface friction was observed when a slime layer was applied to the fresh samples.
- No significant difference was observed between old and new piles. The 40% reduction of shaft friction found in the Dapperbuurt was not confirmed in these tests.

Since it could not be confirmed that sample DW showed severe degradation it is recommended to perform additional tests with more degraded samples of old timber piles.

Since the set up did not allow for testing at higher normal loads, it is recommended to perform additional tests at higher normal loads. It is expected that indentation of the particles will occur at higher normal loads. It seems from the observation of sand particles in the dried wood like indentation can occur at lower normal loads when the wood structure is more degraded.

To see if the friction decreasing effect of slime also occurs in the soft layers, additional tests should be performed using clay instead of sand. Also, if indentation is the cause for measuring the relatively high friction angle in these tests, this would also be confirmed by performing tests with clay, as clay particles are not able to indent into the wood structure.

The performed tests have shown that the shape of the wood samples can strongly effect the behaviour that occurs during the test. To study this further, wood samples with different, well defined, shape effects have to be tested and compared.

Tests on a larger scale are also recommended, for instance in-situ load tests on piles that will be extracted.

5.2. Conclusions and recommendations from the Monte Carlo analysis

From the Monte Carlo analysis, the following conclusions were drawn:

- Using Cholesky decomposition to generate data for the head and tip diameters, subsequently calculating the tapering of the pile worked well for these tests.

- The pile head diameter of 0.25 meters, and the tapering of 8 mm/m, as currently assumed by the municipality are higher than the mean values from the two data sets. For realistic pile lengths of between 10 and 15 meters this results in tip diameters which are higher than what is found from the data sets. This results in calculated pile capacities that are also too high.
- Base capacity provides approximately 80% of the total bearing capacity of a typical timber pile in Amsterdam. When the total capacity is exceeded, and positive skin friction is mobilized in the soft layer, the contribution of the base capacity can decrease to less than 50% of the ultimate capacity.
- The assumed calculation value of the total geotechnical bearing capacity of 100 kN is too high based on these locations and input parameters as most of the computed total bearing capacities were lower than 100 kN.
- The diameter at the tip is the pile parameter which influences the bearing capacity most, after the tip diameter, the embedment is the most influential.
- How much the neutral point moves upward under a certain additional load depends strongly on the depth of the layers which generate most skin friction.
- A potential reduction in the shaft friction does not have a strong effect on the total bearing capacity because friction in the bearing sand layer only provides a small contribution to the total bearing capacity.
- The effect of a reduction in shaft friction due to degradation can have a much larger effect on the ultimate bearing capacity, which can decrease by as much as 20 kN.
- The reduction of shaft capacity causes a decrease in the maximum axial load in the pile, which is favorable for the calculation of the wood strength of the pile.
- The reduction of the shaft capacity can cause the neutral point in the pile to be located higher than without reduction in the case where the layers which can generate more friction are closer to the pile tip. Similarly, the neutral point is lower than if there were no reduction, if these layers are closer to the head of the pile.

From the comparison between the pile dimensions from the data set and the pile dimensions as assumed by the municipality of Amsterdam, it is recommended to re-evaluate and improve the assumptions that are being made. The two data sets provide lots of information that can lead to more accurate assumptions for pile parameters. It must be taken into account that the two data sets are based on piles that were extracted from under houses.

For this same purpose it is advised to perform many more pile extractions in the city of Amsterdam. These extractions must also be performed under bridges and quay walls to ensure that the similar piles have been used here as under houses. Focus must be put on finding relations between the pile parameters, so their uncertainty can be decreased. It can for example be studied if a relation is present between pile parameters and the location and/or age of the pile. Also, relations between the head diameter, tip diameter, tapering and length must be studied in more detail. In this study it was found that the relation between the tip diameter and the head diameter was strongest. But perhaps, when relations are studied for different pile lengths, a different picture arises.

More data must also be gathered on the embedment of the pile tip in the sand layer, as this parameter has a large influence on the calculated bearing capacity of the pile. This can be done by measuring the height of the pile head before extracting the pile. Once there is data available on the embedment, it is probably possible to find a relation between the embedment, the diameter at the tip and the cone tip resistance in the top of the first sand layer. This would make it possible to determine a realistic embedment for each pile assessment.

It is recommended to take the depth of the soft layers which provide most additional skin friction into account when calculating the depth of the neutral point. This is more accurate than assuming a constant amount of skin friction over the soft layers.

In addition it is advised to study the effect of pile groups on the bearing capacity. since the typical Amsterdam foundation consists of two piles under one cross beam and there are always many piles present under one structure. The redivision of loads after one pile in a group settles should also be taken into account during the calculation.

Overall, the conclusions of this thesis indicate that the bearing capacity as it is calculated now is too optimistic. The assumed parameters lead to calculated capacities which are too high, and the effect of a slime layer may lead to even lower bearing capacities. This is all contradicting the reason for conducting this study: which was that the current methods are already too conservative. A reason for these conservative results may be that the calculation method which is used to calculate the base resistance of a pile is in itself too conservative, as was also concluded by de Boorder (2019). It would be worthwhile to investigate whether another, less conservative, calculation method may be used for assessing old piles.

5.3. Additional recommendations

Besides the recommendations that result from the studies that have been conducted in this thesis, some other recommendations are also made.

It is recommended to revisit the Dapperbuurt tests, as there are probably many more conclusions that can be drawn from all these tests. As all the test have been reported very well, with the data still being available for revisitation.

Firstly, it must be studied whether the 40% reduction is also found when the results are studied in a higher level of detail. By for example comparing the test results to calculated values for the base and shaft resistances based on CPT measurements, one could verify some of the simplifications that have been made. Furthermore, it must be taken into account that the time between the compression and tension tests on a single pile was sometimes as little as one day. This could have led to smaller values being found in the tensile tests compared to the compression tests.

Secondly, the Dapperbuurt tests included pile load tests on an additional 37 piles, that were extracted after testing. Of these 37 pile tests, the load displacement curves, pile parameters and the exact locations including nearby CPTs are well preserved. These tests have never been reinterpreted with the purpose of studying a possible reduction in shaft friction. Also, with calculation methods which have been improved since 1974, much more information must be stored in these tests.

Especially in quay walls, lateral loading of the piles must also be considered. A good example of this is the Oudezijdse Achterburgwal, from which piles were extracted. Figure A.1 shows that large lateral displacements of the quay wall occurred. In this case the failure mechanism was not due to the axial loading of the piles, but due to the lateral loading.

References

Anaraki, K. E. (2008). Hypoplasticity investigated: parameter determination and numerical simulation.

Cabalar, A. F., & Canakci, H. (2011). Direct shear tests on sand treated with xanthan gum. *Proceedings of the Institution of Civil Engineers-Ground Improvement*, *164*(2), 57–64.

Chang, I., Im, J., Prasidhi, A. K., & Cho, G.-C. (2015). Effects of xanthan gum biopolymer on soil strengthening. *Construction and Building Materials*, *74*, 65–72.

Chenu, C. (1993). Clay—or sand—polysaccharide associations as models for the interface between micro-organisms and soil: water related properties and microstructure. In *Soil structure/soil biota interrelationships* (pp. 143–156). Elsevier.

Database Amsterdam houtmonster analyse. (2018).

Dataset extracted piles Dapperbuurt. (2018).

Dataset extracted piles Frans Sas. (2018).

de Boorder, M. (2019). Development of a new cpt averaging technique and review of existing cpt based methods for the calculation of total pile capacity.

Dinoloket. (2019a). Retrieved 2019-11-13, from `https://www.dinoloket.nl/ondergrondgegevens` (Boring B25G0009)

Dinoloket. (2019b). Retrieved 2019-03-27, from `https://www.dinoloket.nl/ondergrondmodellen` (Used model is GeoTOP v1.3)

Flemming, H. C. (2011). The perfect slime. *Colloids and Surfaces B: Biointerfaces*, *86*(2), 251–259.

Gans, W. d. (2011). *De bodem onder amsterdam: een geologische stadswandeling.* TNO.

Gard, W. (2019). *Wood structure and porperties.* University Lecture, CIE4110.

Gemeente Amsterdam, Afdeling ruimtelijk beleid. (2009). *Maatwerk - onderzoek naar de technische staat van panden in het kader van 'behoud en herstel"* (Tech. Rep.).

Head, K. H. (1992). *Manual of soil laboratory testing. volume 2. soil classification and compaction tests.*

Hoekstra, J., & Bokhoven, W. (1974). *Systematisch funderingsonderzoek van de dapperbuurt ("systematic foundation research in the dapperbuurt")* (Tech. Rep.).

Ilvessalo-Pfäffli, M.-S. (1995). *Fiber atlas: identification of papermaking fibers.* Springer Science & Business Media.

Kalt, J., & Dusseldorp, J. W. (2018). *Leidraad beoordeling constructieve veiligheid* (Tech. Rep.).

Keijer, H. (2015). *1-2-3 geologie voor ingenieurs.* KIVI, afdeling Geotechniek.

Klaassen, R., den Nijs, P., & van Beusekom, G. (2000). Bacteriele aantasting van houten paalfunderingen. *Literatuurstudie en inventarisatie van de Nederlandse situatie. Stichting Hout Research, The Netherlands.*

Klaassen, R. K. (2008). Bacterial decay in wooden foundation piles—patterns and causes: A study of historical pile foundations in the netherlands. *International biodeterioration & biodegradation*, *61*(1), 45–60.

Klapper, I., Rupp, C. J., Cargo, R., Purvedorj, B., & Stoodley, P. (2002). Viscoelastic fluid description of bacterial biofilm material properties. *Biotechnology and bioengineering*, *80*(3), 289–296.

Korff, M. (2013). *Response of piled buildings to the construction of deep excavations* (Unpublished doctoral dissertation).

Lantinga, C. (2015). *De resterende (geotechnische) draagkracht van bestaande houten funderingspalen.* Technische Universiteit Eindhoven.

Maghsoudloo, A., Galavi, V., Hicks, M. A., & Askarinejad, A. (2017). Finite element simulation of static liquefaction of submerged sand slopes using a multilaminate model. In *19th international conference on soil mechanics and geotechnical engineering* (Vol. 2, pp. 801–804).

Młynarek, Z., Wierzbicki, J., & Bogucki, M. (2015). Geotechnical characterization of peat and gyttja by means of different in-situ tests..

NF3O/SBRCURnet . (2016). *Richtlijn houten paalfunderingen onder gebouwen.* F3O.

Normcommissie 351 006 "Geotechniek" . (2016). *Nen 9997-1.* NEN.

Normcommissie 351 006 "Geotechniek" . (2018). *Nen 8707.* NEN.

Pan, M., Zhu, L., Chen, L., Qiu, Y., & Wang, J. (2016). Detection techniques for extracellular polymeric substances in biofilms: a review. *BioResources*, *11*(3), 8092–8115.

Potyondy, J. G. (1961). Skin friction between various soils and construction materials. *Geotechnique*, *11*(4), 339–353.

Robertson, P. (1990). Soil classification using the cone penetration test. *Canadian Geotechnical Journal*, *27*(1), 151–158.

Robertson, P. (2009). Interpretation of cone penetration tests—a unified approach. *Canadian geotechnical journal*, *46*(11), 1337–1355.

Rosenzweig, R., Shavit, U., & Furman, A. (2012). Water retention curves of biofilm-affected soils using xanthan as an analogue. *Soil Science Society of America Journal*, *76*(1), 61–69.

Schreurs, E. (2017). *Deterioration of timber pile foundations in rotterdam.*

ter Linde, J. (1990). *Inspectie- en beoordelingsmethodiek voor houten funderingen* (Tech. Rep.).

Thomopoulos, N. T. (2012). *Essentials of monte carlo simulation: Statistical methods for building simulation models.* Springer Science & Business Media.

Towler, R. C. J. C. A. B. S., Brett W, & Paul. (2003). Viscoelastic properties of a mixed culture biofilm from rheometer creep analysis. *Biofouling*, *19*(5), 279–285.

Valsangkar, A. J., & Holm, T. A. (1997). Friction angle between expanded shale aggregate and construction materials. *Geotechnical Testing Journal*, *20*(2), 252–257.

Van der Stoel, A. E. C. (2001). *Grouting for pile foundation improvement* (Unpublished doctoral dissertation).

van Tol, A. (2006). *Collegedictaat CTB1410 Funderingstechnieken.*

Vasudevan, R. (2014). Biofilms: microbial cities of scientific significance. *J Microbiol Exp*, *1*(3), 00014.

Wennekes, E., & Grijp, L. P. (2002). *De hele dag maar op en neer - over heien, heiliedjes en hoofdstedelijke muziekgebouwen.*

A

Appendix

A.1. Findings on the Oudezijdse Achterburgwal

The Oudezijdse Achterburgwal is located in one of the oldest parts of the city centre of Amsterdam, it originated around 1400 and is currently in the middle of the red light district. The quay wall of the canal was showing severe deformations, leading to the decision of the municipality to demolish the old quay wall, and construct a new one. In the context of the 'program bridges and quay walls' this was a great opportunity to investigate the state of the quay wall and its foundation piles. This would have also given the opportunity to measure the embedment of the piles in the sand layer, as each pile head location was determined with GPS very accurately.

During the extraction of the piles, an even older quay wall was discovered, which was located below the floor of the demolished quay wall. Another finding was that the connection between the piles and the floor of the quay wall was made using a mortise and tenon joint. The tenon of the joint is shown clearly in the pile head that was used in the shear tests as shown in figure 3.6a in chapter 3.

Figure A.1: Quay wall on the Oudezijdse Achterburgwal showing large horizontal displacements, photo taken by author on 3-1-2019

Figure A.2 shows the CPT data on the location where the piles were extracted. It shows that the soil profile resembles that of the typical Amsterdam profile. Except that the peat layers are much thinner here. This is due to the location being located in the flood plane of the Amstel river, as was already shown in figure 2.2. This caused the peat to have been replaced by river clay.

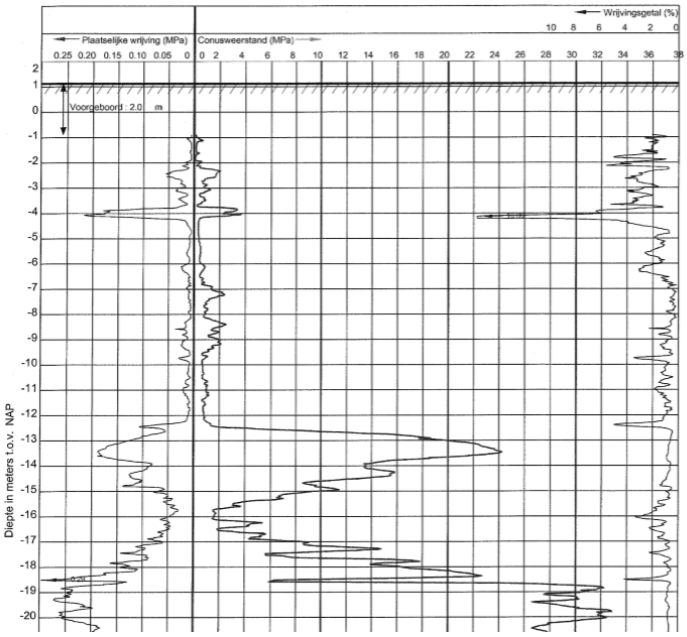

Figure A.2: CPT Oudezijdse Achterburgwal

The initial research plan involved testing several pieces of degraded wood which were going to be taken over the length of the pile in different soil layers. However, after several attempts using various different methods it became apparent that it would not be possible to extract complete piles on this location. The expected cause is that the quay wall had undergone such large deformations that the piles had all broken at 2-3 meters below the pile head. In total 25 pile heads were extracted which became available for research. Pile heads were extracted from the land side and from the water side of the quay wall.

Moreover, samples of wood were taken, to test them for the presence of slime (figure A.3). For this purpose it was important that the pile would not be cleaned, because it was expected that the slime would be lost. Several samples of the pile have been taken to see if there was a slime layer present on the sample.

Unfortunately it was not possible to determine this from the samples that were taken. Even though it is not proven there is suspicion that there was indeed slime. Because when the container with the sample was held up side down and was even shook, the sample stuck to the container as if it had been glued. The samples were stored in a cool box and transported to TU Delft where they were stored at the appropriate temperatures.

The heads of the extracted piles were located at a depth of -1 meters NAP. The length of the total piece of pile head from which DW was taken, was equal to 70 cm, the sample DW was taken at 30 cm under the head of the pile. This piece was therefore probably located in the river clay layer. As mentioned in chapter two and in R. Klaassen et al. (2000), degradation occurs less in soil layers consisting of clay and peat, since there is less oxygen available there compared to sand layers. The pile head from which DW was taken was unfortunately not labeled, so it is not known if this piece was extracted on the land or on the water side of the quay wall.

Figure A.3: Taking slime samples from extracted pile.

A.1.1. IML measurements

Below all the results of the IML measurements on wood sample DW are shown. Measurements 1 to 5 were performed when the sample was wet, 5 to 8 were performed after the sample was oven dried.

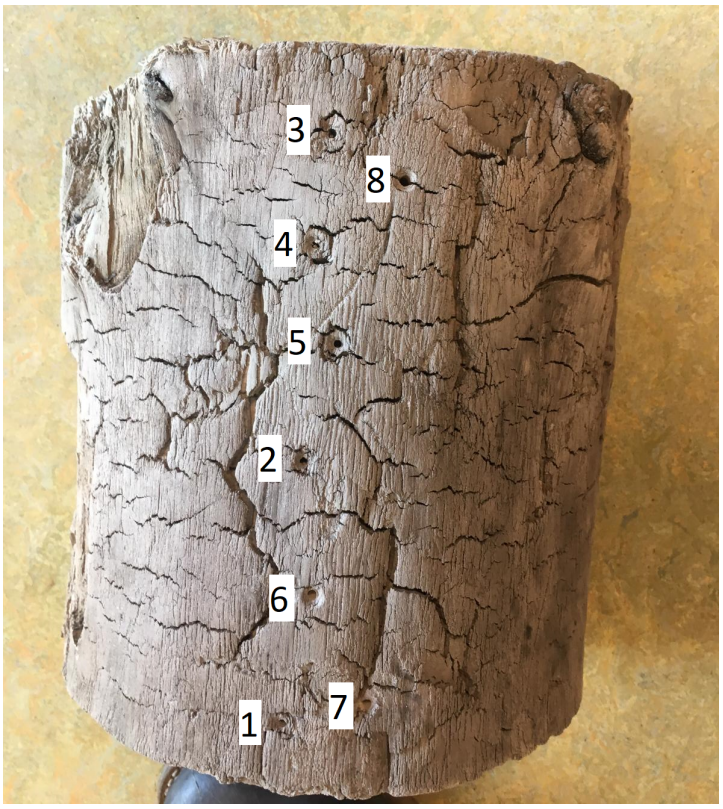

Figure A.4: Locations of all the IML measurements on sample DW.

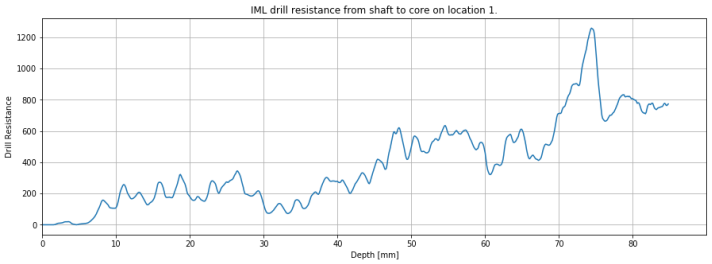

Figure A.5: IML measurement 1.

Figure A.6: IML measurement 2.

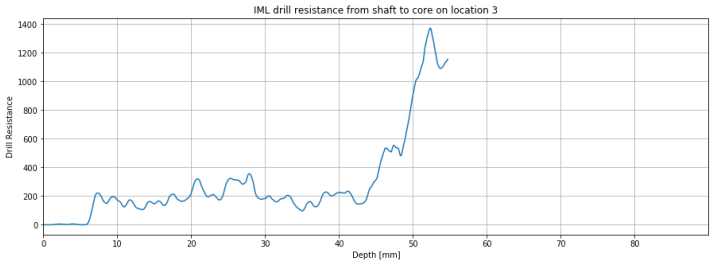

Figure A.7: IML measurement 3.

Figure A.8: IML measurement 4.

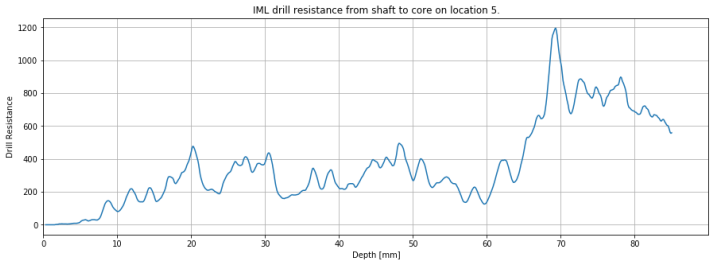

Figure A.9: IML measurement 5.

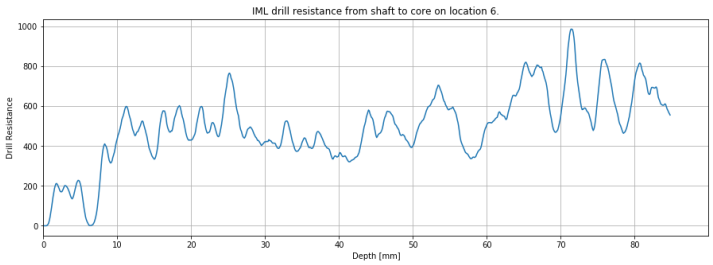

Figure A.10: IML measurement 6.

Figure A.11: IML measurement 7.

Figure A.12: IML measurement 8.

A.2. Sand Properties

Before testing the interface friction between the sand and the timber, more details have to be known about the properties of the sand itself. Therefore, several lab tests have been performed on the sand. The results of these tests will be described below.

A.2.1. Void Ratio

The minimum and maximum void ratios have been determine using the method as described by Anaraki (2008). The equipment which was used in the tests is shown in figure A.13. The mold has an inner diameter of 6 cm and an inner height of 4 cm.

Figure A.13: The Equipment used for determining the minimum and maximum void ratio.

During the maximum void ratio test the mold, without the collar, is filled using the funnel. The tip of the funnel is kept at a minimum distance from the top of the sand pile, and is raised slowly during the procedure. The mold is overfilled by a small amount, this excess sand is striked off carefully before weighing the mold with the sand.

In the minimum void ratio test, the mold with the collar is filled for slightly more than 1/5th of the height. The outside of the mold is then tapped 10 times with the rod, after which the mold is rotated 90°. This is repeated until the layer has been compacter by 100 taps, after this the next layer is placed and compacted. This continues until the mold is filled completely. Then, the collar is removed and the top is striked off.

Using the volume of the mold and the weight of the sand sample, the dry density can be calculated. This is then used in equation A.1 to determine the void ratio.

$$e = G_s \times (\frac{\rho_{water}}{\rho_{sample}}) - 1 \tag{A.1}$$

Where:
G_s = Specific Gravity, equal to 2.67
ρ_{water} = 1000 kg / m^3
$\rho_{sample} = m_{sample}/V_{mold}$

Both the tests for minimum and maximum void ratio have been performed 5 times. The results of these tests are shown in tables A.1. After, the average of the 5 tests was determined, this value was used to calculate the minimum and maximum void ratio. This resulted in a minimum and maximum void ratios of 0.71 and 1.06 respectively.

Test Number	Sample mass [g]
1	179.43
2	177.56
3	173.61
4	176.33
5	177.04
Average minimum void ratio	176.79

Test Number	Sample mass [g]
1	146.25
2	147.04
3	146.19
4	146.78
5	145.98
Average maximum void ratio	146.45

Table A.1: Results for minimum and maximum void ratio tests

When these values were used to determine the relative densities of the core samples, it was found that these were often more than 100%. This indicates that the minimum void ratio that was found in the lab tests was too low. Maghsoudloo et al. (2017) used the same sand in his tests and reported minimum and maximum void ratios of 0.64 and 1.07 respectively. Since these values results in more realistic relative densities, these values are adopted.

A.2.2. Friction angle

The friction angle of the sand is measured using a direct shear box apparatus as explained in chapter two. The test was strain controlled, at a speed of 1 mm/minute, which is the same speed as is used during the shearing of the wood sample.

The sample was dry when placed in the mold, once the shear box was in place, water was added to the container. The sample was then saturated for two hours, after which the tests were performed. The normal loads that were used were 5, 10 and 20 kg. The properties of the two samples are shown in table A.3.2.The sample holder was round with an inner diameter of 63 mm and a height of 21 mm, leading to a volume of $0.065 \times 10^{-3} m^3$ and an area of 0.0031 m^2

	Sample 1	Sample 2
Dry mass [g]	87.77	86.7
Wet mass [g]	107.77	105.98
Dry Density [kg/m^3]	1340.32	1324.43
Bulk density [kg/m^3]	1646.29	1618.95
Moisture content [%]	22.8	22.2
Void Ratio	0.99	1.01
Relative Density [%]	20	14
Degree of Saturation [%]	61.9	59.0

Table A.2: Results for maximum void ratio tests

These sample properties indicate a very loose sample, which is confirmed by the stress path that was observed during the test. Since the aim of the test was to find the constant volume friction angle, it is not a problem that the sample was very loose.

The friction angles that were measured during test 1 and test 2 were 30.5°and 32.5°respectively. Furthermore, an apparent cohesion of 3.6 kPa and 4.6 kPa was measured during tests 1 and 2 respectively. Figure A.14 shows the results of both tests.

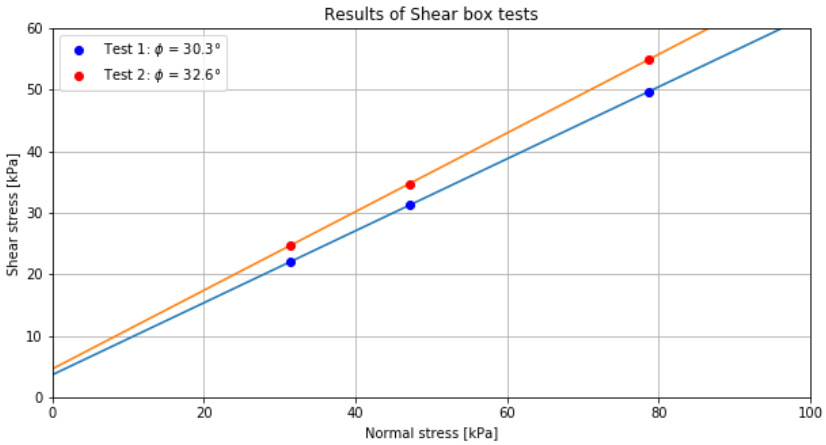

Figure A.14: The results of the shear box tests.

Maghsoudloo et al. (2017) reports a $\phi_{residual}$ of 36 °and a cohesion of 0.0 kPa, which does deviate quite a lot from the one measured in the test. This is probably due to the fact that the samples tested here were not fully saturated, which caused some suction to occur during the tests. This causes the apparent cohesion that is observed during the tests, and also causes a lower observed friction angle.

A.3. Sample properties

The properties of the sand sample inside the box have been determined in two ways. Firstly, by keeping track of how much water and how much dry sand was used to built up the sample. Secondly, by taking several core samples before emptying the box. Results of both are shown below. The box was emptied and refilled once during the tests. The first sample (Box 1) was used for tests 57 to 138, the second sample (box 2) was used for tests 139 to 239.

A.3.1. Whole box

When preparing the sample the amount of water and sand that was put into the box was measured. Using this information an average value of the density in the box can be determined. The inner length and width of the box are equal to 40.8 and 44.6 cm. To make sure the string went through the centre of the hole, the box had to be filled up to 21.4 cm. This amounts to a volume of 0.0394 m^3. The table below shows the properties of boxes 1 and 2.

	Box 1	Box 2
Dry mass [kg]	62.4	61.6
Wet mass [kg]	79.4	78.2
Dry Density [kg/m^3]	1584.1	1563.1
Bulk density [kg/m^3]	2014.6	1983.9
Moisture content [%]	27.2	26.9
Void Ratio	0.685	0.708
Relative Density [%]	89	84
Degree of Saturation [%]	106	101

A.3.2. Core Samples

Using the device shown in figure A.15a core samples were taken on three locations in the box (figure A.16 and figure A.17). From these samples the moisture content and relative densities were determined. The samples were cylindrical, with an inner diameter of 50 mm and a height of 50 mm, leading to a volume of $0.098 \times 10^{-3} m^3$.

Figure A.15: The device used to take the core samples.

Box 1

Figure A.16: The locations of where the samples were taken in the box.

	Sample 1	Sample 2	Sample 3
Dry mass [g]	157.9	153.77	162.12
Wet mass [g]	194.19	188.41	198.33
Dry Density [kg/m^3]	1611.22	1569.08	1654.29
Bulk density [kg/m^3]	1981.53	1922.55	2023.78
Moisture content [%]	23.0	22.5	22.3
Void Ratio	0.66	0.70	0.61
Relative Density [%]	95.3	86	107
Degree of Saturation [%]	93.1	85.8	97.5

Box 2

When the core samples for box 2 were taken, no tests had been run for about 3 weeks. During this time the water level in the box had not been monitored and therefore water had evaporated. This explains why these core samples show much lower moisture contents than in the first box, where sample were taken immediately after testing. The moisture content is therefore not representative of the moisture content that occurred during the tests. The red circle in figure A.17 represents the location of the hole.

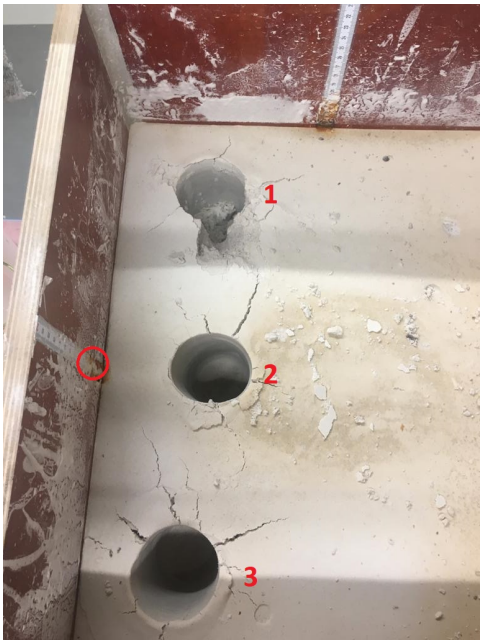

Figure A.17: The locations of where the samples were taken in the box.

	Sample 1	Sample 2	Sample 3
Dry mass [g]	152.89	159.42	155.88
Wet mass [g]	173.93	190.93	178.88
Dry Density [kg/m^3]	1560.1	1626.73	1590.614
Bulk density [kg/m^3]	1774.80	1948.27	1825.31
Moisture content [%]	13.7	31.51	14.8
Void Ratio	0.71	0.64	0.68
Relative Density [%]	83.7	100	90.7
Degree of Saturation [%]	51.7	82.4	58

All in all the two boxes have comparable properties, box 2 is slightly less densely packed. Both boxes do show some variation throughout the box, this becomes clear from the difference between the soil samples. The degree of saturation is much higher when the whole box is regarded. This is due to the fact that this data is from before the testing started, while the cores were taken after the tests with that box are completed. The difference is probably caused by evaporation.

A.4. Results

A.4.1. Test series FW1

The black line in the graphs indicates where the values for the constant volume friction angle is taken. This is at 50% displacement in the tests at 5 and at 10 kg additional normal load, and at 75% displacement in the tests at 15 and 20 kg additional normal load. These values have been chosen because in the latter two tests the peak was more pronounced, and thus a bigger displacement was needed to overcome the peak friction. The numerical results of each test, and the average values at the different loads are given in tables A.3 until A.6.

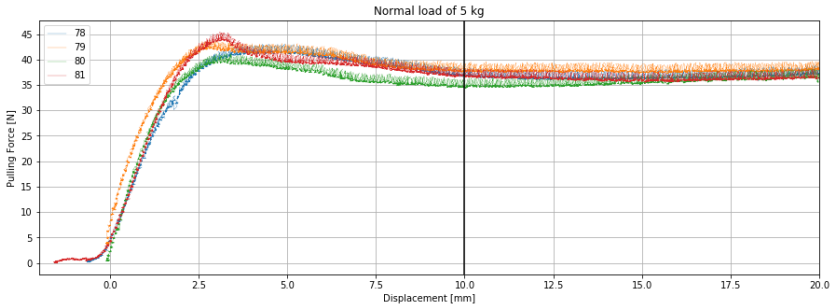

Figure A.18: The results from test series FW1 tests at 5 kg additional load

Tests at 5 kg	
Test Number	Pulling force at 50% displacement [N]
78	36.5
79	38
80	35.5
81	36.6
Average	36.6

Table A.3: Values for pulling force

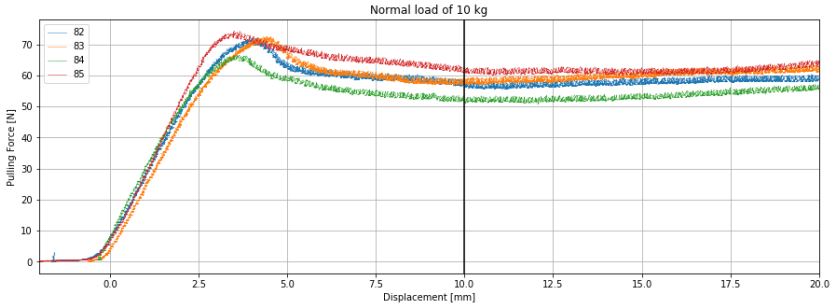

Figure A.19: The results from test series FW1 tests at 10 kg additional load

Tests at 10 kg	
Test Number	Pulling force at 50% displacement [N]
82	58
83	58
84	52.5
85	61
Average	57.4

Table A.4: Values for pulling force

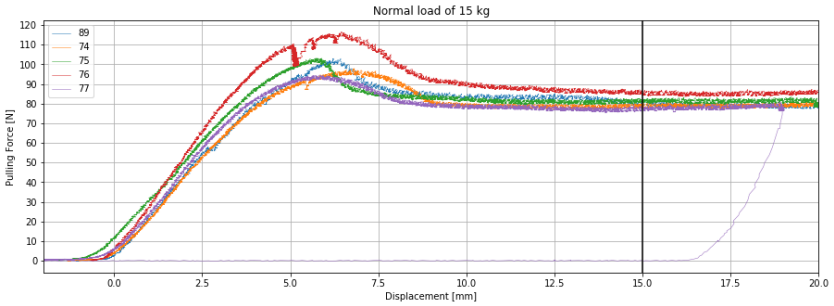

Figure A.20: The results from test series FW1 tests at 15 kg additional load

Tests at 15 kg	
Test Number	Pulling force at 75% displacement [N]
74	80
75	80
76	85
77	78
89	80
Average	80.6

Table A.5: Values for pulling force

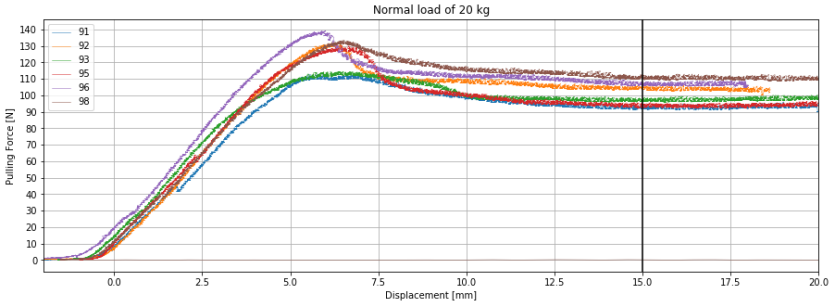

Figure A.21: The results from test series FW1 tests at 20 kg additional load

Tests at 20 kg	
Test Number	Pulling force at 75% displacement [N]
91	94
92	105
93	98
95	95
96	106
98	110
Average	101.3

Table A.6: Values for pulling force

A.4.2. FWS1

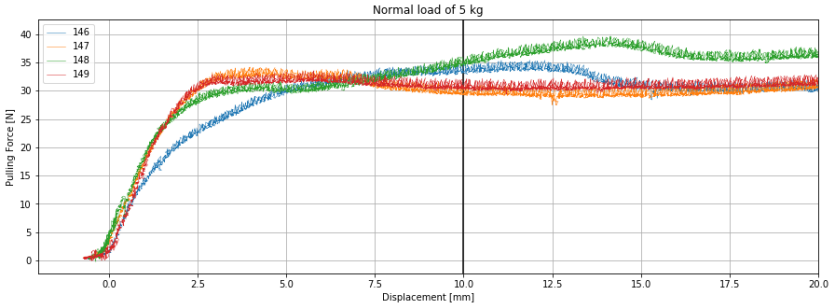

Figure A.22: The results from test series FWS1 tests at 5 kg additional load

Tests at 5 kg	
Test Number	Pulling force at 50% displacement [N]
146	34
147	30
148	30
149	31
Average	31.3

Table A.7: Values for pulling force

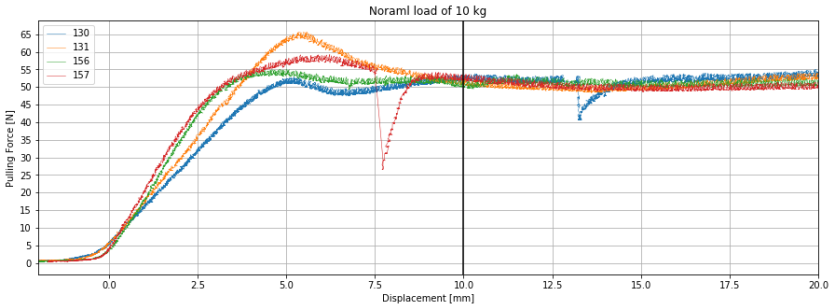

Figure A.23: The results from test series FWS1 tests at 10 kg additional load

Tests at 10 kg	
Test Number	Pulling force at 50% displacement [N]
130	52
131	50
156	50
157	53
Average	51.3

Table A.8: Values for pulling force

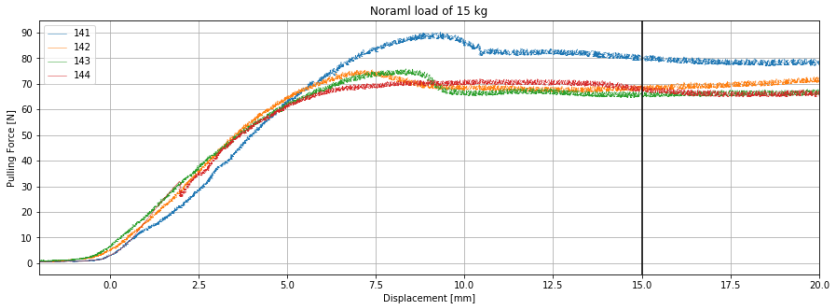

Figure A.24: The results from test series FWS1 tests at 15 kg additional load

Tests at 15 kg	
Test Number	Pulling force at 75% displacement [N]
141	80
142	69
143	66
144	69
Average	71

Table A.9: Values for pulling force

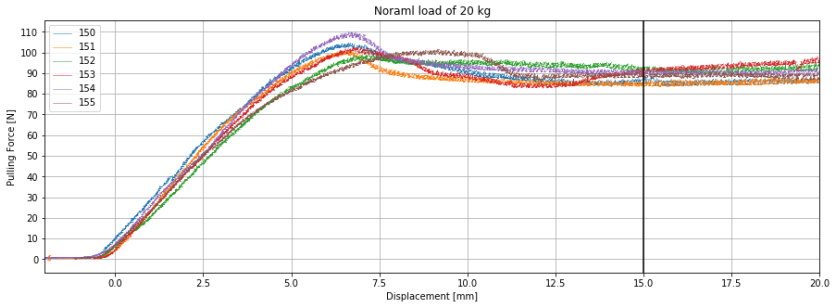

Figure A.25: The results from test series FWS1 tests at 20 kg additional load

Tests at 20 kg	
Test Number	Pulling force at 75% displacement [N]
150	86
151	86
152	91
153	90
154	90
155	90
Average	88.8

Table A.10: Values for pulling force

A.4.3. FW2

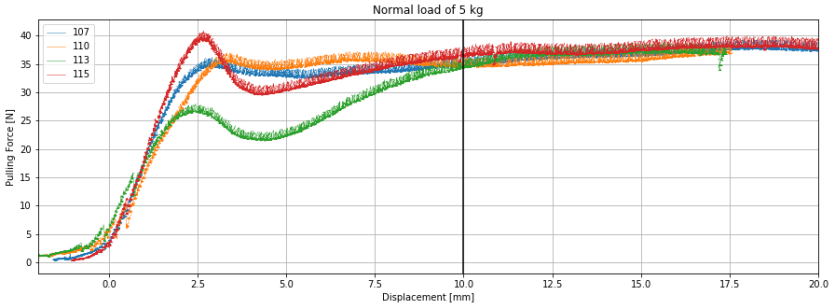

Figure A.26: The results from test series FW2 tests at 5 kg additional load

Tests at 5 kg	
Test Number	Pulling force at 50% displacement [N]
107	35
110	35
113	35
115	36
Average	35.25

Table A.11: Values for pulling force

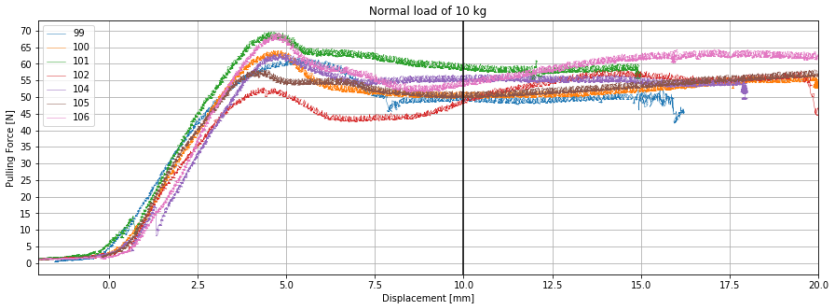

Figure A.27: The results from test series FW2 tests at 10 kg additional load

Tests at 10 kg	
Test Number	Pulling force at 50% displacement [N]
99	50
100	51
101	59
102	49
104	55
105	50
106	55
Average	52.7

Table A.12: Values for pulling force

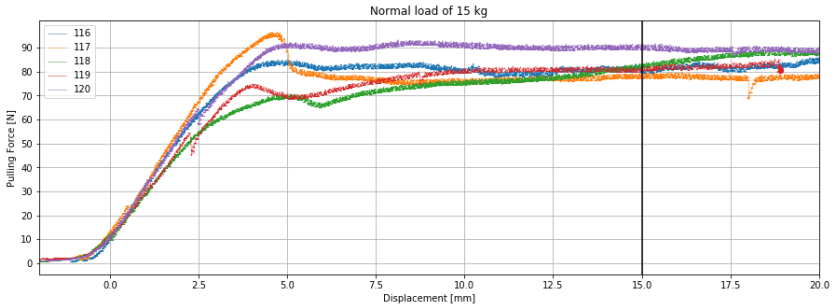

Figure A.28: The results from test series FW2 tests at 15 kg additional load

Tests at 15 kg	
Test Number	Pulling force at 75% displacement [N]
116	80
117	79
118	82
119	81
120	90
Average	82.4

Table A.13: Values for pulling force

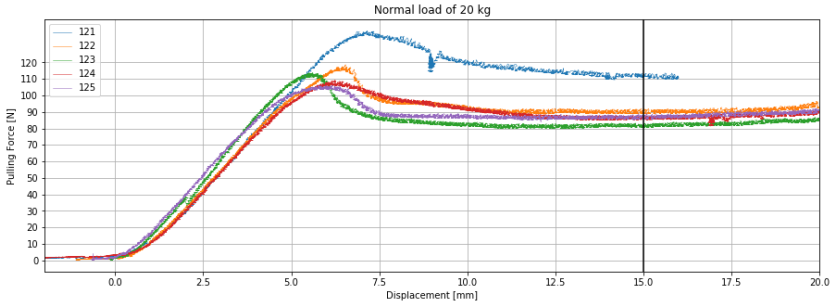

Figure A.29: The results from test series FW2 tests at 20 kg additional load

Tests at 20 kg	
Test Number	Pulling force at 75% displacement [N]
121	112
122	90
123	82
124	86
125	87
Average	91.4

Table A.14: Values for pulling force

A.4.4. FWS2

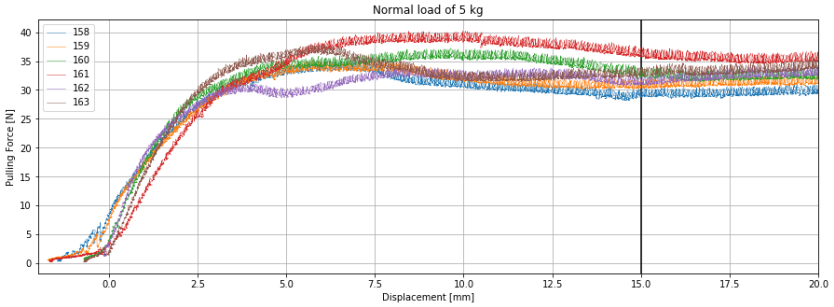

Figure A.30: The results from test series FWS2 tests at 5 kg additional load

Tests at 5 kg	
Test Number	Pulling force at 75% displacement [N]
158	29
159	30
160	33
161	36
162	32
163	33
Average	32.16

Table A.15: Values for pulling force

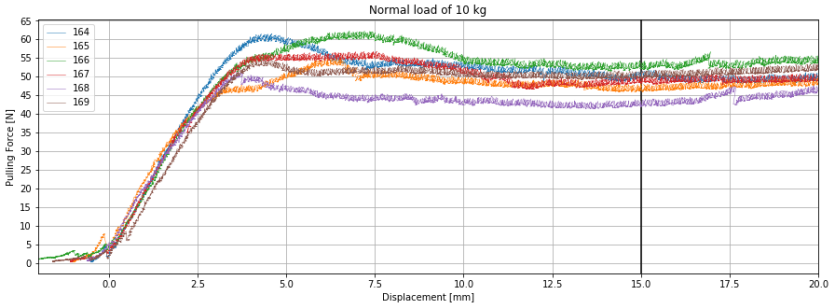

Figure A.31: The results from test series FWS2 tests at 10 kg additional load

Tests at 10 kg	
Test Number	Pulling force at 75% displacement [N]
164	50
165	47
166	54
167	49
168	44
169	50
Average	49

Table A.16: Values for pulling force

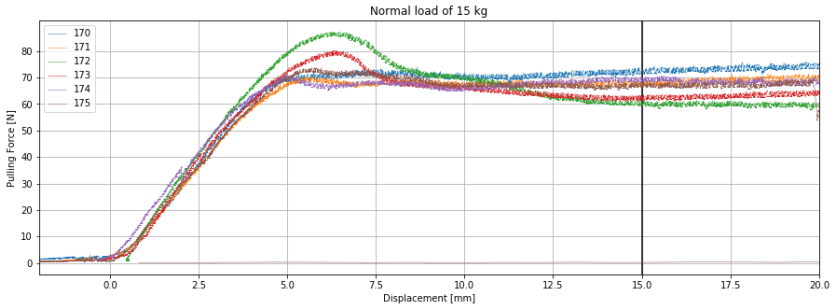

Figure A.32: The results from test series FWS2 tests at 15 kg additional load

Tests at 15 kg	
Test Number	Pulling force at 75% displacement [N]
170	70
171	67
172	60
173	63
174	69
175	67
Average	66

Table A.17: Values for pulling force

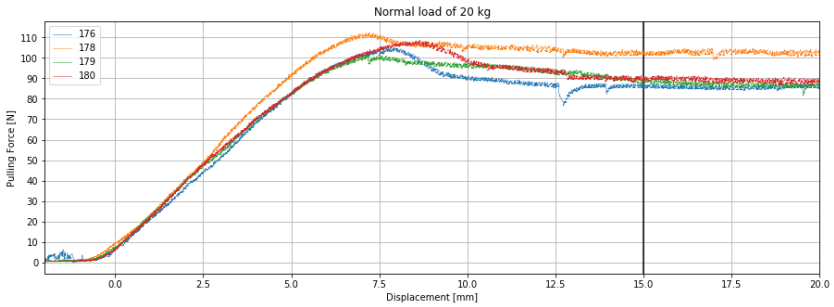

Figure A.33: The results from test series FWS2 tests at 20 kg additional load

Tests at 20 kg	
Test Number	Pulling force at 75% displacement [N]
176	85
178	102
179	87
180	90
Average	91

Table A.18: Values for pulling force

A.4.5. DW

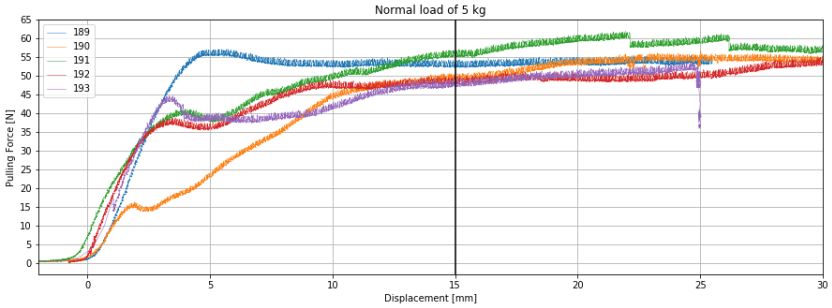

Figure A.34: The results from test series DW tests at 5 kg additional load

Tests at 5 kg	
Test Number	Pulling force at 50% displacement [N]
189	54
190	50
191	56
192	49
193	48
Average	51.4

Table A.19: Values for pulling force

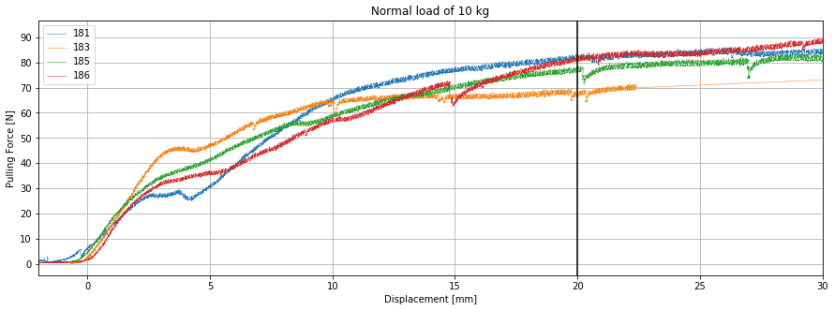

Figure A.35: The results from test series DW tests at 10 kg additional load

Tests at 10 kg	
Test Number	Pulling force at 66% displacement [N]
181	81
183	77
185	69
186	81
Average	77

Table A.20: Values for pulling force

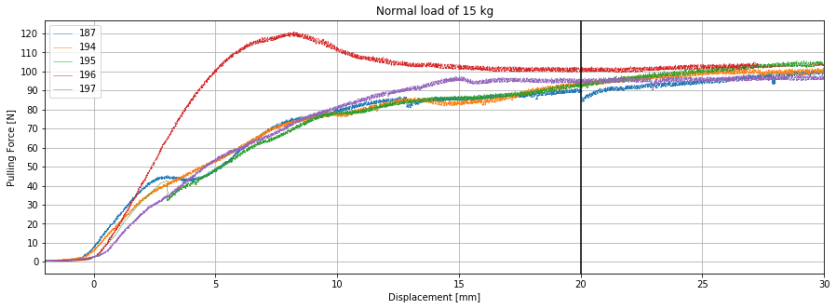

Figure A.36: The results from test series DW tests at 15 kg additional load

Tests at 15 kg	
Test Number	Pulling force at 66% displacement [N]
187	90
194	100
195	95
196	101
197	95
Average	96.25

Table A.21: Values for pulling force

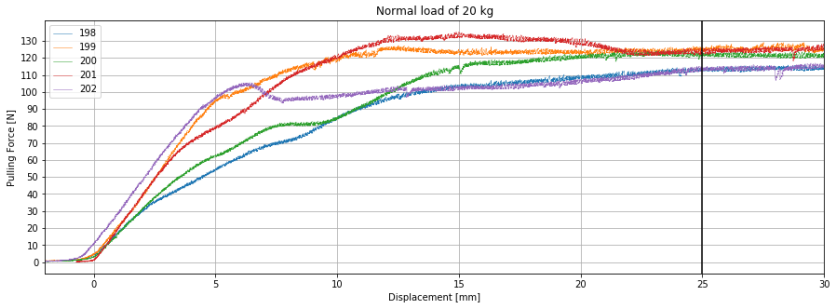

Figure A.37: The results from test series DW tests at 20 kg additional load

Tests at 20 kg	
Test Number	Pulling force at 66% displacement [N]
198	115
199	125
200	121
201	124
202	115
Average	120

Table A.22: Values for pulling force

A.4.6. DWS

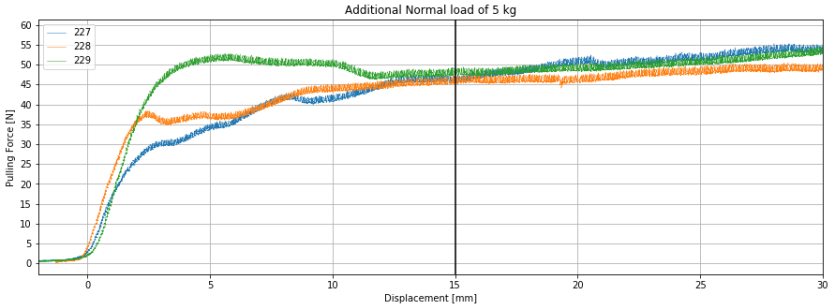

Figure A.38: The results from test series DWS tests at 5 kg additional load

Tests at 5 kg	
Test Number	Pulling force at 50% displacement [N]
227	48
228	46
229	47
Average	46

Table A.23: Values for pulling force

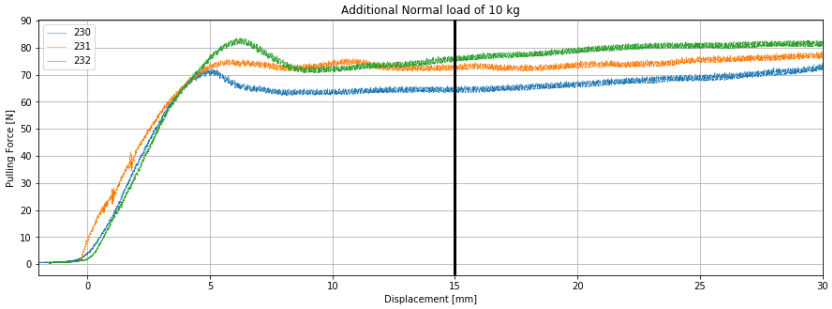

Figure A.39: The results from test series DWS tests at 10 kg additional load

Tests at 10 kg	
Test Number	Pulling force at 50% displacement [N]
230	65
231	73
232	76
Average	71.3

Table A.24: Values for pulling force

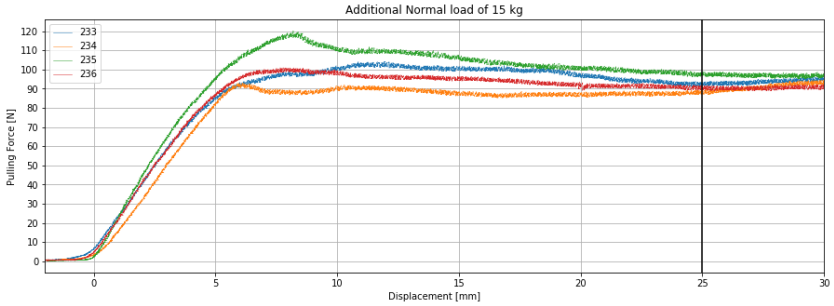

Figure A.40: The results from test series DWS tests at 15 kg additional load

Tests at 15 kg	
Test Number	Pulling force at 83% displacement [N]
233	93
234	87
235	97
236	90
Average	91.75

Table A.25: Values for pulling force

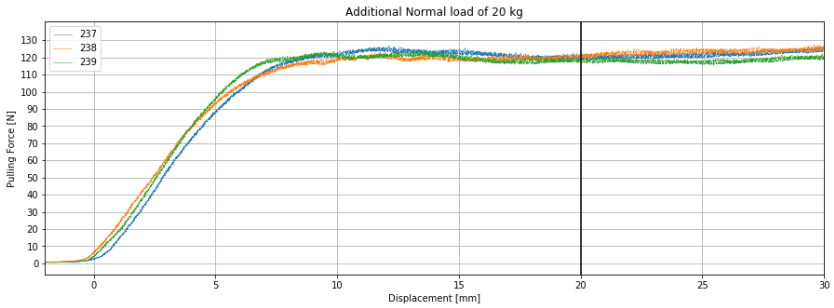

Figure A.41: The results from test series DWS tests at 20 kg additional load

Tests at 20 kg	
Test Number	Pulling force at 66% displacement [N]
237	120
238	120
239	120
Average	120

Table A.26: Values for pulling force

B

Appendix

B.1. CPTs of the Locations

The Robertson IC method requires data of the vertical (effective) stress at each depth to correct the CPT values. Therefore it is needed to interpret the CPT manually before running the Monte Carlo analysis. The interpretation of the layers and the corresponding unit weight are given below. The interpretation is based on the CPT data and on D-foundations software developed by Deltares. The unit weights are determined based on results of tests performed for the Dapperbuurt tests, for the North-South line project and on the NEN 9997-1.

Soil type	Top [m NAP]	Bottom [m NAP]	$\gamma_{sat}[kN/m^3]$
Sand fill	0.49	-1.4	17
Clay	-1.4	-2.7	16
Sand	-2.7	-3.3	17
Peat	-3.3	-4.9	11
Clay	-4.9	-7	16
Wad Sand	-7	-8	18,5
Clay	-8	-9.2	16
Was Sand	-9.2	-10	18.5
Peaty Clay	-10	-11.6	15
Sand (First Sand layer)	-11.6	-13.5	20

Table B.1: Soil Profile and Parameters on location 1.

Soil type	Top [m NAP]	Bottom [m NAP]	$\gamma_{sat}[kN/m^3]$
Sand fill	0.66	-1	18
Sandy loam	-1	-7.5	19
Peaty Clay	-7.5	-10.2	14
Clay	-10.2	-12.5	15
Peat	-12.5	-12.7	12
Sand (First Sand layer)	-12.7	-15	20

Table B.2: Soil Profile and Parameters on location 2.

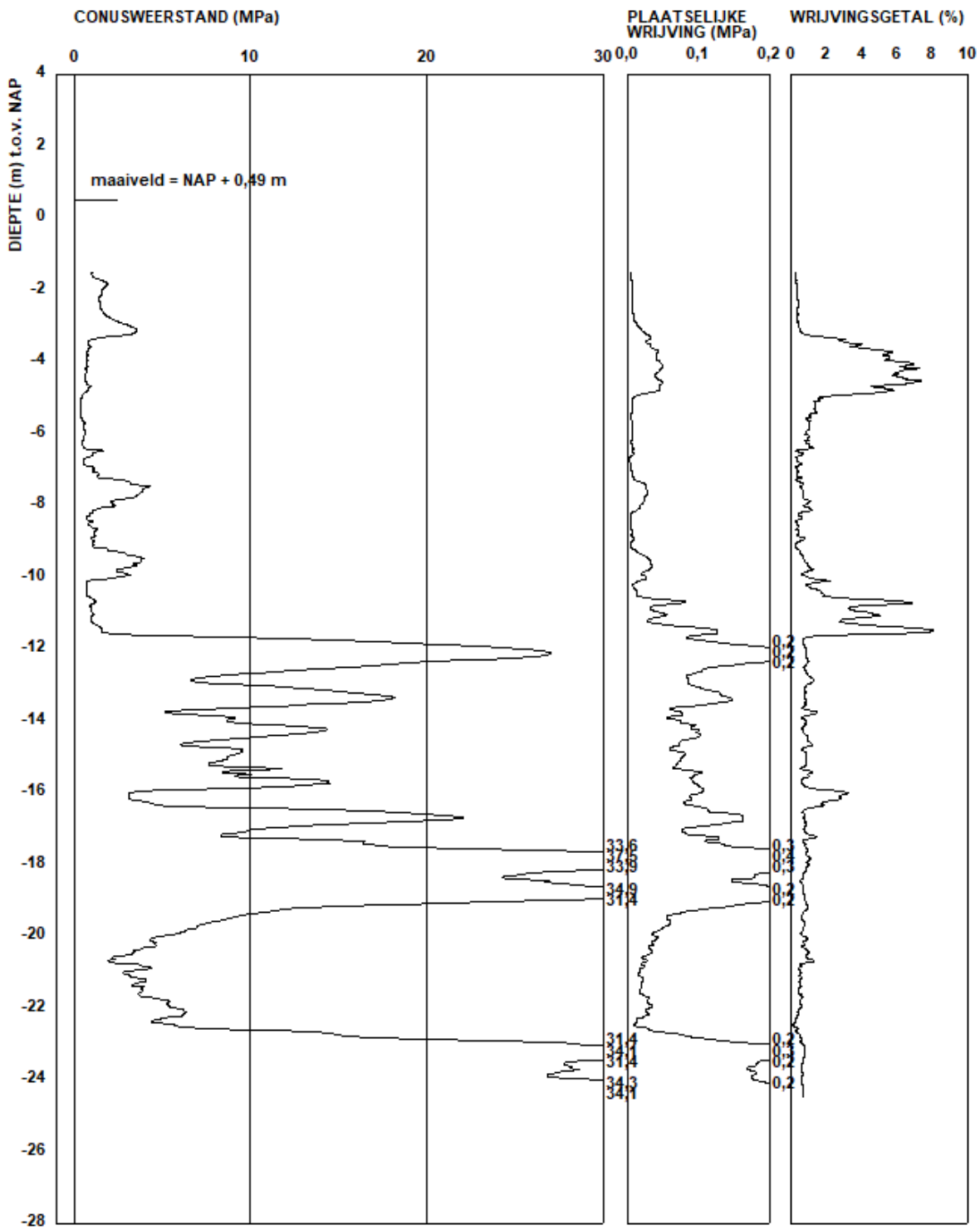

Figure B.1: CPT Data on Location 1

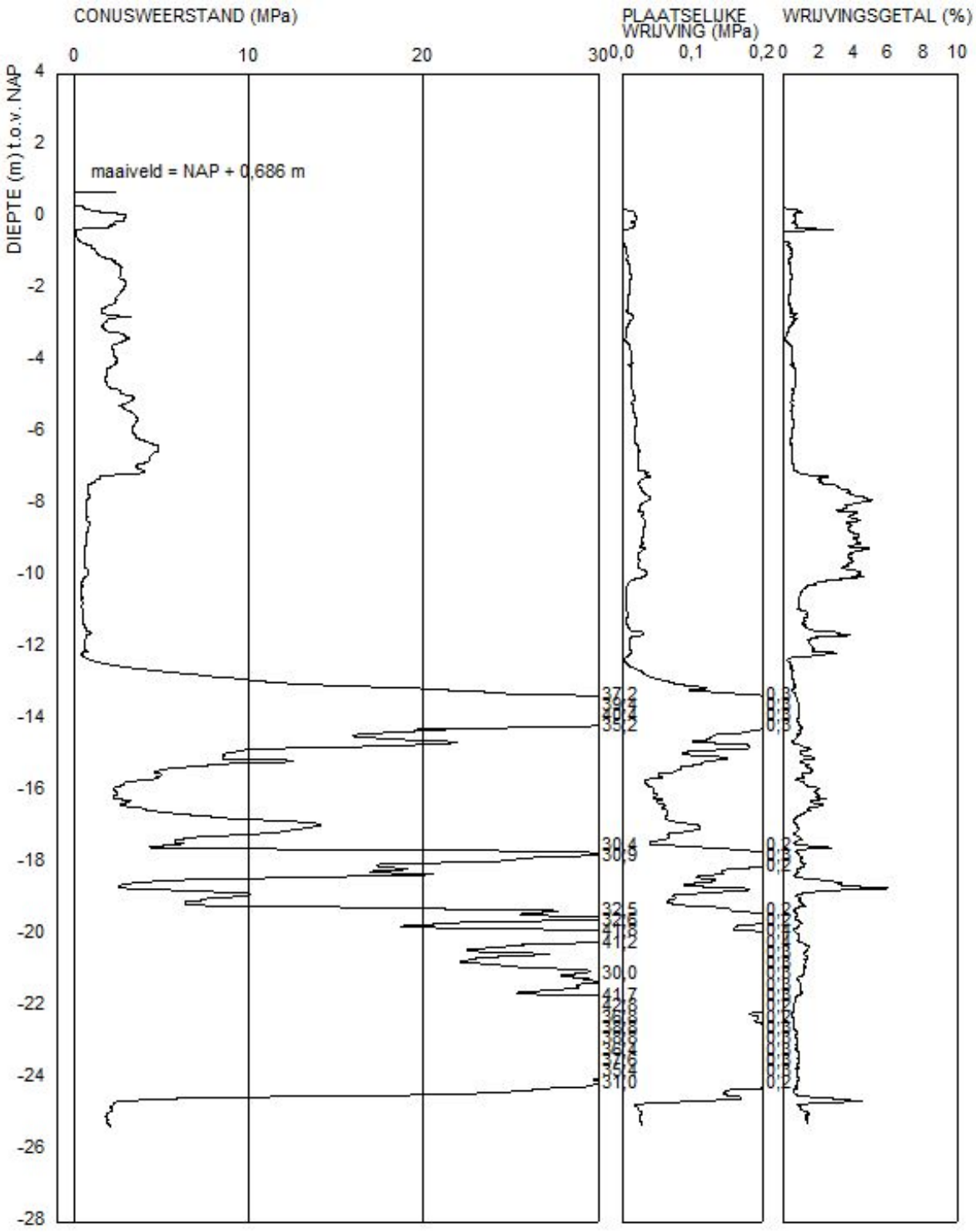

Figure B.2: CPT Data on Location 2

B.2. Parameter Analysis

Relation Dt and Dh

Figure shows that using the tapering and the head diameter for the Cholesky decomposition gives results which don't match as good, as well the data points as the tip diameters. Since tip diameter is more important parameter than tapering in the calculations, using the correlation between the two diameters gives the best approach

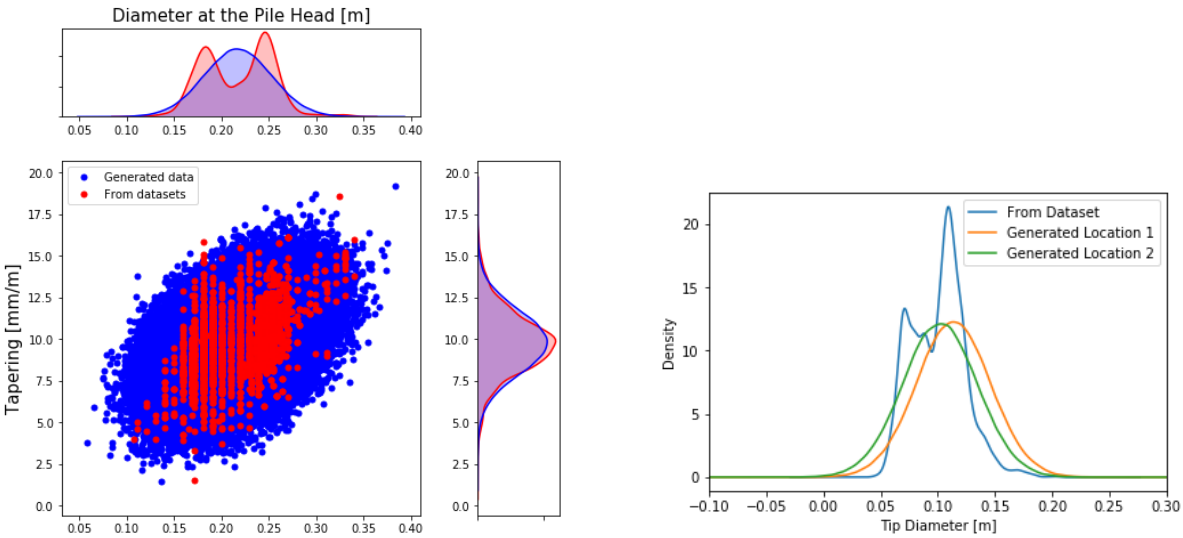

(a) Distributions of generated data and dataset

(b) PDF for tapering on two locations and from dataset

Figure B.3: Results from Cholesky decomposition

The distributions which followed from the analysis were compared to the distributions from the original data set. This showed that the best fit with the original data was found when a relationship was prescribed between the diameter at the head and at the tip. From these parameters the tapering was calculated.

B.2.1. Results

Location 1

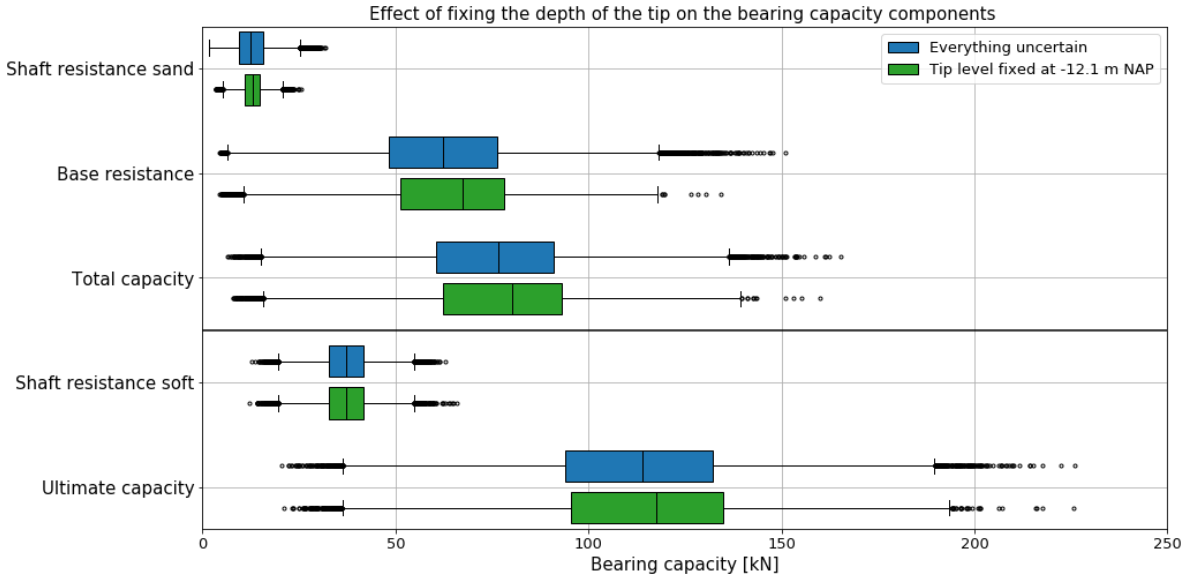

Figure B.4: Box and Whisker plots for all bearing capacity component with all parameters uncertain and with the depth of the pile tip set at -12.1 NAP

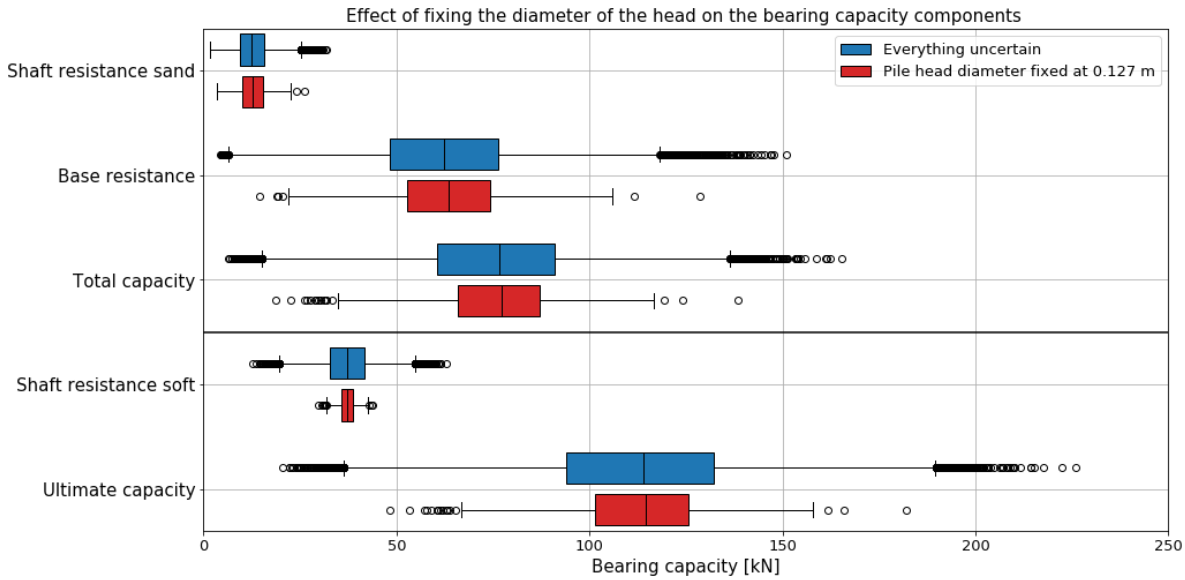

Figure B.5: Box and Whisker plots for all bearing capacity component with all parameters uncertain and with the head diameter set to 0.217 m

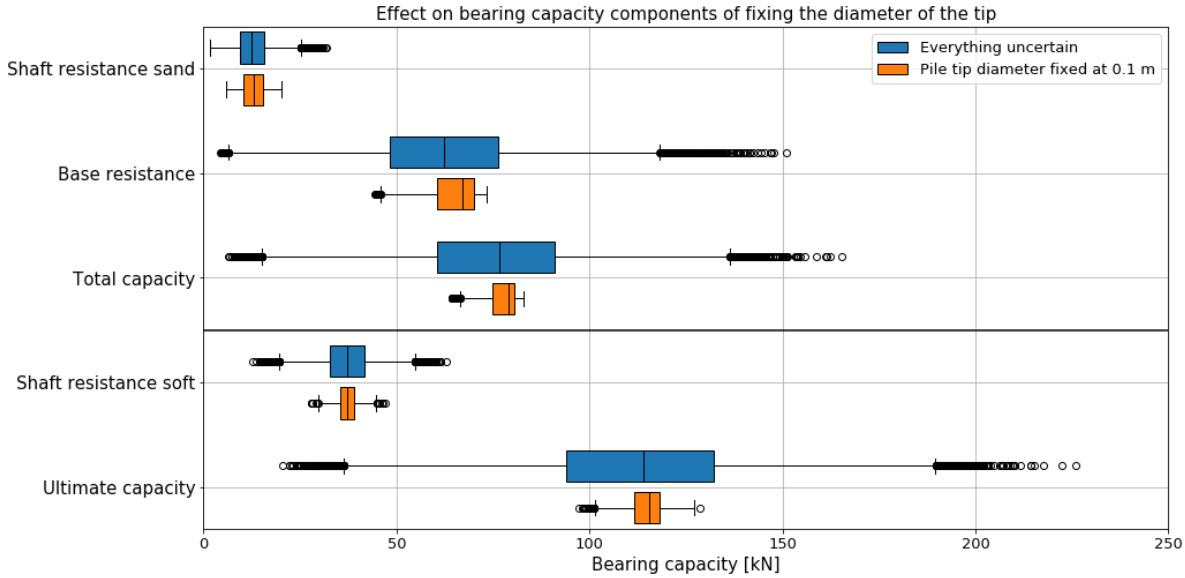

Figure B.6: Box and Whisker plots for all bearing capacity component with all parameters uncertain and with the tip diameter set to 0.1 m

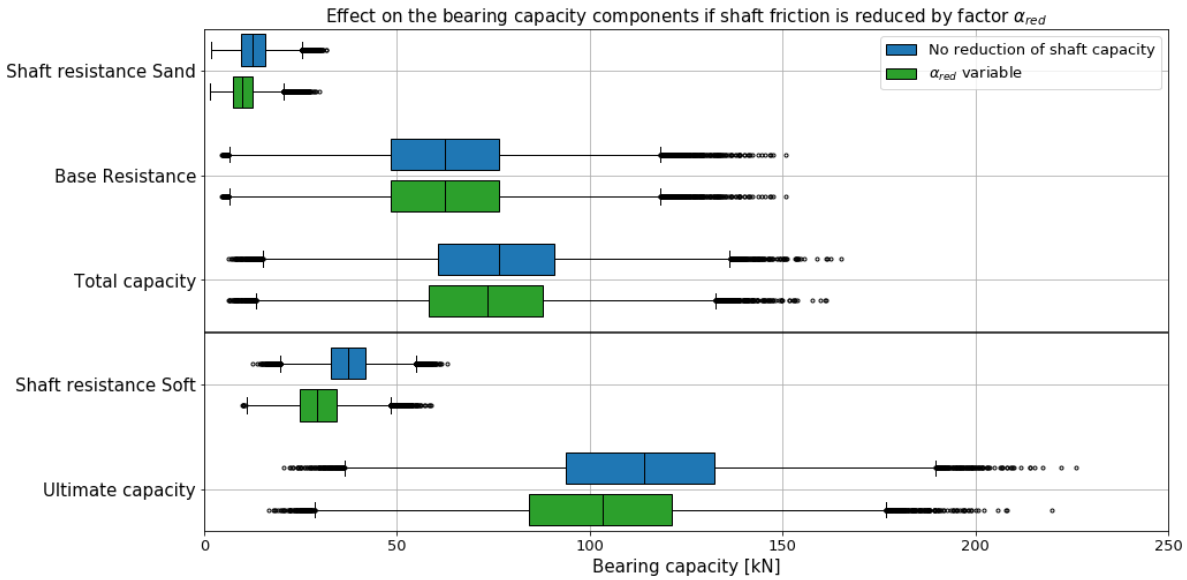

Figure B.7: Box and Whisker plots for all bearing capacity component with tip diameter fixed at 0.1, depth set at -12.1 NAP and α_{red} varying

Location 2

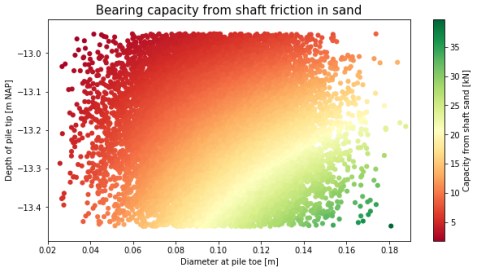

Figure B.8: Shaft capacity in the sand layer for different tip diameter and embedment

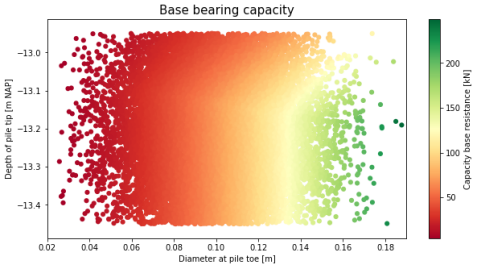

Figure B.9: Base resistance for different tip diameter and embedment

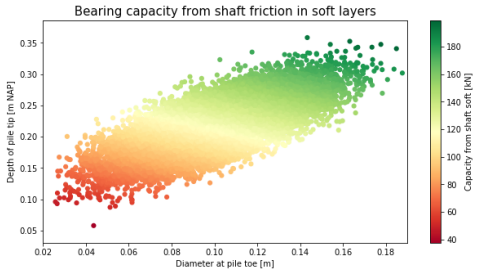

Figure B.10: Shaft capacity in the soft layers for different tip and head diameter

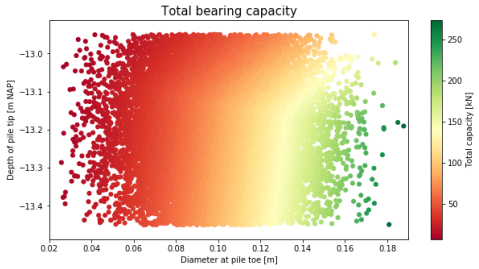

Figure B.11: Total capacity for different tip diameter and Embedment

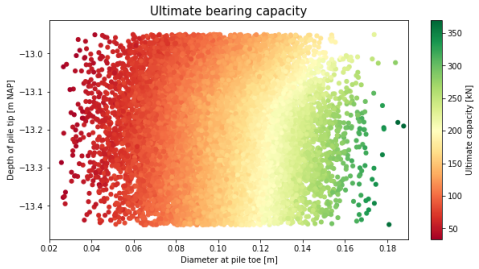

Figure B.12: Ultimate capacity for different tip diameter and Embedment

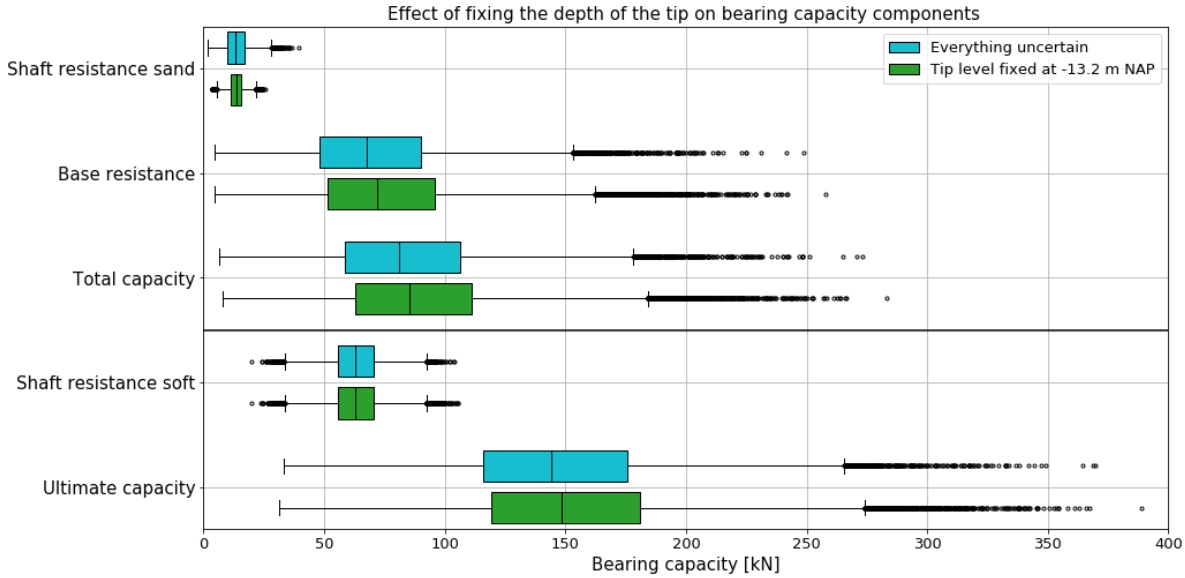

Figure B.13: Box and Whisker plots for all bearing capacity component with all parameters uncertain and with the head diameter set to 0.217 m

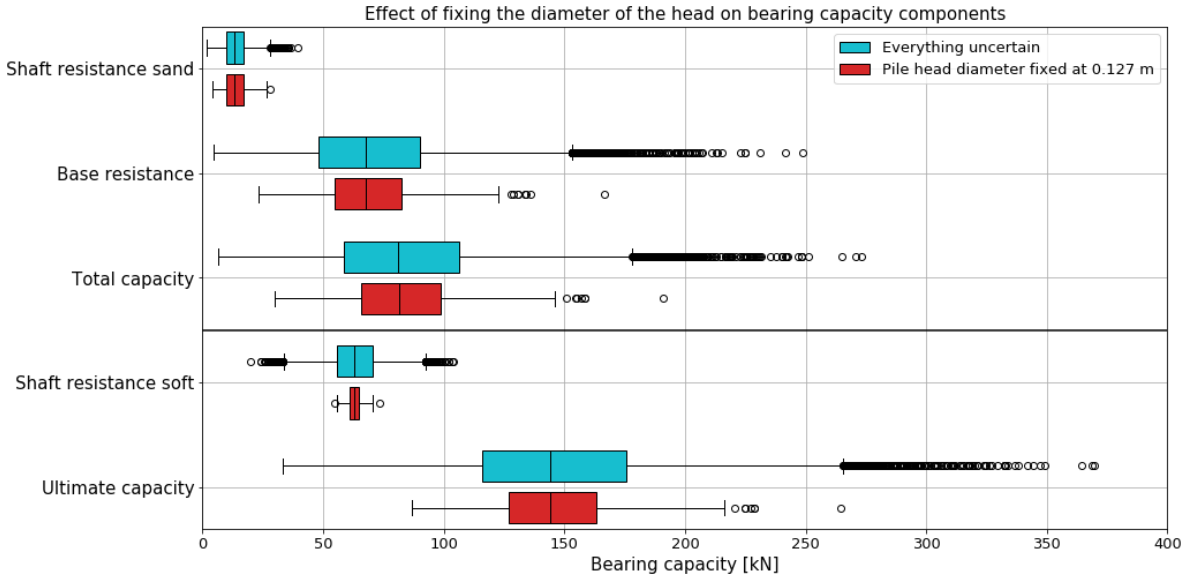

Figure B.14: Box and Whisker plots for all bearing capacity component with all parameters uncertain and with the head diameter set to 0.217 m

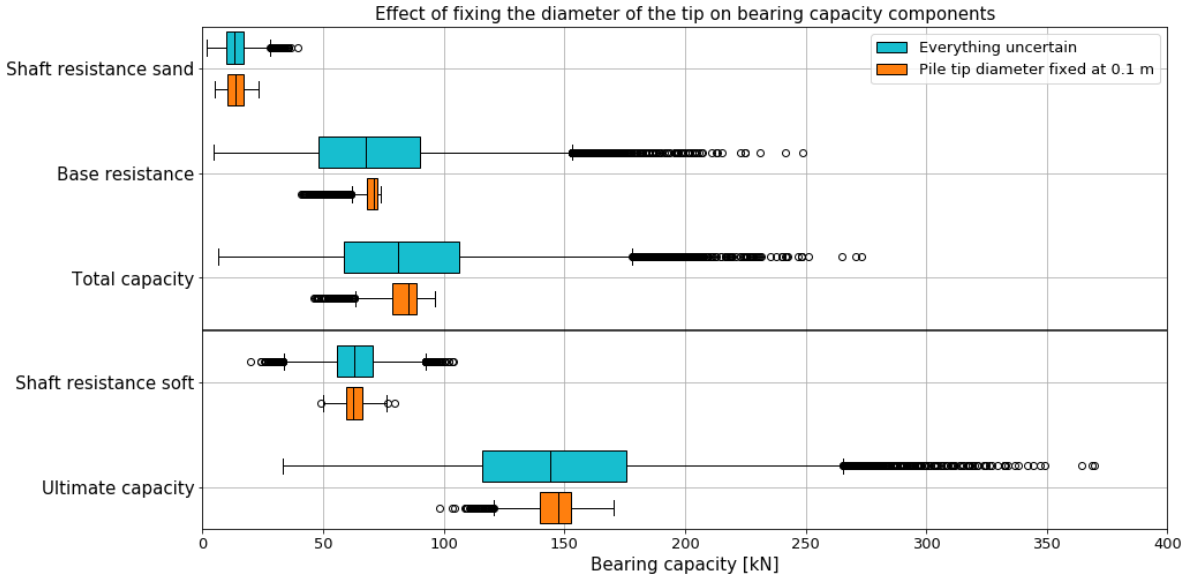

Figure B.15: Box and Whisker plots for all bearing capacity component with all parameters uncertain and with the tip diameter set to 0.1 m

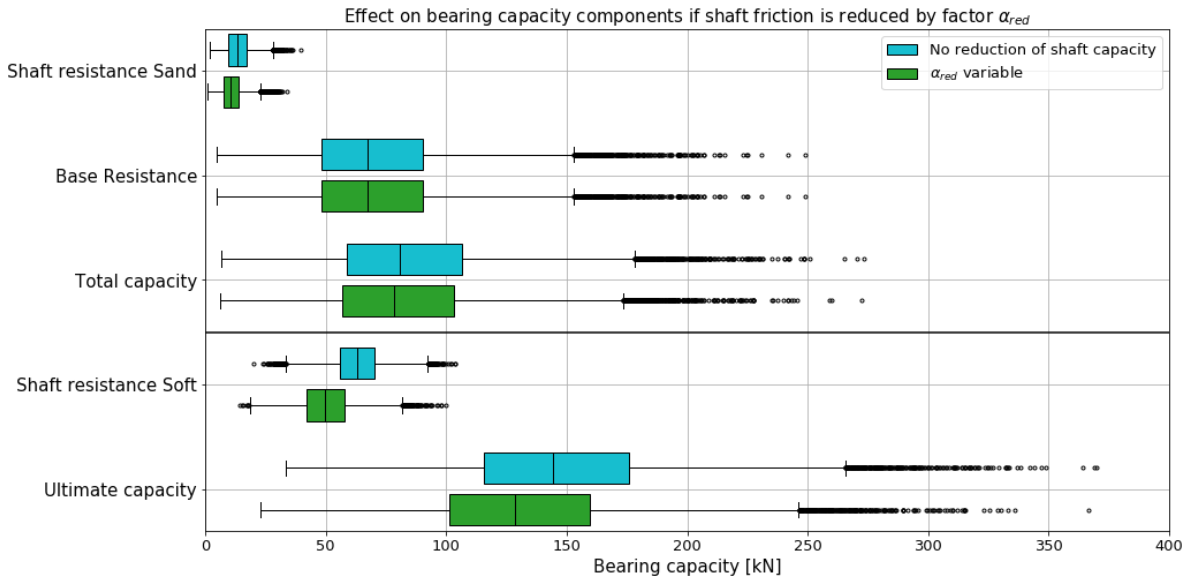

Figure B.16: Box and Whisker plots for all bearing capacity component with tip diameter fixed at 0.1, depth set at -13.2 NAP and α_{red} varying